IMPACT BEHAVIOR OF ORTHOTROPIC STEEL PLATES AND PLATE ELEMENTS WITH BISERRATED AND CLOSED RIBS

by

EKREM MEHMET CELEBI, Dipl. Ing.

DISSERTATION

Presented to the Faculty of the Graduate School of

The University of Texas at Austin

in Partial Fulfillment

of the Requirements

for the Degree of

DOCTOR OF PHILOSOPHY

THE UNIVERSITY OF TEXAS AT AUSTIN

May, 1971

The research was financially supported by the U. S. Naval Facilities Engineering Command Contract No. NBy 78667 N00025-67-C-0026.

Ekrem Mehmet Celebi

May 1971

IMPACT BEHAVIOR OF ORTHOTROPIC STEEL PLATES AND PLATE ELEMENTS WITH BISERRATED AND CLOSED RIBS

Publication No. _____

Ekrem Mehmet Celebi, Ph. D.
The University of Texas at Austin, 1971

Supervising Professor: A. Anthony Toprac

The impact behavior of orthotropic steel plates with biserrated and closed trapezoidal ribs was investigated. Orthogonal-anisotropic characteristics for a deck plate is achieved by stiffening ribs equally spaced and parallel to the span. Nine full size specimens with single or multiple ribs, serrated or closed were tested.

Orthotropic steel plate with biserrated ribs had been developed by the Naval Facilities Engineering Command, U. S. Department of Navy and is named as AMMI system. The AMMI structural system was used to build many kinds of naval structures because of the material and weight savings due to serrations. Since most of the naval structures operate under severe loading conditions the response to impact of the AMMI system needed an investigation.

The prime objective of the study was to find out how much energy could be absorbed by various specimens. The study was carried out so that the impact capacities of the closed and serrated multiple rib specimens could be compared with those of single rib specimens. The impact and static response of the orthotropic plates and their primary elements are discussed in detail.

TO

MY MOTHER

AND

MY FATHER

ACKNOWLEDGMENTS

It has been a distinct privilege to have had Professors Anthony A. Toprac, Eugene A. Ripperger, James S. Noel, Ching H. Yew, and Joseph A. Yura as members of the Supervising Committee. The author is indebted to all of the members of the committee who generously offered their time, and supplied their enthusiasm, knowledge, and experiences to this project. Sincere thanks are extended to the late Dr. Ervin S. Perry, a previous member of the committee for his guidance and constructive suggestions, and also to Professors Enrico Volterra and Eric B. Becker for their interest and support.

The author expresses his thanks to his friend Mr. Cecil W. Thomas, Research Assistant in the Biomedical Engineering Department, for his help and assistance. Without the programs he developed for the XDS930 computer this work would have been much more difficult to accomplish.

Handling of the immense volume of data was only possible due to the existence of powerful computers at The University of Texas. Helpful consultation of Mrs. Florence Turk at the Computation Center is gratefully acknowledged.

The author acknowledges also with the deepest gratitude the encouragement and support of his wife Elfi.

Appreciation and sincere thanks are due to Mr. Robert Garcia who worked hard during the tests. Thanks also to Miss Kathy Huebinger for typing the first draft and to Mrs. Pat Theiss for typing the final manuscript.

The author would like to thank all who participated in this project directly or indirectly, and his colleagues for their advice and interest.

The author acknowledges also his appreciation to his colleagues at the Middle East Technical University, Ankara, Turkey for their support and for making his leave of absence possible.

Dynamic loads were applied by dropping a free fall mass onto a cushioning material resting on the specimen. Impact force, deflections, and strains at various locations of the midspan section and support reactions were measured and registered on a multichannel magnetic tape recorder. Test data on the analog tape were then sampled at every millisecond time interval and digitized. Finally the digitized information was reduced and analyzed by digital computers.

The closed rib specimens were stiffer than the serrated specimens. In other words, the same impact force deflected the serrated rib specimen more than the closed rib specimen. The effect of stress concentrations, the notch effect due to serrations became more evident under impact. Serrated rib specimens yielded earlier than the closed rib specimens. Closed rib specimens possessed more reserve strength and energy absorption capacity beyond initial yielding.

The serrated rib specimens failed always by buckling of the deck plate at or close to the impacted location, and carried much lower impact force at ultimate than the closed rib specimens. The closed rib specimens did not buckle, except very locally and only when excessively deformed after successive impacts.

There was one case only in which the high velocity impact on serrated single rib specimen caused the cracking of the weld tip since buckling of the deck plate, was excessive. Otherwise no fractures were observed.

Theoretical considerations to predict the deflection of the impacted single rib specimens are also discussed in this study. It is seen that the shape of the load is important for the correct prediction of deflection.

Based on the impact test results, pertinent conclusions are derived and recommendations for further study are included.

TABLE OF CONTENTS

NOTATION

A	Area of the cross section, Constant, inclination of the straight line
a	Acceleration, Deceleration
B	Constant, intercept of straight line
$[C]$	Damping matrix of an element or structure
c	Damping constant
CL	Closed (rib specimen)
c_{cr}	Critical damping coefficient
E	Young's modulus, Electromotive force, Voltage
e	Strain
$\dot{e}$	Strain rate
$\bar{F}$	Calibration constant of Statham accelerometer, Straingage factor
$\{f(t)\}$	Force vector
f	Frequency
G, g	Acceleration due to gravity
GN	Value set on gain switch
I	Impulse $= \int P\, dt$
k	Spring constant , stiffness
L, l	Span length, half span lentgh (when specified)
$[M]$	Mass matrix of an element or of structure

M_p	Plastic Moment
m	mass
P	Force
P_i	Impact force
P_u	Predicted ultimate load in static tests
P'_u	Measured ultimate load in static tests
R	Resistance, Voltage divider (resistor)
r	max amplitude of the steady state solution
S	Section modulus of a cross-section
S_t	Top section modulus of a cross-section
S_b	Bottom section modulus of a cross-section
SR	Serrated (rib specimen)
$\{u\}$	deformation vector
T	Period of vibration, Impact duration
t	Time
V	Volt
v	velocity
v_o	Initial impact velocity
X, Y	Coordinate axes
X_1	Maximum amplitute
x	Amplitute
z	Distance from the center of gravity of a section to a reference axis
Z	Plastic section modulus of a cross section

γ	Specific weight
δ	Deflection
δ_c	Plastic deflection due to collapse load
θ	Angle of rotation
μ	Damping coefficient
ρ	Specific mass = γ / g , Damping constance as the percentage of critical
Δt	Incremental time
	Axial stress
σ_y	Yield stress
$_{dyn}\sigma_y$	dynamic yielding stress
τ	Ratio of circular frequency of the system to its natural circular frequency
Σ	Summation
ζ	Phase angle
ω	Circular frequency
ω_o	Natural Circular frequency

CHAPTER I

INTRODUCTION

1.1. General

The investigation reported herein was concerned with the impact response of the orthotropic steel plates. A detailed discussion of previous investigations, scope and the limitations of this present study are described in this chapter. The type of specimens tested, instrumentation employed, test procedures, and the test results are discussed in the following chapters.

1.2. Historical Developments

The idea of orthotropic plates was conceived early in this century as the result of engineer's efforts in Europe, primarily Germany, to obtain optimum structural performance from materials. The recognition of the load carrying capacity of the deck allowed the design of lightweight steel bridges.

Orthotropic or orthogonal-anisotropic plate is distinguished from ordinary plate by equally spaced stiffening ribs rigidly connected to one side of the plate generally parallel to the span. The ribs not only increase the flexural rigidity of the plate in the longitudinal direction, but also help to distribute the loads in the transverse direction. Orthotropic steel plates with different types of ribs are shown in Fig. 1. The open rib forms are easy to manufacture, but they are torsionally less stiff compared to hollow rib forms.

The extensive application of orthotropic steel plates was possible only after improvements in welding technique were developed. The economic conditions of Germany, following the Second World War, speeded the development of long span bridges using orthotropic steel plates. The

material and weight savings due to the structural efficiency of the orthotropic plate had also been recognized long time ago both in England and America.

These plates were used primarily in bridges as deck elements and later on as web elements for box girders. Parallel to these developments in bridge structures orthotropic plates found extensive application in ship decks, both in oil tankers and cargo ships. Military demands due to the Vietnam war stimulated further usage of orthotropic plate structures in portable and adaptable units.

Recently Dr. A. Amirikan (1)* of the Naval Facilities Engineering Command (NAFVAC) of the United States Department of the Navy, introduced a new orthotropic plate with trapezoidal hollow ribs which were serrated at alternate locations of the two faces of the rib-webs. The new structural element was called "orthotropic steel plate with biserrated ribs" (Fig. 2). The Naval Facilities Engineering Command of the U. S. Navy utilized this structural system, AMMI system, as the deck element in several structures. The biserrated ribs resulted in weight reduction and allowed relatively large size prefabricated modules of the AMMI system. These advantages soon speeded the utilization of the AMMI system to build pontoon bridges, floating and portable harbors, lighters, tugs, submerged fuel bunkers, offshore service platforms, floating and dry docks (2).

Because of the unusual loading conditions in the war zone and of the serrations on the ribs, and since no experimental data was available, it was deemed necessary to investigate the behavior of orthotropic plates both with biserrated and closed ribs under static, fatigue and impact loading. An example of the closed rib orthotropic plate is shown in Fig. 3.

The response to static and fatigue loads of these elements have been studied prior to 1970 in the Structural Fatigue Laboratory of The University of Texas at Austin and reported in References 3, 4, 5, and 6. The response of the orthotropic plates under impact loading has been studied and is reported herein.

*Number in parenthesis refers to corresponding item in the References.

1.3. Literature Review

Though the area covered by the general expression "impact loading" is large and diverse and has appealed to the interest of many scientists for some centuries, almost none of the results of the previous theoretical studies apply to the current investigation. A detailed literature survey related to the studies of impinging bodies is contained in References 7 and 8. Part of the reported work is concerned with material properties under impact. Some others discuss the stress wave propagation due to impact in infinite media, and others in half space or in rods.

The deformation of an impacted simple beam has been studied for almost two centuries. Recent efforts were directed toward reducing the restrictions on the geometry of the cross section, the beam supports and the material behavior. The shape of the impacting mass was usually considered to be spherical. The duration, magnitude and the shape of the contact force needed to be known to predict the response theoretically.

The theoretical impact studies on rectangular and circula are rather few. They were generally based on elastic behavior, for which the deflections were small compared to the plate thickness and the material behavior was linear. The thickness was considered to be constant overall. The load on the plate was uniformly distributed and caused bending of the "middle plane" of the plate. No deformation or distortion of the element of the "middle plane" was expected. None of these assumptions are valid in a study of the behavior of an orthotropic plate.

The experimental impact studies on plates have been carried out mostly on small size plates either to investigate the stress wave propagation in the plate and correlate the results with theory, or to find the penetration, perforation, or scabbing of metallic plates due to high or hypervelocity impact, when the plate is hit by a bullet or shock front of an explosive detonation.

According to the author's knowledge, neither theoretical nor experimental studies have been made on the impact response of orthotropic plates.

1.4. Content of the Study

This study is divided into three chapters. The first is the introductive part. It contains the general statement of the problem, the aim and scope of the investigation, its restrictions and limitations.

The second chapter of this work contains extensive information related to the experiments. This chapter is divided into paragraphs corresponding to the steps followed in the experiment and includes specimen details, the test setup, test procedure and instrumentation, and the data reduction methods.

The last chapter contains discussions of the results. From the reduced and analyzed data, force/time, force/deflection, force/energy, and stress/time relations are established with a separate paragraph for each relations. A summary in tabular or graphical form for each relation was prepared. Representative examples of the relations are pointed out in this chapter referring to the numbers given to the figures and tables. Supplementary information for each relation is given in corresponding appendices. The reader may find necessary information in the appendix pertaining to each relation following the explanations given in the discussion paragraph. At the end of each paragraph conclusions are given.

The last chapter also contains a special paragraph for conclusions based on the results of this study. At the end recommendations for further studies are included.

1.5. Objectives of the Study

The objectives of this study on the impact response of the orthotropic plates with biserrated and closed ribs are:

1. How much energy will the orthotropic steel plate absorb?
   (a) elastically
   (b) when yielding initiates at extreme rib fibers
   (c) when deck plate buckles
   (d) when a certain level of displacement is reached
   (e) ultimately

2. How will the ultimate energy absorption capacities vary?
   (a) with the type of rib (biserrated or closed)
   (b) with the number of ribs (one, three, four)

3. How will the different orthotropic plates deflect under impact?
   (a) with the type of rib (biserrated or closed)
   (b) with the number of ribs (one, three, four)

4. Is the impact behavior of orthotropic plates different from its static behavior?

5. How will the shape of the impact pulse (its amplitude and duration) vary?
   (a) with the type of the rib (biserrated or closed)
   (b) with the number of ribs (one, three, four)

6. When and what kind of failure of orthotropic plates will occur under impact?
   (a) will there be any fracture?
      (1) at welds
      (2) around serrations
      (3) in the deck plate
      (4) or elsewhere
   (b) will there be buckling in all orthotropic plates? where and how will this develop?
   (c) will the failure be local or cover the whole plate (to declare it out of service?)

7. Can any qualitative comparison be established between the stresses of the impacted and statically loaded orthotropic plates?

A general study of the impact response of the orthotropic steel plate would have involved the effects of many parameters such as: the geometry of the orthotropic plate including the form and the location of the ribs, the support conditions, the material behavior of the plate, the mass ratio of the impinging mass and of the plate, the material characteristics and the initial impact velocity of the mass, the physical environment in which the impact occurs, etc. The combined effect of all these parameters create the most important variable in such a study, the time dependent impact force, also referred to as "the forcing function." The forcing function is also influenced by the shape of the contact surface between the impinging object and the plate, and by the shape changes during impact. The forcing function is itself a function of the total

response characteristics of the investigated element including its local behavior.

In static loading the deflection is related only to the material and geometric properties of the specimen together with the force applied to it. However, for dynamic loading, all interactions between the parameters are time dependent. Therefore, the following decisions governed the objectives of this study:

(1) Experimental investigations are to be made to study the response characteristics of the orthotropic plate elements and the orthotropic plates under impact loadings.

(2) The test series to contain single, three, and four-rib specimens (Fig. 4 to 8). The single-rib specimens represent the orthotropic plate elements. The multi-rib combination of the plate elements constitute the orthotropic plate.

(3) Distinctions to be made among the specimens based on whether or not their stiffening ribs have web serrations (Fig. 2 and 3).

(4) The tests to be performed in such a manner that comparison of the response of multiple versus single and closed versus serrated rib specimens could readily be made.

(5) This study to produce the time dependent relations of the impact force, the displacement of the specimen, the strain measurement at certain locations of the specimen, and the support reaction.

(6) From these measurements the following relations to be derived:

   (a) The force-deflection characteristics mainly at the impact location for each specimen, and also at other locations.

   (b) The work time relation as a measure of how much energy the specimen is capable of absorbing. This relation is obtained from the force deflection curve at the impact location by numerical integration using millisecond time steps. The integration begins when impact is initiated and it ends when the incremental work approaches zero.

   (c) To obtain the relation between the energy absorbed by the specimen and the impact force.

   (d) To find the stress-time relations at locations where the strains were measured.

(7) To derive pertinent conclusions from the established relationships.

1.6. Restrictions and the Limitations of the Investigation

In the previous paragraph, the objectives of this investigation were described. In this experimental study as many parameters as possible were studied. The limitations of the parameters depended on the available equipment at The University of Texas. Due to complex nature of the geometry of the specimen on one hand, and due to the lack of any prior knowledge regarding the behavior of such structural elements under impact loading on the other hand, no attempt was made to justify experimental measurements with calculations based on existing theories. Theoretical deflections were calculated only for specimens with a single closed rib and were compared to those measured experimentally. It is seen that at best the theory may provide an approximate solution, if the shape, the amplitute and the duration of the time dependent impact force is estimated close enough to those experienced during the tests.

Even in the case of static loading within the elastic limit, the experimental and theoretical results differed more than 10 percent (6). A literature survey indicated that beyond the elastic limit there existed no comparison between theory and experiment. Using the general matrix notation the force deflection relation of the statically loaded system can be written as

$$\{f\} = [S]\{u\}$$

where $\{f\}$ is the static force vector
$\{u\}$ is the displacement vector
$[S]$ is the stiffness matrix of the plate

The above mentioned discrepancy between the theoretical and experimental results indicate that the stiffness characteristics of the orthotropic plate has not been established theoretically accurately enough.

In the case of dynamic loading the force deflection relation is even more involved, and can be expressed with general matrix terms as

$$\{f(t)\} = [M]\{u''\} + [C]\{u'\} + [S]\{u(t)\}$$

where

$\{f(t)\}$ = time dependent forcing function as represented by vector

$[M]$ = mass matrix of the system

$[C]$ = damping matrix of the system

$[S]$ = stiffness matrix of the system

$[M]$, $[C]$, $[S]$, are all related to the geometry and material behavior

$\{u(t)\}$ = time dependent deflection function as represented by vector

$\{u''\}$, $\{u'\}$ = second and first time derivatives of the deflection function as represented by vector

This matrix equation can provide an accurate solution to the problem to the extent that the mass, damping, and stiffness matrices are capable of representing the characteristics of the system.

It was mentioned earlier that prior theoretical studies were restricted to very specific and assumed conditions and were far from representing the actual behavior of the system.

The tests needed a good variety of expensive and sophisticated instrumentation, which was available in this University. Yet data could simultaneously be registered only in six available channels of the recording instrument. Even with this limited number of channels almost 1.6 million data points were produced. Such a large amount of data could not be reduced without the computers. Displacement and strain measurements could only be measured at certain locations at the mid-span. Force measurements were made only by one accelerometer on the mass and the support reaction could only be registered by means of two load cells. For more recording at other locations of the specimen, more elaborate and costly recording instruments would be required, even then one would be limited by the capacity of the existing computers.

CHAPTER II

EXPERIMENT

2.1. General

This chapter will be concerned with the details of the conducted experiments. To fulfill the objectives of the study nine prototype orthotropic steel plate specimens were tested under impact. The test specimens are described in detail in the following paragraph. The specimens were distinguished from each other by the number of their stiffening ribs and whether or not the ribs were serrated at alternate web locations. Single rib specimens were referred to as plate elements, whereas the multirib specimens constitute the orthotropic plate.

The specimens were subjected to impact loads by a falling mass of 1197 lbs. from different heights with initial impact velocity up to 56.7 ft./sec. The test setup, the test procedures followed, and the instrumentations employed are discussed in this chapter. Detailed information regarding the instruments and their calibration and operation are included in Appendix IV.

During the tests impact forces were measured by an accelerometer attached to the impacting mass. The displacements and strains of the midspan section were measured using transducers and strain gages. The support reactions were measured by the load cells placed under each rib. The test data were recorded on a multichannel magnetic tape recorder. Registration and recording were automatic and controlled electronically during the period of load release and impact. The methods used for data reduction and analyses are described at the end of this chapter.

Although there were many impact tests performed prior to this date at The University of Texas at Austin and other universities, this study differs greatly from those with reference to the test specimens,

test demands, setup facilities and procedure undertaken in the phase of data reduction.

2.2. Specimens and the Test Setup

In this section the specimens, coupon tests, test site, test setup are described. The methods followed in testing is explained and information is given about why cushioning material during the test was needed and how cushions were made and tested.

2.2.1. Specimens. Of the thirteen specimens tested in this program the first four, which were not virgin specimens, were used to improve the test setup and to check the instrumentation. The data registered during these trial tests were not reduced.

The nine prime specimens are summarized in Table 1 and their details are shown in Figs. 4 to 8. Table 1 contains the abbreviated names given to each specimen. In graphical or tabular representation of the test results, the specimens are referred by these abbreviations. For example CL-3-1 stands for the closed three rib specimen, which is the first of its type, similarly SR-1-2 is the second of the serrated single (one) rib specimen. The specimens differed from each other in their widths, number of stiffening ribs and according to whether the ribs were biserrated or closed. The shape of the rib and the shape of the serrations were the same for all specimens. The thickness of the top plate was 1/4 in. and that of all ribs 3/16 in. The span length was 10 ft. for all specimens tested.

The serrations in biserrated specimens were cut with an automatic flame cutting machine (Fig. 9). The corners of the trapezoidal serrations were of 3/4 in. radius to reduce the notch effect. The cut lines were very smooth throughout the length. All serrations in each rib were first cut, prior to bending of the ribs into trapezoidal cross-sectional form.

The bent rib plates were welded to the lower side of the top plate. Figure 10 schematically shows how the rib plate was bent after being flame cut and how it was welded to a top plate to create a biserrated single rib specimen. The welding operation was carried out by skilled welders carefully avoiding warping during the manufacturing process of the specimens. The welding sequence for serrated rib specimens was specified in the shop drawings. A.W.S. E - 7018 or equivalent type of electrode was used for welding.

The supports of all specimens were also unique. A 1/4 in. thick plate of 12-3/4 in. height was welded against each end of the ribs. This supporting web was then welded to a strip of 6 or 8 in. width base plate.

2.2.2. Coupon Tests. The mechanical properties of the A 36 steel used in the specimens were determined with the coupons obtained from material of the same heat.

Figure 11 shows how the 30x30 in. plate was cut into strips to make the test coupons. In this figure the roll direction and the numbers given to each coupon are indicated. The coupons were machined to a standard coupon size with an 8 in. gage length according to A.S.T.M. A370-65. The test results and those taken from the mill test report are tabulated in Tables 3, 4 and 5.

The overall mean values of the coupon tests are as follows:

- yield strength 41.24 ksi
- ultimate strength 60.92 ksi
- max elongation 29.21 % (8 in. gage length)
- Young's modulus 31.07×10^3 ksi

The mill report (Table 5) gives also the chemical compositions of the important elements in steel together with their heat number. The yield and ultimate strength values reported by the steel producer are higher than those obtained in coupon tests. The average Young's modulus cited above is rather high. In further calculations, static Young's modulus of steel is taken as $E = 29.5 \times 10^3$ ksi., a value established in the literature by very accurate tests.

No dynamic tests were made on coupon specimens. Instead in Fig. 12, the ratio of dynamic and static tensile yield stress values are shown as a function of loading time. Figure 12 contains the test results of several steel specimens (7) with different carbon content. A similar relation of the dynamic and static yield stresses of mild steel as a function of strain rat e is shown in Fig. 13 (9). In this figure there is also an empirical formula given, to predict the dynamic yield limit of mild steel for an assumed strain rate.

Figures 12 and 13 are included in order to estimate the impact yield stress to be used in Section 3.3 when theoretical plastic deflections of the impacted closed single rib specimen are predicted. The estimate is made on the basis of strain-rates obtained during the impact test of the orthotropic plates.

2.2.3. Test Site. The drop facility located at the southeast corner of the Engineering Science Building of The University of Texas at Austin was chosen to be the test site for this study. The following specification of the test site as designed originally (10) is given.

	Lower Limit	Upper Limit
. Drop height	.0 ft	85 ft
. Impact velocity	.0 fps	74 fps
. Weight of mass	248.5 lbs	2500 lbs
. Specimen area	.0 ft^2	2 ft x 2 ft
. Specimen height	.0 ft	limited by the stability of stack during impact.

The photographs of the test facility as they were originally designed are shown in Figs. 14, 15, and 16.

Although the test site seemed to be suitable for this study, major changes were needed (Figs. 16, 17, and 18). The following improvements were performed:

(1) The distance of the guide wire anchor locations originally 36 in. was changed to 108 in. Further separation was not possible due to original design limits of the site. The new spacing between the guide wires made it possible to test the multi-rib specimens and furthermore created the possibility of moving the specimen so that the drop mass could strike on locations other than the central position of the specimen (Fig. 19).

(2) The change in guide wire locations required redesign of the supporting arms of the falling mass. The improvement made can be seen in Figs. 16 and 19.

(3) Since measurements and observations were required also on the lower side of the specimen, a supporting system at higher elevation than the original concrete anvil (Fig. 17) had to be added to the test site. Two special girders (depth 37" x 3/8", flange width 11-7/8") were anchored to the concrete floor to serve as main supports throughout the test. The front and the plan view of the new test site is shown on Fig. 18.

2.2.4. Test Setup. The test setup shown in Fig. 19 consisted of:

(1)** Special girders to support the specimen and elevate it to a level appropriate to work under the specimen.

(2) Load cells to measure the support reactions; there were as many load cells as the number of ribs at each end. Only two of the outputs were recorded due to limited numbers of channels in the magnetic tape recorder, the others were spacers.

(3) Specimen placed on the load cells. Around each load cell 4 anchor-bolts were tightened to hold the specimen in place (Figs. 17 and 19). To avoid the lateral movement of the whole system after impact, especially for high drops of over 240 in., chain and hoist arrangement was used at the supporting girders (see Fig. 81).

(4) Load distribution pad--A 24" x 10" x 2" steel plate weighing 142 lbs was used to distribute the impact load. Steel pipe-halves were welded on the pad to avoid the confining pipe from tilting during and after impact.

(5) Confining pipe--A steel pipe 12-1/4" long, 6-3/8" inside diameter, and weighing 18 lbs placed on the load distribution

**The number refers also to the parts mentioned in Fig. 19.

pad served to contain and confine the cushioning material in it.

(6) Cushioning cylinder--Specially made out of crushable lightweight concrete (see also paragraph 2.2.4). Its weight varied from 9 to 14 lbs.

(7) Aluminum plunger--A cylindrical solid aluminum piece placed on the top of the cushioning material, to crush it at the early stages of impact and confine it in the confining pipe. The weight of the plunger was 14 lbs.

(8) Freefall-mass, also known as "drop-mass," hits first the aluminum plunger when released from the desired height. The quick release hook mechanism, which was used to release the drop weight is shown in Fig. 16. The total weight of the drop mass was 1197 lbs.

2.2.5. Cushioning Material.

2.2.5.1 General. As explained above, the cushioning material was placed in a steel pipe with an aluminum plunger on top of it. A lightweight vermiculite concrete was used as cushioning material throughout the test. Information about its preparation and its strength characteristics is given in the next section.

The main purpose of cushioning was to tailor the load pulse with a positive slope after certain rise time. The best possible form would be a near rectangular pulse shape resulting in a constant impact force of a desired duration. This shape was generally achieved in low impact tests with short rise and decay time. As pointed out in Reference 11 and 12, the pulse shape greatly influences the impact response of the test specimen. The pulse form is also effected by the impact response, resulting in a mutual interaction. Among the various materials employed in previous studies (12, 13, 14, 15 and 16) lightweight concrete proved to be the most satisfactory for the type of experiments described herein.

During impact the cushioning cylinders were dissipating part of the impact energy and decelerating the falling mass slowly, so that the value measured by the accelerometer, especially at the time of first contact was within the capacity of the accelerometer. Without cushioning

material proper recording would have been more difficult.

2.2.5.2. Preparation and Strength of the Cushioning Material. The following mixture was used to prepare the lightweight concrete cushioning material:

Vermiculite	30 lbs
Cement	47 lbs
Water	75 lbs

The mixture was prepared using a 5-1/2 cubic foot mixer and poured into standard 12" x 6" concrete test cylinders which were left inside the laboratory for two days before they were stripped off the forms and cured for twenty-eight days or longer. At least one week prior to their use they had to be removed from the room and left inside the laboratory to dry.

The vermiculite used as aggregate is a micaceous mineral, which expands and exfoliates during its fabrication due to heat and other chemical reactions. Chemically it is a hydrated magnesium-aluminum-iron silicate. The type used for the cushioning material had a trade name "Zonolite Plaster Aggregate No. 3." Its density was 8.1 lbs per cubic foot. The sieve test results are as follows:

100% passed through sieve No. 4 ; (.1870 in. = 4.760 mm.)
75% passed through sieve No. 8 ; (.0940 in. = 2.380 mm.)
3% passed through sieve No. 50; (.0117 in. = .297 mm.)

Type I, Portland cement was used in all mixtures.

The strength of the cushioning cylinders was not the primary concern of the experiment. All static tests indicate a minimum ultimate strength of 180 psi.

For the sake of qualitative comparison Fig. 20 shows the stress-strain diagrams of the cushioning material obtained during the static

and dynamic tests. The static tests were made on specimens which had the same material mixture as the specimens used throughout the impact tests.

In each test, the specimen was placed inside the confining steel pipe in the same way as in the actual test and the plunger was placed on the top of the specimen. The testing machine pressed the plunger against the specimen and crushed it gradually. The specimen for Test I was 28 days old with density of 33 lbs/cu. ft. while the specimen for Test II was 6 months old with density of 43 lbs/cu. ft.

Test III and IV are from Reference 125. The specimens used in these dynamic tests differed both in mixture and size from those used in the static tests.

The results of Test III are based on the impact mass (of 236 lbs weight) dropped in free fall on a standard cylinder (density = 50 lbs/cu.ft.) with 720 in./sec. impact velocity.

Test IV is the result of an impact test obtained with an air-gun dynamic test instrument. In this test the weight of the impact mass was 103 lbs and the impact velocity 720 in./sec. The circular impact area was 12.56 in.^{2}. The length of the specimen was 6 in., and its density was 50.5 lbs/ft.^{3}. Figure 20 indicates that the strength of the vermiculite cushioning material did not vary much with the kind of mixture or with the size ratio of the specimen at least during the confining stage. Confinement of the test cylinders began above the stress level of 200 psi.

2.3. Test Procedure and Instrumentation

2.3.1. General. This section covers the part of the experiment beginning with the time of positioning of the test specimen into the desired location until the end of the test. This period of time can be divided into two parts. The first was the time spent to install all necessary equipments and to check them for proper functioning. The second was the time required to perform the test and record the data on a magnetic tape recorder, in photographs and sometimes in 16 mm film. Figure 21 shows schematically how the instruments were connected.

The test data were obtained in using the following instruments:

Accelerometer - for force measurement (Fig. 16)
Load cells - for measurement of support reactions (Fig. 17)
Transducers - for displacement measurement (Fig. 22)
Strain gages - for strain measurement (Fig. 22)

The readings from the above instruments were recorded in data recording instruments. As mentioned earlier, Appendix IV contains a detailed account of the data measuring and data recording instruments (see also Figs. 23 to 25).

2.3.2. Testing and Recording. After the specimen was aligned into the proper test position it was subjected to impact load by dropping a mass weighing 1197 lbs from the desired height. During the long period of time devoted to improve and adopt the test facilities to this experimental study, experience was gained in deciding the drop height without causing harm to the specimen at the early stage of impact test.

In total, 160 tests were performed on 9 specimens. In all tests the impact location was at midspan. The load distributing steel pad (Fig. 19) was placed at the center of the specimen width when single rib specimens were tested. The drop height was gradually increased till the impact of the load caused the failure of the specimen. The multi-rib specimens were impacted at locations other than the central location within the elastic region. Then the drop weight was removed to the central impact location and the drop height of the mass was gradually increased until the failure of the specimen occurred.

The different impact positions along the midspan section of the specimen are indicated in Fig. 26. This figure also shows the numbering system used to designate different locations for each specimen. Numbers were given in sequential order first to the ribs, then to the locations between the ribs. This system of numbering proved to be very useful in the computer program during data reduction (see also paragraph 2.4.4).

During the test, the following data were recorded time dependently:

(1) The impact force acting on the specimen,

(2) the displacement of the specimen at several locations, mainly at the midspan section. In single rib specimens also at the quarter span location,

(3) the strains, only at several locations of the midspan cross section, generally in the longitudinal direction. In multi-rib specimens, at the lower side of the deck plate between two ribs both longitudinal and transversal directions,

(4) the support reactions, each rib was supported on one loadcell, for both right and left supports.

Since there were six working channels in the magnetic tape recorder, only six instruments would be registered during each test. Tests were repeated for different combinations of 6 instruments several times, keeping the drop height of the mass and impact location on the specimen unchanged. Due to differences in the cushioning material it could never be expected to have exactly the same behavior for an instrument which was used in two consecutive tests. However, the observed change in the behavior was slight in most cases.

The data measuring instruments could be divided into two groups. The first group included accelerometers, strain gages, and load cells which had output voltage in the order of millivolts. They all were connected through a calibration box to the Redcor Instrument Amplifiers. The second group included five displacement transducers with different capacities of linear output range. All of the outputs of the transducers were in the order of volts, and needed to be reduced to the level acceptable by the capacity of the recorder. The procedure used to achieve this is explained in detail in Appendix IV. Each transducer was calibrated frequently during the tests; their characteristics were almost unchanged. The transducer's output needed no amplification prior to recording, and hence the transducers were connected directly to the recorder as schematically shown in Fig. 21. The digital voltmeter was to monitor the output prior to and after the test.

Before each drop, a preliminary run of the tape to record and monitor the recording level assured the proper functioning of the instruments. Checks were then made for broken wires or misconnections between the several input and output plugs and for possible wrong choice in gain set. Prior to each pad positioning the quick release mechanism was checked for malfunctioning.

Drop height was measured for low drop levels to within 1/16 in. accuracy. Above 72 in., the drop height was read from an electronic counter, a device which was originally designed for the drop facility. The counter indicated the number of turns of a precisely dimensioned drum which was rotating in contact with the main winch cable. The accuracy of the measurements for this counter was better than 5 percent. After all adjustments and checks necessary prior to the test were accomplished, the tape recorder was started to run in recording level, instructions were given to the test participants to be alert, and at the end of countdown the drop mass was released by doubly secured electronic push button switches. The mass struck first the plunger, crushed the cushioning cylinder inside the confining pipe and loaded the specimen impulsively (Figs. 27 and 28). The rebound and secondary impact varied according to the initial impact velocity, the cushioning material and the specimen characteristics. After almost every impact test the free fall mass, confining pipe, plunger, and heavy steel pad were thrown back into the air. When the mass dropped two or more times on the system, a wooden supporting system caught the mass and prevented damages on the confining pipe and the clamps on the pad. After a few seconds, vibrations damped out and the magnetic tape recorder was stopped and played back. The tape containing the test data recording will be referred to as "Analog Tape" hereafter.

During the play back, the output of each channel of the magnetic tape recorder was connected to a storage oscilloscope (Appendix IV, paragraph 4.2) one at a time (Fig. 23). The voice channel reproduced the time of countdown, the click of the release mechanism and the impact strike.

Just prior to impact, the oscilloscope was manually triggered and the record made in that specific channel was stored on the screen of the scope. This check was repeated for all tests in every channel. If for some reason the instruments had malfunctioned or the gages were broken or the gain set in the instrument amplifier was not the correct one, the test was repeated, if the specimen had not failed totally by that time.

2.4. Data Reduction

2.4.1. General. The readings recorded on the magnetic tape were in analog form and represented the time history of the output voltage of the measuring devices. Since these readings could not be reduced directly by the digital computer the next step was to digitize or periodically sample the analog test tapes.

2.4.2. Digitizing of the Analog Tape. The analog form of test readings contained in tapes were digitized using the XDS 930 computer of the Engineering College of The University of Texas (Fig. 30). Recorded on the analog tape the information represented a continuous record which needed to be sampled at certain time intervals so that the test could be regarded as a collection of a finite number of measurements at certain times rather than be continuous and infinite. Furthermore, each of these finite numbers of data had to be a number rather than a voltage. This sampling (chopping of continuous data at time intervals) and the conversion of voltage to a representative numeric value was done by the XDS 930 computer. Based on the response of the instruments used during the testing and recording, the time interval between samples was chosen to be one millisecond. Since the test data were recorded either on 4 or on 6 channels simultaneously, the computer had to be also fast enough to recognize these 4 or 6 values, convert them to numbers, and store these numbers on the digitized tape before the second part of the data in the next time interval arrives. The choice of millisecond satisfied this restriction on computer capability.

Schematic description of the digitizing stage is shown in Fig. 30. Each of the output channels of the recorder before entering the computer was connected to a transistor type filter (Figs. 31 and 32) to get rid of noise above 90 hertz. Although all cables during the test were shielded and the cable connections were grounded, the recorder and electronic noise in the near surroundings were enough to produce noise which was also recorded on the tape. The early trials showed that no further data analyses would have been possible without filtering the tape information during digitizing. In order to digitize at certain intervals of time, pulses had to be sent to the computer by a pulse generator. An electronic time counter was used to monitor the frequency of the pulse generator (Figs. 30 and 32), thereby allowing exact adjustment of the sampling frequency. Both counter and the pulse generator needed 30 minutes of warm-up time so that the time interval of one millisecond was constant during digitizing.

First the digitizing program was loaded to the XDS 930 for the digitizing process to begin. Depending upon the availability of the units of the computer either the card reader or magnetic tape or the paper tape unit was used for this purpose. This program produced a file on the digitized tape for each drop test. The file consisted of its name and four records (two seconds) of digitized data for that test. The file name was in code which specified to which test the data belonged and how many channels had been recorded. It further specified the number of records in which the data was stored and the number of data samples which were in each record. All this information was fed to the computer through its teletypewriter unit (Figs. 29 to 33) and the program prepared from this the corresponding coded file name or title and put it onto the tape. So the computer was ready to digitize the data. The analog data was played back by the same magnetic tape recorder used during the tests (Fig. 32). From the loudspeaker of the recorder the countdown time prior to the drop weight release, and the contact of the drop mass could be heard. Before each drop, the tape was listened to for a better orientation. On the next run of the tape the sense switch on the computer command console (Fig. 29) was set just before the mass hit the specimen.

Setting the sense switch initiated the digitizing of 2000 values or two seconds of each channel. After a few seconds, the first 500 points or one half-second of data for the first channel appeared on the scope display of the XDS 930 computer. By switching the specified sense switch on the command console, the data in each channel were viewed sequentially on the scope. Each time the picture on the scope was replaced by the next one (Fig. 29). The data was stored on the tape in digital form in the records of that file and the line printer of the computer printed the same values on the paper.

The tapes produced on the XDS 930 by digitizing the information from the analog tapes will be referred to as "Digital Tapes" hereafter (Fig. 30). In four steps (or records) 2000 values of data for each channel were stored in each file. Since the beginning of digitizing was rather arbitrary, the scope pictures assured that the initial impact time was not missed (Fig. 29). If it was missed, the same digitizing was repeated easily. In all the tests, the time between the instant of first impact and the end of the rebound period was less than 100 millisecond. A span of time of 2000 milliseconds was long enough to damp out the vibrations caused by the impact. The concern of the test was only the first 100 millisecond period after the initiation of the impact. Prior to this period, the mass was just released and falling. After this period the mass fell a second or more times on the specimen from the rebound uplift. Therefore, it was again a relatively uninteresting period.

2.4.3. Reduction of the Digitized Tape. Due to reasons mentioned above, only five percent of the information on the digitized tape describes the impact response of the specimen tested. The rest was relatively unimportant. In the early stages of the work a program was written for CDC 6600 computer of The University of Texas at Austin to reduce and to analyze the entire test data in one step. However this could not be done as it was impossible to detect the beginning of each test using the same criteria. To detect the beginning the program which calculated arithmetic means and standard deviations of every 25 of 2000 data points and the first standard deviation value higher than a set one was hardly

satisfied. If for some reason a noise with high amplitude passed the filter during digitizing, the program tried to evaluate this instance as the beginning, and consequently other program mistakes occurred and the program stopped. Furthermore, unnecessary data on the tape required a big storage in the core of the computer during analyzing so that the run priority of the program was reduced. Therefore, it was decided to reduce data by XDS 930 computer, observing the test information on its scope and storing only the important part of the test on a new tape. A Fortran program handling a similar reduction of biomedical test data was used for this purpose. The schematic description of the capabilities of the program is shown in Fig. 33. The program written for the XDS 930 computer accomplished the following:

(1) To read the title of the file and analyze from it the name of the test, the number of channels, and the number of points that were stored thereafter.

(2) To read the data for all channels from the primary digitized tape and sort them continuously for every channel. In the original digitized tape, information was stored 500 points for all channels in four consecutive orders.

(3) Since the program was also capable of reducing 60 cycle noise mathematically using some fourier transforms, there was a choice as to which of the channels would be the reference channel.

(4) When desired, the first 500 points of the reference channel could be displayed on the screen of the scope.

(5) The picture on the scope could be shifted with any steps of points in either right or left direction (Fig. 29). By this great flexibility of the program, the beginning and the end of the test period could visually be detected on the scope. Upon adjusting the beginning point to the far left of the scope, the right side of the function could be stretched or compressed against the origin. In other words, by fixing the origin of the function on the scope, the number of samples of the data on the scope display could be increased or decreased at any desired rate. In this study, it was decided to plot on the screen altogether 130 points of which the first 100 belonged to the beginning of the test from the instant the drop weight struck the specimen. Between 101 to 110 it was blank, and the last 20 points belonged to the points between 1981 and 2000 milliseconds

in the original digitized tape. This last part is plotted only to see how the measuring device behaved two seconds after the instant of switch set at the digitizing stage. It had more qualitative than quantitative value.

(6) After accepting the display of data on the scope to be valuable for the test results, the data of 130 points stored on a new tape could either be printed on the line printer or plotted on the Calcomp 11 inch paper plot. A great portion of the test was plotted this way by Calcomp while in the meantime data was stored in a new tape. This new tape is used for the final analysis and reduction which will be explained in the next chapter. These final tapes will be referred to as "Reduced Digital Tapes."

2.4.4. Analysis of the Reduced Digital Tape.

2.4.4.1. General. The final analysis of the test data was carried out in several steps on the CDC 6600 computer of The University of Texas. The main task was to evaluate the measured and recorded test results. The reduced digital tape produced on XDS 930 computer was the primary input. Another input source of the program was the cards for each test, containing information such as the identification number and the date of the test, how many channels of the recorder were registered, the type of specimen (closed or serrated, single, three or four ribs), coded names for every instrument in the order of channel numbers, date on which cushioning material was produced, how much it crushed during impact, what was the weight of the cushioning cylinder just before the test, and which of the program options (like printing, plotting or on tape storing of parts or whole analyzed information) should be executed for each test.

Paragraph 2.4.4.2 describes the capabilities of the Fortran program used as first stage evaluation of the test data. Analyzed information in the first stage was stored on another tape which will be referred to later as the "Analyzed Tape." The information on this tape was the final results of the tests. For further studies, this tape supplied the needed information such as force, displacement, energy, and strain with respect to time. A series of programs were also written to extract information from the analyzed tape, to plot them on graphs or to punch them on cards.

2.4.4.2. Program to Evaluate Test Results from Reduced Digital Tape. The Reduced Digital Tape containing all of the test data was analyzed on the CDC 6600 computer because of its high speed and great storage capacity. A FORTRAN program named "Program Test" was written for this purpose. The main features and the flow diagram of this program are given below. The CDC 6600 computer had been designed for 60 bit word length, whereas the XDS 930 computer, which prepared the reduced tape 12 bit word length. To be able to work with this tape on CDC 6600 a subprogram called "DCIFER" was used for the appropriate word length conversion.

The main features of the program TEST are as follows:

(1) To analyze the test data from reduced digital tape, one test at a time, but capable of analyzing an unlimited number of tests sequentially. The information related to each test, instrument, and cushioning material was read into the computer from the cards. Following the last test a blank card was used to terminate the program. The program was able to analyze any one of the tests. The only restriction was that the cards had to be in the ascending order with respect to their sequence number; otherwise, the program would stop with corresponding error message. The sequence need not be consecutive. A subprogram called HOPFILE which referred back to DCIFER to find the exact location on the reduced digital tape such that the information read by the card matches the test data on the tape.

(2) The program TEST evaluated the measurements considering the different calibration constants related to each instrument and the different gain switch sets related to each channel. It distinguished the various instrument locations on the specimens, and the different types of specimens. These different distinctions and separations of decisions were achieved by naming the instruments with a code name consisting of five alphanumeric characters. The first character stands for the type of the instrument:

A - Accelerometer

B - Bottom Gage

T - Top Gage

C - Load Cell

D - Displacement Transducers.

The first, second and the third alphanumeric characters specify the individual characteristics of the instruments; for example:

A22 is accelerometer no. 7422

A17 is accelerometer no. 7417

D51 is the first of the transducers with $\pm$ 0.5 in. linear range

D32 is the second of the transducers with $\pm$ 3.0 in. linear range

and likewise for the other 17 devices. The fourth character of the coded name is used to represent the location number of each instrument on the specimen. Location numbers are shown in Fig. 26. In addition to the seven location numbers letters A and B are used to specify the locations of the Load Cell A and Load Cell B. If displacement transducers were attached at 1/4 span length their locations were also designated with A and B referring to the Load Cell along that rib. The last character, an integer form 1-4, represented the gain levels 10, 30, 100, 300, respectively. The subroutine SHIFT1 was used to interpret the coded name to select the desired character or character combinations.

(3) Program TEST converted the voltage output of each instrument to the dimensioned values which they really measured. This program was able to find the maximum magnitudes and how many milliseconds after the beginning of the impact the maximum occurred. The program was capable of giving plots and printed output for force, displacement, support reactions, and strain measurements with respect to time. The combination of force and displacement measurements eliminating the time axis lead to the force-displacement curves for that test. The force displacement relation of the devices at the impact location was used then to calculate the energy time relation as performed by the impacting force while the specimen was deflecting under it. Plots and printed outputs were also available for this relation. The strain measurements were used to compute the strain rate and the stresses. The restricted number of channels did not allow the use of more strain gages. The strain gages were in general parallel to the ribs. On the lower side of the top plate of the specimen between ribs, gages were installed in the lateral direction. The stress calculations of the dynamically loaded specimen were made based on the assumption that steel is a Voigt type visco-elastic material. This assumption allowed the stress calculations to be formulated as

$$\sigma(t) = E\, e(t) + c\, \dot{e}(t)$$

where

$\sigma(t)$ = Stress in ksi at instant (t)

E = Young's Modulus (29.5×10^3 ksi for steel)

$e(t)$ = Strain at instant (t)

$\dot{e}(t)$ = Strain rate/per sec. at instant (t)

c = Coefficient of viscous damping, taken to be $.85 \times 10^4$ from reference 20, page 86.

(4) Program TEST also contained options for printing and plotting of the outputs. The options increased the efficiency of the program in cases such as storing whole test results on a new tape (Analyzed Tape), or punching of the maximum force, work done due to deflection, stress values with the computed parameters related to the drop heights or density of the cushioning material or the crushing percentage of the cushioning, etc. The punched results on the cards were used later in different programs as input for further studies.

The flow diagram of the program is given below:

FLOW DIAGRAM OF THE PROGRAM "TEST"

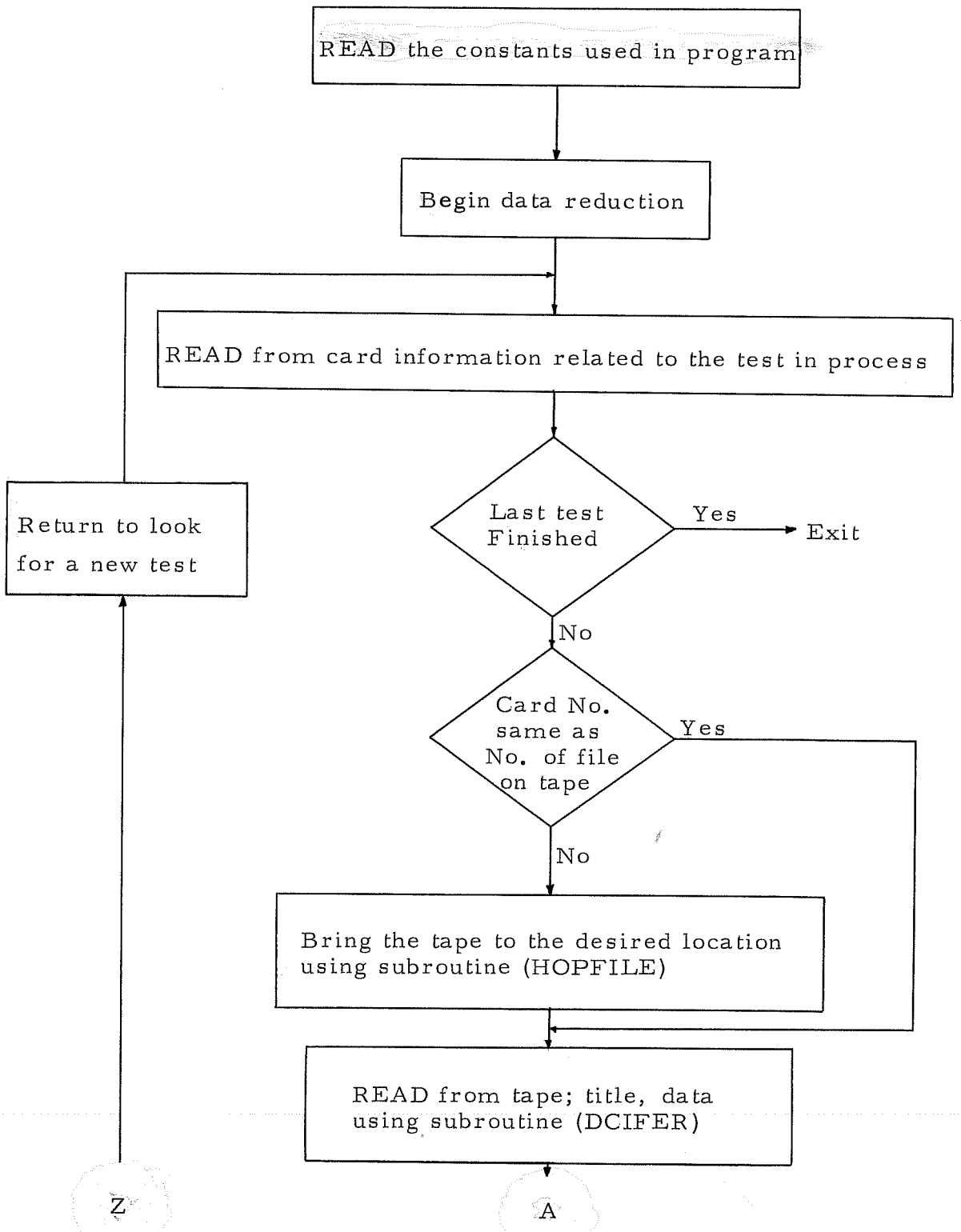

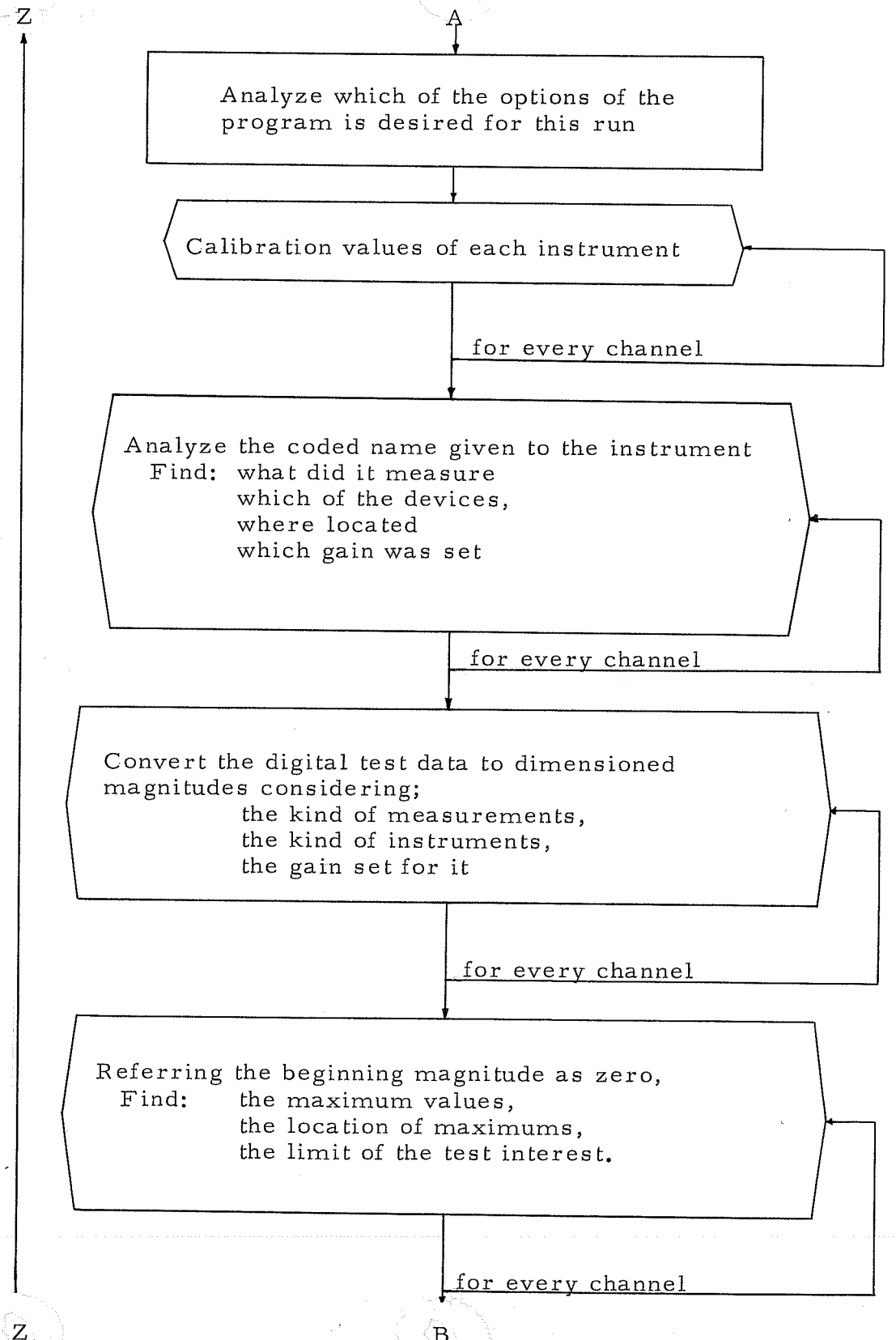
Z
A
Analyze which of the options of the program is desired for this run
Calibration values of each instrument
for every channel
Analyze the coded name given to the instrument
Find: what did it measure
which of the devices,
where located
which gain was set
for every channel
Convert the digital test data to dimensioned magnitudes considering;
the kind of measurements,
the kind of instruments,
the gain set for it
for every channel
Referring the beginning magnitude as zero,
Find: the maximum values,
the location of maximums,
the limit of the test interest.
for every channel
Z
B

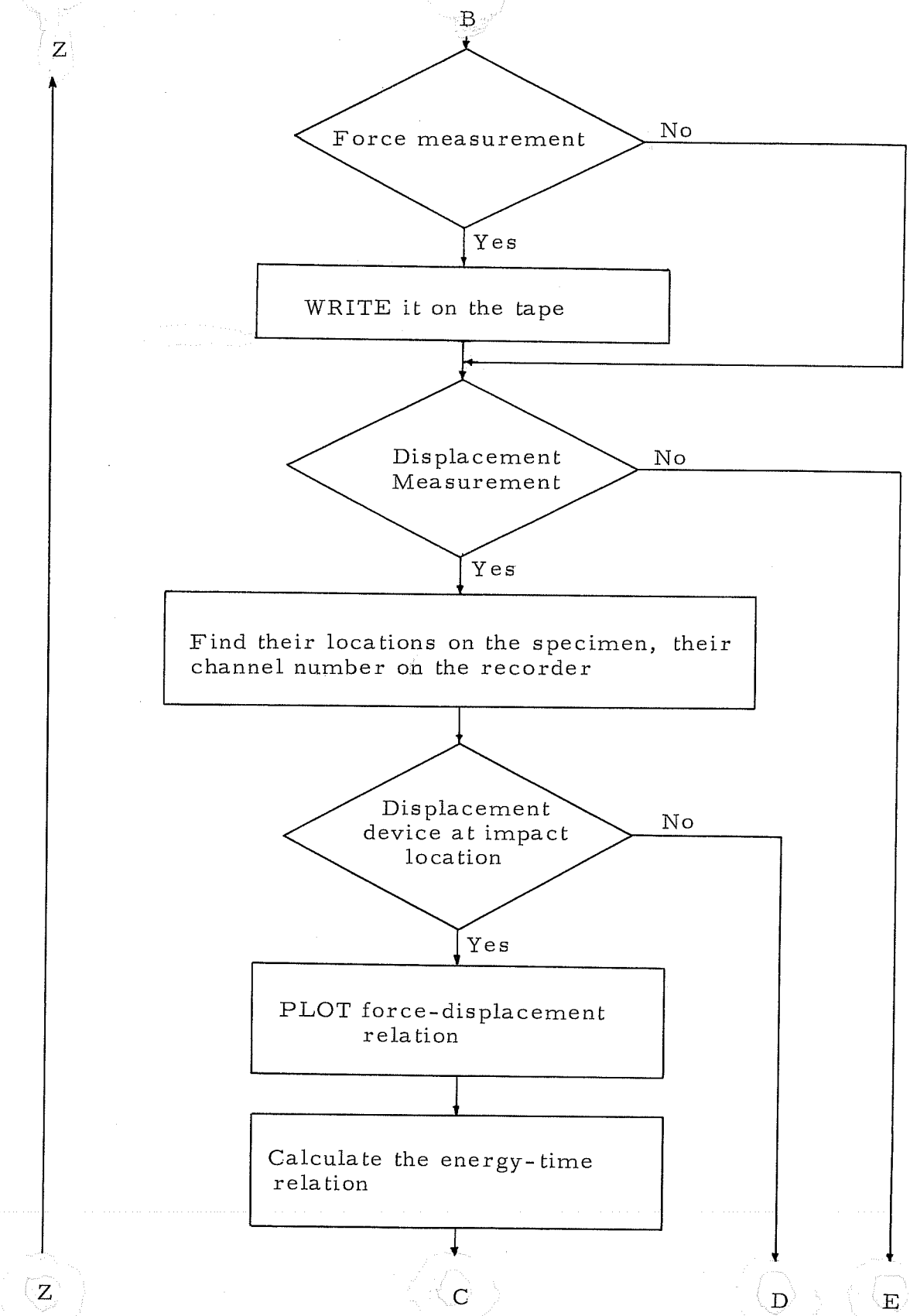
B
Force measurement
No
Yes
WRITE it on the tape
Displacement Measurement
No
Yes
Find their locations on the specimen, their channel number on the recorder
Displacement device at impact location
No
Yes
PLOT force-displacement relation
Calculate the energy-time relation
Z
Z
C
D
E

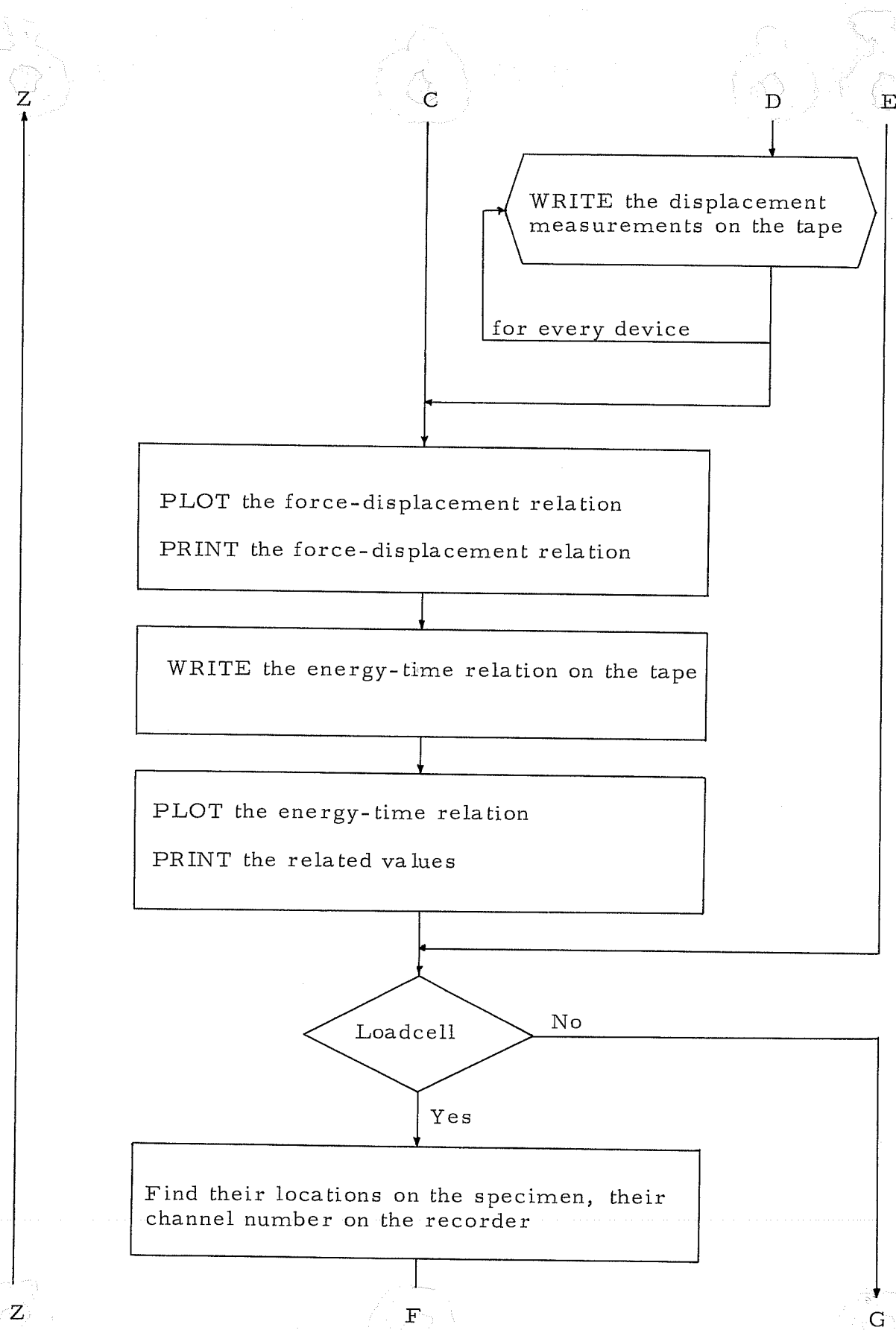
Z
C
D
E
WRITE the displacement measurements on the tape
for every device
PLOT the force-displacement relation
PRINT the force-displacement relation
WRITE the energy-time relation on the tape
PLOT the energy-time relation
PRINT the related values
Loadcell
No
Yes
Find their locations on the specimen, their channel number on the recorder
Z
F
G

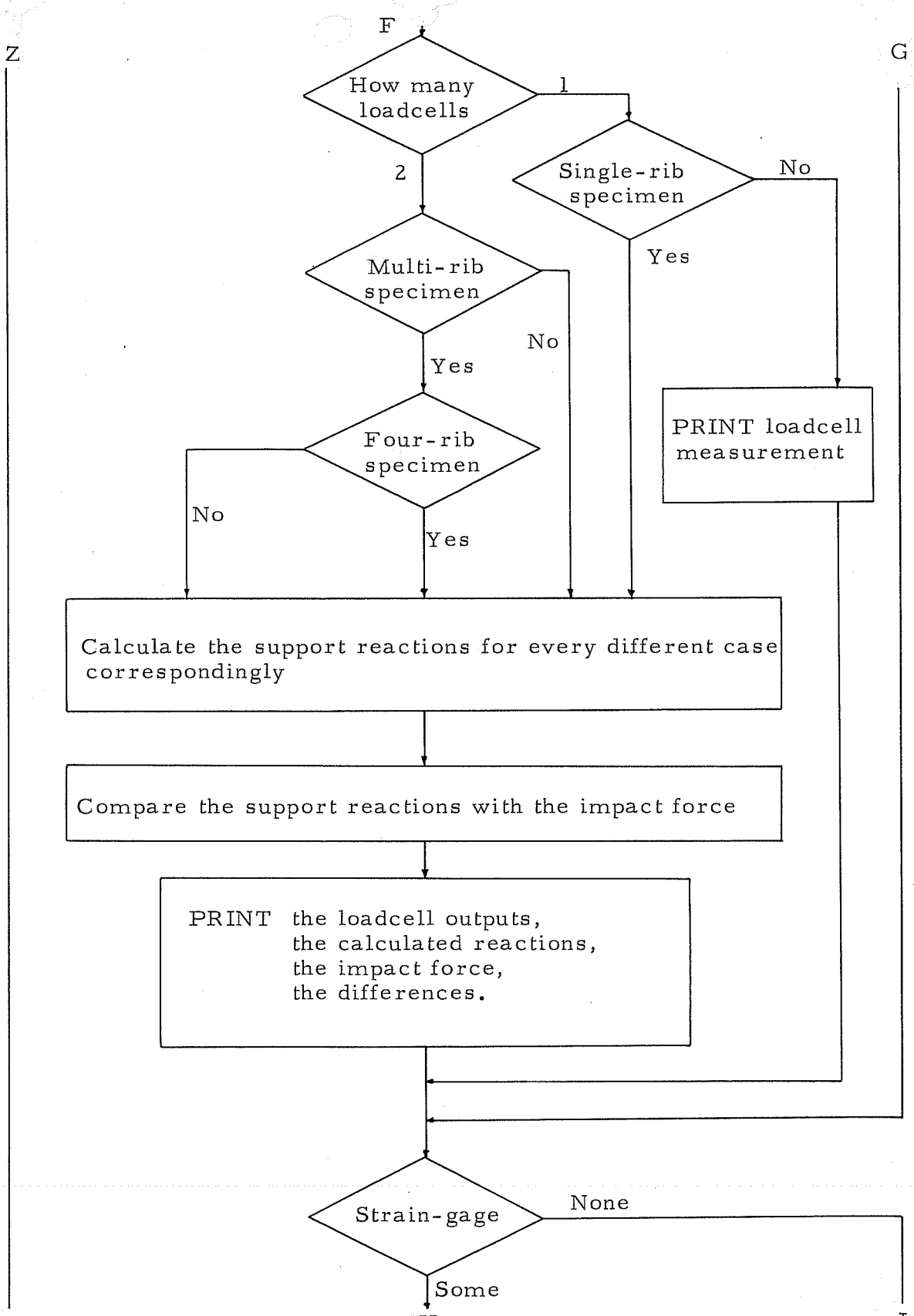
F
Z
G
How many loadcells
1
2
Single-rib specimen
No
Yes
Multi-rib specimen
No
Yes
Four-rib specimen
No
Yes
PRINT loadcell measurement
Calculate the support reactions for every different case correspondingly
Compare the support reactions with the impact force
PRINT the loadcell outputs,
the calculated reactions,
the impact force,
the differences.
Strain-gage
None
Some
Z
H
I

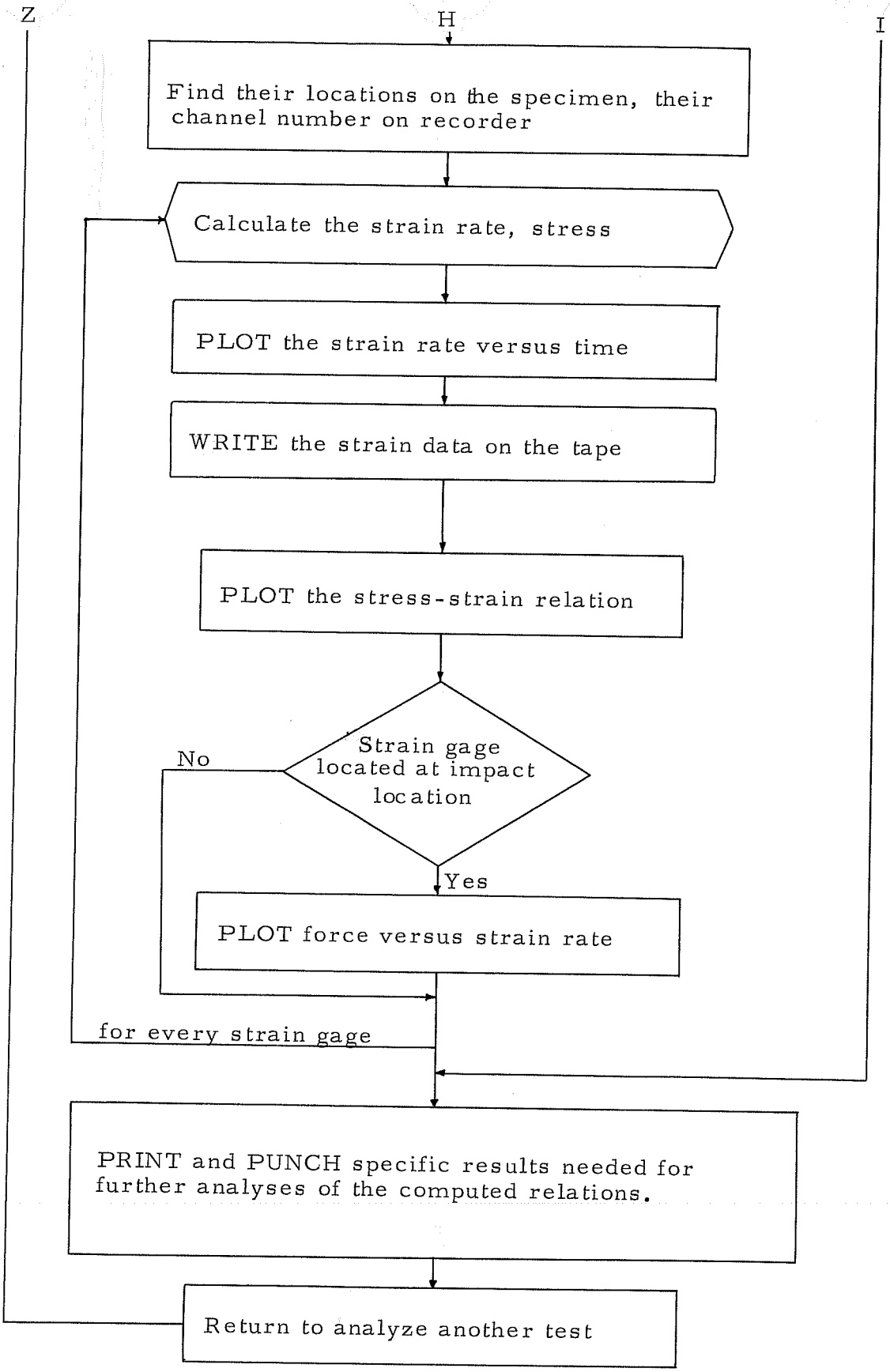
Z
H
I
Find their locations on the specimen, their channel number on recorder
Calculate the strain rate, stress
PLOT the strain rate versus time
WRITE the strain data on the tape
PLOT the stress-strain relation
Strain gage located at impact location
No
Yes
PLOT force versus strain rate
for every strain gage
PRINT and PUNCH specific results needed for further analyses of the computed relations.
Return to analyze another test

2.4.4.3. Extraction of Information from the Analyzed Tape. Several programs, each with different purposes, were written to extract the information from the analyzed tape. Although one longer program could serve for the same purpose, these were written separate and independent to minimize the time to develop them.

The programs were used to obtain the following relationships:

(1) Force/Time
(2) Force/Displacement
(3) Force/Energy
(4) Stress/Time

The programs served mainly to read certain parts of the analyzed tape, to combine or compare the findings, and plot and/or print or punch the desired information. If the instruments functioned well during the experiments and there was no partial saturation of the input, or if no data input mistakes were made, then the "Program Test" analyzed the specific test and also stored the results on the analyzed tape.

However, if there were no data available, no storing could take place on the tape at that test, and at that part of the test a special remark was made in the corresponding file. To avoid the uncertainty in reading back the analyzed tape, precautions were already taken by the "Program Write Tape" abbreviated as WRTP. For each test, whether it could be analyzed or not, one file with a file number was reserved on the tape. The sequence of the file numbers was the same as the number of the test. Each file was composed of records. Each record contained the following information.

(a) File Number
(b) Record Number
(c) Yes or No (according to whether the data were to be stored or not)
(d) If "Yes", how many data points were stored,
(e) The code indicating the instrument and its location on the specimen,
(f) The final test results.

In the extraction programs, the same questions were asked to determine for each test which instrument did or did not measure and what was measured. Accordingly, proper records of the desired files were written on the tape, and later read to plot the analyzed data.

Each program had further features and options. For example, one could write the appropriate labels of the plots or draw the cross section of the specimen used in that particular test. Besides the non-changing parts of the labels, there were parts like the abbreviated names given to each different specimen, the drop height from which the impact mass was released, the impact velocity of the mass as calculated from the drop height, the test number, the location of impact, the locations of the instruments which registered the plotted data. The computer program used the component parts of the label to decide which options were to be executed. The drawing of the cross section with the location numbers on it was performed by the subroutine "DRWSEC--draw sections", after recognizing the name of the specimen which specified type of specimen.

Each graph was also labeled with the location numbers of the data measuring instruments. The location of the label itself on the plot needed to be arranged in the proper manner by the computer program. This task was especially important when the data of more than one instrument had to be drawn on the same plot as it was the case of some of the Force/Deflection Relation plots of the multi-rib specimen.

In the case of the Force/Time Relation, there were two slightly different programs written; one to plot the relation in Calcomp graphical units of computer, and the other to obtain punched data cards acceptable for the Dynamic Beam Column Program. This program was used to calculate the displacements of the impacted beam for a given forcing function. The punched data cards supplied this theoretical method a direct and non-imaginary forcing function.

Flow diagrams or printed copies of the data extraction programs are not included.

CHAPTER III

TEST RESULTS

3.1. General

The procedure involved in recording, reducing, analyzing and representing the data obtained throughout the test has been explained in previous chapters. This chapter is devoted to discuss the findings, which are presented in form of tables and figures. The test results obtained by the measurement of force, displacements, and strains are in general very satisfactory when their trend and magnitudes are qualitatively compared with those obtained in static tests (6). The methods and devices applied to measure the force, displacement, and strain quantities were essentially different from each other in static and impact cases. In a few tests, some of the instruments malfunctioned and naturally it was not possible to obtain any data in those cases. The load cell measurements did not give any representable results. Therefore, there will not be any discussion about the support reactions in connection with the different specimens or impacting force.

The data measurements are categorized in the following manner:

force/time relation
force/deflection relation
force/energy relation
stress/time relation

Each of these relations will be discussed in the following paragraphs.

3.2. Force/Time Relation

The impact force acting on the specimen was obtained from the accelerometer/time records. A Statham accelerometer having an operating range of $\pm$ 500 g was used for measuring impact deceleration. Information about the accelerometer characteristics is given in

Appendix IV, paragraph IV. 7. The accelerometer was rigidly bolted to the top of the impinging mass which was dropped on the specimen from different heights. The weight of the cushioning and plunger assembly was almost 1/40th of the weight of the impinging mass. The effective impact force on the specimen was assumed to be approximately equal to the force obtained from the deceleration measurements, neglecting thereby the effect of the cushioning mass.

The analysis of the acceleration/time record yielded a computer plot for each test. Typical plots showing the force/time relation of each specimen were gathered in one figure. Figure 34 was prepared for the closed single-rib specimen. Figures 35 and 36 correspond to serrated single rib, Fig. 37 for closed three rib, Fig. 38 for serrated three rib, Fig. 39 for closed four rib, and finally Fig. 40 for serrated four rib specimens.

Each figure indicates the changes of the pulse, its amplitude and impact duration for different test for the specimen. The force/time relations differed slightly even for two subsequent drops from the same height, on the same specimen. This was mainly due to differences in cushioning materials. Another reason for the changes in the pulse was due to superposition of the vibration modes of the impacting system and the measurements of deceleration. Although an electronic filter was used during digitizing to filter noises above 90 Hertz, the force/time plots showed the existence of 80-85 Hertz noise (Figs. 35 to 40, also Fig. 43). This frequency seemed to be the natural frequency of the complicated mass system. The acceleration/time curves showed free vibrations during digitizing with 12-13 milliseconds period following the first impact pulse. The vibration of the arms and other parts of the mass was consistent and was the same throughout the tests. Its effect on the measured force was minor in low impact test and diminished even in high impact tests when the force became comparatively larger.

It is interesting to note in Figs. 35 to 40 that the force amplitude in the low impact tests, (with drop height less than 30 in.) did not vary greatly for different specimen groups. Maximum force remained about

20 kips. The shape of the pulse was nearly half sinusoidal or even flatter becoming almost trapezoidal. The rise time was between 4 and 7 milliseconds. The maximum impact force seemed to happen after 30-35 milliseconds followed by a relatively long decay time.

When drop height of the impinging mass was increased the pulse shape became parabolic and for very high drops it became triangular especially on closed rib specimens (Figs. 34, 37 and 39). The ultimate tests showed that the maximum impact force carried was greatly different among the closed rib specimens. The serrated single rib specimens kept their quasi half sinusoidal form of force/time relation during the failure stage. Failure criteria in this study were excessive deformation for the closed rib specimen and buckling for the serrated rib specimen. When the specimen was unable to withstand further impact loading, it was considered to have failed. The pulse shape for ultimately loaded serrated multi-rib specimens was triangular, similar to the closed rib specimens.

Observed changes in impact duration from one test to another were negligible. For most of the tests, the impact duration was about 60 milliseconds. The measured maximum impact force in the impact duration of T could be used for the comparison of test results. However, the impulse $I = \int P_i(t)dt$ and a mean impact force $P_{mean} = I/T$ were considered as better measure for the comparison.

The summary of the force/time relations on different specimens, grouped according to the rib numbers and serrations are given in Tables 6 through 9. The instant and the magnitude of the maximum impact force, the Impulse I, the impact duration T and the mean impact force mean P_i are given in these tables. The test number, location of the impact (see Fig. 28), the drop height of the impinging mass, and its initial impact velocities are also listed in the tables.

Tables 6 and 7 contain the test results of the closed single rib and serrated single rib specimens respectively. Similarly in Tables 8 and 9 summary of the force/time relations of closed and serrated three rib specimens and of closed and serrated four rib specimens are cited. These tables are intended to show only the most

important information related to the force/time relations. The summarized information was obtained from the printed computer outputs of the tests. Since no prediction could be made prior to tests regarding the drop which will fail the test specimen, the drop height was increased rather arbitrarily according to the experience obtained from the earlier tests. The impact force or impulse values presented in the tables show the increasing trend as influenced by the increase of drop heights.

For easy comparison the ultimate test results of tables 6 to 9 are combined in Table 10 in which also the ultimate static loading capacity of different specimens are given.

It is seen here that the maximum impact forces were well above the static ultimate values and the calculated mean impact forces were slightly below. The type of the observed failure of the specimen was also mentioned in this table. There was no closed multi-rib specimen tested under static loads (6). Using the values of Table 10 and referring to the capacities of the single rib specimen to be 100 percent, the relative capacities of the multi-rib specimens were calculated. Table 11 contains comparisons of mean, and maximum impact forces, and of static ultimate load. For example, considering the maximum impact force obtained for serrated single rib specimen be 100 percent, the maximum force of serrated three rib specimen was 450 percent and of serrated four rib specimen 720 percent. Similar comparison was given for closed rib specimens as 100, 463, and 195 percent. The last value pertaining to the four rib specimen should be disregarded. The ultimate capacity reached in this specimen was lower than that expected. This was due to yielding in rib 3 during previous low impact tests. In Test No. 157 propagation of yielding was faster when the mass was dropped from a height of 552 in. The specimen did not fail thereafter and withstood three further high drop impacts, during which no data could be registered.

In the lower section of Table 11 comparisons of mean, maximum impact force and of static ultimate load were made to express the capacities of the closed rib specimens in terms of the serrated ones.

In general, closed rib specimens had more capacity than the serrated rib specimens. The maximum impact force sustained by closed single rib specimens was 3.58 times that of the serrated ones. Similarly, closed three rib specimen endured 3.70 times greater impact force than the serrated three rib specimen. The closed four rib specimen could not be compared with the serrated four rib specimens for the same reason given in the last paragraph.

The first part of Table 11 is graphically shown in Fig. 41. The relative capacities of the specimens are given in the ordinate and the abcissa indicated the rib numbers. There were no two rib specimens tested. The graph did not aim to represent a continuous relation between the ordinate and the abcissa. The values for single, three or four ribs were just connected by straight lines to indicate the trend. The capacity of the closed four rib specimen, as given in Table 10, is excluded from Fig. 41. The value obtained from Test No. 157 (Table 10) would be misleading and hence the expected trend is marked in Fig. 41 by dotted line.

In Fig. 42 the impulse for various specimens obtained from ultimate impact tests (Table 10) is shown. From this figure it can be seen that the closed three rib specimen can endure 3.46 times more impulse than the closed single rib element. In the serrated rib specimens, the impulse was almost linearly increasing with the number of the ribs. However, when the impulse of any closed rib specimen was compared with the impulse of the corresponding serrated rib specimen, the values of the closed rib specimen were 3 to 4 times greater than those of the serrated ones.

The study of the above cited comparison revealed the following facts:

(1) Multi-rib specimens endured more force than the summation of the individual capacity of each rib (Fig. 41), both in static and in impact loading.

(2) The rate of increase of impact force capacities was higher in closed rib specimens when compared with that of serrated rib specimens.

(3) Calculated mean impact force from the impulse was in general smaller than the corresponding static ultimate (Table 10).

(4) The closed rib specimens, either single or multiple rib, were all very efficient in load carrying compared to the equivalent serrated rib specimens (Table 11). This will be discussed again in the sections 3.3. and 3.4.

(5) The impulse values obtained from ultimate impact tests were 3 to 4 times higher for closed rib specimens when they were compared with the impulse of serrated ones (Fig. 42).

(6) The impulse rate in serrated rib specimens was almost linear with the number of ribs (Fig. 42).

(7) For closed rib specimens, impulse rate was higher than that for serrated ones.

3.3. Force/Deflection Relation

3.3.1. Experimental Findings. Force/deflection relation was established from the time dependent force and displacement measurements, eliminating the time axis. Force/time relation was discussed in the previous paragraph indicating the existence of the vibration of the mass system on the force recordings. Because of practical reasons any further smoothing of the curve was not undertaken except the filtering of frequencies above 90 Hertz as data were digitized. By this it was accepted that the possible error in force measurements would be within the usual limits of engineering accuracy. The displacement/time records were smooth, but delayed only 2-3 milliseconds behind the force records. The delay was assumed to occur due to cushioning.

Similar smooth records were also obtained in strain measurements. In both displacement and strain records the free vibration of the test specimen following the first impact had a natural period of around 20 milliseconds. This value did vary in different tests on different specimens between 18 and 21 milliseconds. Neither the number of ribs nor the serrations seemed to have great effect upon the natural frequencies. The natural frequencies of a beam with the geometric

properties of closed and serrated single rib specimens were also calculated for comparison (Table 12). If the beam mass was assumed to be concentrated at the center of the simple supported beam, the natural period of closed rib case was found to be 27 milliseconds and of serrated one 26 milliseconds. With uniformly distributed mass over the span, the calculated natural period was closer to that observed, 22 and 21 milliseconds for closed and serrated rib specimens respectively. The values calculated on the basis of half of the beam mass concentrated at the center of simply supported beam and total mass on the center of the fixed end beam were much lower than the natural periods of specimens observed.

In Fig. 43 the force/time and displacement/time records of Test No. 6 are shown in dotted lines. The delay between two records is also marked. It appears in this figure as if the maximum displacement happened 8 milliseconds prior to the force reached its maximum, which was not true in reality. The force could not increase when the specimen rebounded already. The error in predicting the instant of maximum force due to vibration of the mass was mentioned in the discussion of force/time relation. In Fig. 43 the force/time curve is smoothed out as a continuous line, which also shifted the instant of maximum force value to the instant of maximum displacement. The force/displacement relations from the recorded and smoothed force/time relation are shown in Fig. 44.

A computer program was written on Calcomp plotting units of the Computation Center of The University of Texas to plot force/deflection relation from the recorded force and displacement relations. Typical examples of plots are shown in Figs. 45 and 46. Other examples are given in Appendix I. In the same appendix some of the test characteristics related to or derived from the force/deflection relation are presented for each test in tabular form and in plots. These tables contain information such as test number, drop height, impact velocity, impact force, displacement at certain locations with the time in milliseconds relative to the first contact, attained energy at that time

and the total duration of impact. Impact duration for the tests on multi-rib specimens is not included in these tables.

From the force/displacement plots, it is possible to distinguish three different groups of force/deflection relations:

(1) Plots indicating the elastic behavior of the specimen
(2) Plots showing partial yielding
(3) Plots with the total failure of the specimen after ultimate tests.

The first group of plots is omitted in the present study due to the shift of maximum displacement instant prior to the instant of maximum force. The second group of plots indicated that the maximum force was reached prior to maximum displacement (Fig. 45). These plots were obtained from the high impact test results. As mentioned in force/time relation (paragraph 3.2), the relative effect of vibration of the mass system on the force measurements, was less for the high drop tests. The plots indicated the initiation of local yielding at the maximum impact force which decreased and soon after rebound followed. A permanent deflection was observed when the force value dropped to zero. A second group of force deflection curves was obtained when the specimens were impacted with moderate impact velocities. Low, moderate, and high impact velocities were relative quantities and differed according to the specimen. The initial impact velocity and the drop height of the mass was included in the top line of each calcomp plot. The value of the remaining deflection due to yielding, changed with the magnitude of the initial impact velocity which in turn controlled the acting impact force on the specimen.

Second group of plots compared to the third group of plots indicated clearly the reserve strength of the specimen beyond local yielding. This can be seen by comparing the force/displacement relations obtained through the consecutive test numbers 89, 90, 91 or in test numbers 154, 155, 157, 158 (Tables 13 and 15).

The third group of plots indicates the total failure of specimen when the impact force gradually decrease and the displacement continued

to increase for a much longer period of time than needed to reach maximum force value (Fig. 46). The highlights of the tests for important drops are presented in Tables 13 through 16. Table 13 corresponds to three rib specimen and Table 14 pertains to the serrated three rib specimen. Tables 15 and 16 indicate the highlights of the tests of closed and serrated four rib specimens respectively. Information for single rib specimen is given in "test characteristics tables" in Appendix I preceding the plots of the force/deflection relations.

With the help of Tables 13 through 16 and also of the deflection measurements taken by dial gages before and after the tests, the deflected shape of the specimens were obtained (Figs. 47 through 55). The deflection of the specimens was measured as the vertical distance from the original horizontal position to the top of the deck plate. These measurements were accurate only to within 1/16 of an inch.

The deflected shape of the specimens after total failure was reproduced along at least three lines as indicated on a section drawing in the deflection figures. There were also marked static and impact deflections at important instants of some tests (Figs. 47 through 55). The impact forces at those instants or static loads were also shown there. In some of the tests the load distribution pad may have been placed (especially in static tests) at 90 degree rotated position. These cases were indicated with explanatory asterisks.

In addition to the above deflection figures, there were figures for the multi-rib specimens to show their deformed midspan section during impact (Figs. 56 through 60). On each of these figures there was also a small sketch indicating the impact location by an arrow with the maximum impact force (in kips) reached in that test. The test number and drop height of the mass are also included in the sketch.

In Figs. 56 through 60 there are two deflection curves for one test to show the difference between the maximum impact deflection during the test and the shape of the section just after the test. In all of these figures the deflection of the section could only be qualitatively drawn since deflection measurements during impact was limited to the

number of devices and of the recording channels. The actual shape of the specimens after or during the tests can be seen in several photographs taken during the experiments (Figs. 74 through 86).

The static deflection of midspan section of serrated multi-rib specimens (6) were drawn in Figs. 56 through 60, together with the deflected shape of similar specimen under impact. These figures allowed to obtain general ideas on the responses of the identical specimens under static and impact loads. Figure 61 shows the response of the serrated three rib specimen. The deflections of the serrated four rib specimen in three different tests are shown in Figs. 62 and 63. In these figures, at some deflection levels, the static and impact forces, the instant in millisecond after the impact and the attained energy in (kips. in.) are also included.

Since imperfections and eccentricities greatly influence the initiation of buckling, it is hard to establish a general statement from these figures about whether buckling occurs earlier under static or under impact loads. Further one test result contradicted the other, and the exact shape of the deck plate just prior to buckling had not been measured. Buckling initiated usually over the serrations closer to the free edge of the specimen and propagated inwards. Determination of the instant buckling occurred in impact tests was based on force/time and displacement/time measurements. The computer outputs were carefully studied for the test during which the actual buckling was observed. At the instant of buckling the force magnitude sharply decreased and displacement values rapidly increased.

In the serrated three rib specimen, buckling under static load occurred when the central deflection was about 2 inches and at the instant of buckling under impact load the specimen had almost 3.5 inches deflection (Fig. 61). In the serrated four rib specimen buckling seemed to occur in both cases at around 2 inches of deflection (Figs. 55 and 62). In serrated single rib specimens the deflections at which buckling occurs were different for static and for impact loading (Figs. 48, 49, 64, and 65).

Serrated rib specimens seemed to be sensitive to buckling, especially when the impact force was concentrated in a small area. Preliminary tests conducted without the load distributing steel pad, showed that buckling of the deck plate occurred earlier because of local deformation just under the cushion. For example in one of the preliminary tests the serrated single rib specimen buckled even when the impact mass was dropped from only a 10 in. height.

However, in later tests with a load distribution pad it was observed that specimen SR-1-1 buckled when impacted from 120 in. height (Test No. 48) and specimen SR-1-2 buckled when impacted from 36 in. height (Test No. 66).

On the other hand, for a closed single rib specimen even without a load distribution pad there was no problem of buckling except locally when impacted with a very high impact velocity. If the serrated single rib element was impacted without the load distribution pad at impact location, buckling occurred at the center serration. Otherwise the buckling location was shifted to a serration closest to one of the edges of the load distributing pad. This again indicated the effect of force concentration upon buckling and also upon the total impact behavior of the orthotropic steel plates with biserrated ribs.

In Appendix I there is a qualitative comparison of impact and static load displacements for the serrated three rib specimens of Test No. 97 and 98. Any deflection comparison for the closed multi-rib specimen is not available since no closed multi-rib specimen was tested statically.

The static load-deflection curves of Reference (6) are drawn together with the impact force/displacement relations (Figs. 64 through 67) obtained in Test Nos. 18, 62, 105, and 120. Figure 64 corresponds to closed single rib specimens. The yield and predicted ultimate loads are marked on the static load displacement curve. These loads are also marked in Fig. 65 which shows the characteristics of the serrated single rib specimen. As seen in Figs. 66 and 67 corresponding to serrated three and four rib specimens, the ultimate impact forces were much higher than the static ultimate values.

Table 17 was prepared for a better comparison of impact and static forces when the specimen had reached a certain deflection during the tests. The L/400 and L/200 of the span were considered arbitrarily to be the specified deflection values for this comparison which resulted to 0.3 and 0.6 inches respectively. In Table 17, the test number, mean impact force, impact location and the initial impact velocity are included. Furthermore asterisks are used to indicate whether the specimen yielded or failed during that impact. Within the L/400 deflection limit only Test No. 132 showed yielding of SR-4 (serrated four rib) specimen. Due to larger inertia, the multi-rib specimens needed higher impact velocity on the impinging mass to reach the same deflection as the single rib specimen. In Test No. 132 the high impact velocity caused high impact force and yielding occurred.

The specified deflection limit L/200 seemed to be more critical to reach for the majority of the specimens, without yielding. All of the serrated multi-rib specimens (Test Nos. 105, 89 and 120) had yielded and the specimens in the last two have buckled under impact. The maximum impact force at this instant (L/200 deflection) were almost 80 percent higher than the static load. The static test results (6) of both serrated and closed single rib specimens showed yielding within L/200 deflection range. There was practically no difference in static loads to yield the serrated or closed single rib specimens (static P_y = 11.2 kips at 0.44 in. deflection of closed single rib specimen and static P_y = 10.6 kips at 0.54 in. deflection of serrated single rib specimen).

Both in closed and in serrated single rib specimens yielding due to impact occurred at the same midspan deflection, but the force required to deflect the closed rib specimen was about 53 percent more than that required to deflect the serrated rib specimen. This indicates the superiority of the closed rib specimen under impact as compared to the serrated one. Maximum impact force for the serrated single rib specimen was 20 percent more than the static load and for closed rib 40 percent more. The single rib specimen did not yield when impacted to deflect as much as the specified value L/200 = 0.6 in. (Figs. 64 and 65).

Specimen CL-1-1 deflected 2.49 inches when first yield sign appeared and at that instant the impact force was P_i = 30.4 kips (Test No. 25 in Fig. 47). Serrated single rib specimen SR-1-1 deflected 2.67 inches as yielding initiated when P_i = 19.8 kips (Test No. 50 in Fig. 49).

A general relative comparison of the static and impact response of the specimens is shown in Fig. 68. The static test results are shown by the dashed lines and impact tests are drawn by solid lines. The figure was prepared using the force/displacement relations of ultimately loaded static and impact tests. The impacted specimens were declared as failed during these tests, except the two marked by asterisks in Fig. 68 (C1-4-1 and SR-1-1). These two specimens did not reach higher impact loads since they yielded and therefore they should not be included in conclusive decisions. Figure 68 also shows that the closed rib specimens are efficient compared to the serrated specimens during impact. Static ultimate loads required more deflections than the maximum impact forces. The straight lines in Fig. 68 were just used to connect the ultimate load locations on the graph with the origin. It naturally did not show the actual force/deflection relations. This was merely used as a simplified way of representing the immense data obtained.

3.3.2. Theoretical Considerations. There exist theoretical methods to predict the displacements, moments, shears, and stresses when the beam or plate is impacted. In almost all of these studies the specimen was assumed to have a solid cross section in contrast to the test specimens of this study. In addition, the striking mass of these studies had either no defined shape when assumed acting like a point load or was spherical when the contact force between the impacting mass and the specimen was taken into consideration. The specimen was idealized either by a single spring system in its simplest form or consisted of lumped masses with many degrees of freedom when the method was developed for the use of computers. Most of the methods treat the problem like the force vibration of an elastic system.

The main difference among these approaches was in the solution of the differential equation for the forced vibration problem. The

assumptions, the representation of the forcing function, and the solution of the equation along the time axis and also along the geometric axes of the system were the important parts of these works. Analytical studies were also performed to predict the plastic deformation of beams and plates. A detailed discussion of different theoretical methods to predict the displacements of elastically or plastically impacted beams and plates is covered in References (7) and (8).

It could be possible to compare theoretical results with the experimental results. However, it is beyond the scope of this study to enter into such a diverse task of comparison of different theoretical methods and their accuracy in predicting the behavior of the impacted specimens. For example, to show the difference between theory and experiment, the following calculations were performed.

The force/deflection characteristics of the closed single rib specimen when impacted from 10 in. in Test No. 6 was arbitrarily chosen for the first comparison. As mentioned previously, during this test the behavior of the specimen was elastic. It was assumed that the chosen specimen would respond like a beam since it was a single rib specimen. The closed form of the cross section was stiffer than the serrated rib specimen and less affected by the load concentrations which caused local or stability type of failures.

The calculated deflection was based on the "Dynamic Beam Column 8 - DBCT" computer program (17). This program used the mathematical model of a beam with the lumped masses concentrated at certain beam stations. The program was developed using the finite difference method to solve the problem of the forced vibration of the beam within the elastic limit. The beam element between the specified stations was assumed to be rigid. The transverse deflection of the beam stations (or joints) was considered to be the only degree of freedom of the system. The relative rotations of the rigid beam elements between the stations were derived from the deflections of the stations using the finite difference method. The program did not include the internal damping effect of the material.

The above mentioned program was used for the following loading conditions to compare with the results of impact Test No. 6.

(1) The force pulse as obtained in the form of punched computer output directly from the analyzed data of Test No. 6.

(2) Triangular force pulse with the same peak as in the test.

(3) Rectangular pulse with the amplitude of mean impact force calculated from the impulse/impact duration of Test No. 6.

(4) Peak force as obtained in the test, applied constantly for the time duration t, such that $(P_{max}) \times (t)$ = impulse of the test.

The time dependent force was assumed to be concentrated at the midspan so that the distributing effect of the loading pad is not considered in the computer solutions. The resulting deflection/time relations are plotted in Fig. 69. The computed force/deflection relations are shown in Fig. 70 together with the result of Test No. 6. These figures lead to the following comments:

(1) Maximum deflection value of the experiment on closed single rib specimens could be closely calculated by the DBCT program provided that the forcing function is known.

(2) There was a phase difference in the computed solutions when the shape of the loading was varied for the same impulse.

(3) The effect of damping was visible during the test and during the visual inspection of the data on the scope of the digitizing computer. However, the "Dynamic Beam Column" program did not consider any damping. The program is also not capable of differentiating whether and when the impinging mass is separating itself from the beam during impact, especially during rebound. In fact, the mass did never separate from the beam according to the program.

Another attempt was made to predict the plastic deflection using the method developed by Symonds (18). This method neglected the elastic deformation of the beam when the beam was plastically deformed. It assumed only plastic hinges at the center and at two other locations

symmetrically located to the central one. The plastic hinge in the specimen was spread all along the length of the loading pad, mainly concentrated in the corners of the pad. The theoretical study assumed unrestrained support conditions, whereas the specimens of this program had to be restrained for the physical test.

The motion of the beam was considered by Symonds to occur in three stages. In the first stage it was assumed that the beam with the coordinate origin at the center moved as a rigid body when loaded, until the moment at the center reached the plastic moment capacity of the cross section. The equation of motion was written for this stage relating the time dependent force with the time derivatives of the displacement. At the second stage, the plastic hinge formed at the center and at the straight beam halves rotated relative to each other. The rotation angle was assumed to be small. The third stage provided the occurence of one additional hinge on both beam halves. A detailed discussion of the method is also given in Reference (7), which points out that the rotation angle should be within ten degrees to avoid significant errors in the predicted results.

The central rotation angle is given by the formula

$$\theta_o = 0.037 \, (\rho A \, M_p^{5/3} \, L^{1/3})^{-1} \, (I^2)_{max} P_i^{2/3}$$

where

$$I = \int_0^{\tau} P_i(t) \, dt$$

$$M_p = {}_{dyn}\sigma_y \cdot z$$

z = Plastic modulus of the cross section

$z = 12.13 \text{ in.}^3$ for closed single rib specimen

$A = 6.196 \text{ in.}^2$

$\rho = \gamma/g = 7.187 \times 10^{-4}$ lbs. sec.^{2}/in.^{4} (steel)

${}_{dyn}\sigma_y = 55$ ksi assumed depending on the results obtained in References (7, 9). See Figs. 12 and 13.

$L = 60.00$ in. for half span

The plastic deflection at midspan is calculated with

$$\delta_p = L \sin \theta_o$$

The data of Test Nos. 18, 26, 23, 38, and 39, on closed single rib specimen were used to evaluate the above deflection formula. (For the experimental results of the same tests see Appendix I "Some Test Characteristics on CL-1-1 and CL-1-2 Specimens").

The predicted plastic displacements and the experimental values (Table 18) were far from being considered satisfactory for this type of test and specimen. The calculated values were 2.74 to 5.85 times smaller than those measured. Only for the Test No. 23 there was an acceptable correlation between the predicted and measured values with the measured plastic displacement 9 percent less than the predicted one.

If the measured maximum impact force is considered to be the possible static collapse load to deform a plastic hinge on a simple beam, the plastic deformation could be calculated with the formula (see Reference 19).

$$\delta_{collapse} = \frac{40}{27} (P_{collapse}) \frac{L^3}{48\ EI}$$

The calculated collapse deflections with this less elaborate formula and the measured values of the above mentioned tests are shown in Table 19. This simple approximation gave quite satisfactory results. The predictions varied from the measured displacements by ± 20 to 30 percent.

3.3.3. Implied Results

The differences between the predicted and measured values were expected. To compute the deflections of the orthotropic plates more extensive studies should be made using a general theoretical formulation. No theoretical prediction of deflection has been made for the serrated single rib or for any of the multi-rib specimens.

It should be remembered that in all of the impact tests cushioning material controlled the shape of the pulse. Any theoretical method to predict the behavior of impacted specimens should consider an actual pulse shape to obtain a reasonable comparison of the theoretical and the experimental results.

The findings from the studies on the force/deflection characteristics of the specimen can be summarized as follows:

(1) The force/deflection characteristics of the impacted orthotropic steel plates and of single rib elements are presented in Tables and Plots (Figs. 44 through 67, Tables 13 to 19, and Appendix I).

(2) The force/deflection behavior of the specimens under impact was also compared with the behavior of the statically loaded similar specimens of Reference (6).

(3) In high impacts on serrated multi-rib specimens, the required impact force was at least 80 percent more than the static load (Figs. 66 and 67).

(4) Comparison of the static and impact forces measured during the tests as the specimen reached a certain specified deflection like (L/400, L/200) is given in Table 17. The (L/400) deflection limit could be reached in almost all test series elastically, but multi-rib specimens yielded prior to L/200 limit. Statically loaded single ribs also yielded within this limit but the impacted single ribs did not.

(5) Impacted closed and serrated single rib specimens yielded at almost the same midspan deflection but the force required to deflect the closed rib specimen was almost 53 percent more than the force needed to deflect the serrated single rib specimen (Figs. 47 and 49).

(6) The transverse load distribution capability of the multi-rib specimen under impact condition was rather poor. The impacted location had considerably more displacement when compared with the neighboring locations of the specimen in the transverse direction of the same section (Figs. 61 and 62).

(7) The serrated specimens deflected more than the closed rib specimens for the same level of force (Fig. 68). (C1-4 specimen was an exception. See the reasoning given in paragraph 3.2).

(8) The deflection of the closed single rib specimen was calculated with only two of the existing theoretical methods for the comparison.

(9) The verification of the elastic impact behavior was based on the computer program "DBCT (8)" (17). The force/time relation of the impact Test No. 6 was used as the forcing function for this program. Although there was some phase differences, still the calculated displacement values correlated reasonably well with the measured quantities (Fig. 69). The program was also used to calculate the deflections of the same specimen by changing the shape of the actual forcing function to triangular or rectangular form. For the triangular shape, the location and the magnitude of maximum aplitude were the same as in the case of the forcing function of the impact Test No. 6. For the rectangular shape the amplitude of the force was mean P_{impact}. In both cases the impact duration was the same as in the test. A third forcing function of rectangular pulse shape was also tried with the amplitude of the maximum impact force for a calculated duration of time with the impulse the same as in the actual test. The results showed that the program was very sensitive to the shape of the forcing function. The calculated deflections were not correlating with the measured values any more if the shape of the pulse varied from the real form with the same impulse (Figs. 69 and 70).

(10) The theoretical plastic deflections calculated for closed single rib specimen using the method developed in Reference (18) did not correlate with the measured deflections (Table 18). Simple beam deflection formula for the static collapse load gave very good results, when the collapse load was replaced by the maximum impact force of the test (Table 19).

3.4. Force/Energy Relation

This relation was developed for those tests in which the displacement at impact location was recorded. The energy was calculated as the integral of the area under the force/displacement curves. Since the test data were sampled during digitizing at every millisecond and the data was stored on tapes, the integration step in the computation was chosen to be a millisecond. Thus the program calculated the incremental area under force/displacement curves for every millisecond time interval. The integration was carried out up to the

instant of maximum displacement. At that instant the incremental energy approached zero. The computer printed out the value of "attained energy" for every millisecond. There was also another program to produce calcomp plots in which force versus attained energy was presented. The force/energy relation obtained on specimen CL-3-1 during Test No. 89 was shown in Fig. 71. Further similar plots are included in Appendix II. The instantaneous values of the attained energy are given in Tables 13 through 16 to indicate the energy characteristics of individual tests. These tables were referred to the discussion of force/displacement relation.

Tables 20 and 21 are prepared to summarize the energy levels obtained in the important tests. These tables indicate the value of the attained energy at the instant when:

(a) no yielding has occurred,
(b) yielding initiated at a certain rib,
(c) specimen failed totally,
(d) absolute maximum energy was obtained.

The corresponding deflection at each instant is also given in the last column of these tables. The deflection measurements refer to the original (or straight) position of the beam and not to the position of the specimen prior to each test. The impact force at that instant and the corresponding drop height of the impact mass are also included in these tables.

The calculation of impact energy was based on the recorded test information. As mentioned earlier, especially in low impact tests, the force/time records were influenced by the vibrations of the mass and of its supporting system. Therefore, for those tests the calculated energy was inaccurate. Fortunately the impact energy of the low impact test was less important in this test series. The ultimate energy absorption capacities of specimen resulted in high impact tests, and the effect of vibration of the mass system on the force/time records in these tests was very minor.

From Tables 20 and 21 , Fig. 72 was obtained by plotting the attained energy versus the displacement at the initiation of yielding and at failure due to buckling or excessive deflection. The failure criteria was mentioned earlier in section 3.2. From these tables the most critical values of the attained energy of different type of specimens are collected in Table 22. This table summarizes the possible energy absorption capacities of different test specimens at certain stress limits. The limits were distinguished as elastic or at yielding or at total failure. This separation of limits was made upon studying stress/time relations. The stress/time relations will be discussed in the following paragraph. The highest value in energy calculations as reached prior to the initiation of yielding in stress/time record was considered to occur within elastic range. For the two serrated single rib specimens the values were 16.2 and 30.3 kips. in. Considering the possible inaccuracies in low impact force records a mean value of energy (23.2 kips. in.) was presented in Table 22 for serrated single rib specimens. It can be seen that the table values did not vary with the number of ribs of the specimen, when the impact behavior was elastic. Only when impacted beyond yielding, multi-rib specimens showed higher energy absorption capacity than single rib elements. This is probably due to the fact that the multi-rib specimens did not deflect as easily as the single rib specimens because of the higher ratio of mass of the specimen to the free falling impacting mass (see also 7, p. 62). The higher impact force was achieved by the higher impact velocity and by the rigidity of the specimen resulting in high rates of strain. At high strain rates the specimen began to behave plastically. When the multi-rib specimens were impacted within the elastic range, impact force was low and specimen did not deflect much, and so the calculated energy was also low. For this reason, in Table 22 the absorbed energy of the multi-rib specimen is shown to be at least as much as companion single rib specimens, when impacted below the plastic range. In Fig. 73 the energy absorbed by the specimens during ultimate impact tests were plotted against the rib numbers. Data pertained to two closed and two serrated rib specimens are shown in Fig. 73. The dotted line in this

figure represents the energy absorption of the specimen at the ultimate load and the straight line shows the ultimate energy absorption capacities prior to rebound.

It is seen that the closed three rib specimen absorbs at ultimate level 2.53 times the energy as compared to its single rib element. Closed four rib specimen is not included in the comparison for reasons cited in paragraph 3.2. The energy absorption capacities of the serrated rib specimens was less than the capacities of the closed rib ones. Closed single rib specimens absorbed almost as much energy as the serrated four rib specimen. The ultimate energy absorbed by serrated three rib specimen was only 25 percent above the capacity of the single serrated rib. The serrated four rib specimen absorbed 442 percent energy of the serrated single rib. The low energy value of the serrated three rib specimen was due to early buckling in this specimen as compared to four rib specimen. In three rib specimen yielding at the extreme fibers of its impacted central rib initiated immediately after buckling. The impact location in four rib specimen was between ribs two and three. The four rib specimen could resist impact with its two ribs below the load distributing pad. If the loading pad was placed on the central rib as in the case of three rib specimen, only the impacted rib had to absorb the energy until its failure. The neighboring ribs could come into the picture after the central rib deflected excessively. This shows the beam-like behavior of the orthotropic plates under impact. It is believed that a transverse steel diaphragm across the ribs at the midspan could considerably improve the plate-like behavior of the multi-rib specimens.

Based on the test results and the observations following conclusions are derived:

(1) Energy absorption capacities of the serrated rib specimens were considerably smaller than those of similar closed rib specimens (Fig. 72).

(2) The ultimate energy absorbed by the closed single rib specimen is 3.86 times the serrated single rib specimen. Similar ratio for three rib specimens is 7.85.

(3) The energy absorption capacity of the three closed rib specimen is 2.53 times the capacity of its primary single rib. The same ratio for the serrated three rib specimen is rather low, being only 1.25. Serrated four rib specimen absorbed 4.42 times the energy of the serrated single rib specimen.

(4) The energy level reached, when yielding started, was low in serrated specimens as compared to the closed rib specimens. The rate of increase of the energy values by the number of its ribs for the closed rib forms is higher as compared to the serrated ones. (Compare the dotted lines drawn in Fig. 72.)

(5) Closed rib specimens had higher energy absorption capacity beyond first yielding than the serrated rib specimens (Fig. 73).

(6) Failure of the serrated rib specimens was due to buckling of the deck plate at the serration next to the impact location.

(7) The failure criterion for closed rib specimens could be a specified magnitude of the deflection at impact location although no definite value has been set in this study.

3.5. Stress/Time Relation

This relation was derived from the time dependent strain measurements. The application of strain gages and measuring technique is discussed in Appendix IV.8. The derivation of stress magnitude from strain measurements is not a simple procedure when the strains are time dependent.

At an instant, impact stress at one location of the specimen is not to be compared with the stress at other locations. For the impact creates in the material a moving stress wave. The stress and the strains of the impacted system are localized. The impact stress is, in general, a function of the velocity of the stress wave and of the material characteristics.

In this study the instrumentation and the test set-up was not planned to measure the stress wave velocities, to use then these measurements to calculate the stresses. The stress calculations

were based on the assumption of viscoelastic behavior of the material and on the time dependent strain measurements.

The strain gages were applied with the idea of monitoring the strain rates to obtain rather qualitatively the stresses at the desired locations. The restrictions on the monitor stations were already mentioned in paragraph 1.3. In all of the tests, strain gages were limited to the locations distributed along the midspan section of the specimens. The locations were numbered beginning from left to the right rib and continuing with the locations between the ribs (Fig. 26).

There were bottom and top strain gages. Bottom gages were placed at the lowest fiber of the rib to measure the longitudinal strains. Top strain gages were attached to the lower side of the deck (or top) plate between two ribs if the specimen were the multi-rib type, and one inch from the edge if it were a single rib specimen. Similar to bottom gages, most of the top gages were directed parallel to the ribs in order to measure the longitudinal strains. However, in multi-rib specimens, there were also top gages in the transverse direction. The transverse gages measured very small strains indicating clearly the beam like behavior of the impacted orthotropic plates when yielding was not present.

When the impact was high enough to yield the impacted rib, then membrane stresses occurred in the plate in the transverse direction. The rate of transverse strains were higher than those of the longitudinal strains at the same location of the specimen. This indicates that the load distribution occurred only when the impacted rib was deflected excessively. The load transferred to the neighboring ribs caused naturally those ribs also to deflect.

Since there were six recording channels and one was reserved to register the impact deceleration, only five strain gages could be monitored at a time in each test. The calculation of the stresses in this study was performed using the relation

$$\sigma(t) = E\, e(t) + c\, \dot{e}(t)$$

where

E is Young's modulus of steel assumed to be 29.5×10^6 psi

c coefficient of viscous damping from Reference (20) p. 86, Table 2.5.1

c = $(0.70 \text{ to } 1.00) \times 10^4$ psi sec.

e(t) and $\dot{e}(t)$ = the measured strain and strain rate at certain instant (t).

The above formulation of stress assumes a viscoelastic behavior of the material. Coefficients of the viscosity for different metals is given in Reference (20). These were originally obtained experimentally by Kotano Kondo and Seibei Konno.

In the stress calculations c is taken to be 0.85×10^4 psi sec., which is the mean table values (20). In the tests in which no yielding occurred, the strain rates varied between 0.001 sec^{-1} and 0.230 sec^{-1}. Only in high drop impact tests where the specimen yielded or failed totally, the strain rate was between 2.0 and 2.5 sec^{-1}. It reached the maximum value of $\dot{e} = 2.964$ sec^{-1} in Test No. 133 on serrated four rib specimen.

The calculated stresses versus time were plotted on the calcomp plot. The example plots are shown in Appendix III. In multi-rib specimens the plots show stress/time relations registered at more than one location. The maximum stresses at different locations did not occur at the same time, as expected. Besides the calcomp plots of stress/time relations, Tables 23 through 30 show the relation between stresses at several locations of the multi-rib specimen and the impact force. The stresses for single rib specimen under impact and under static loading are given in Table 31. The attained energy values were included in these tables to distinguish the level of energy attained prior to or after yielding occurred.

From the dynamic test results of different types of steel, it can be approximately assumed that the dynamic lower yield stress would be 50 or 60 percent higher than the static yield stress. For A 36 steel used in the test specimen, this will result in a dynamic yield stress of 54 to 57.5 ksi. Any calculated impact stress above the value of 60 ksi indicates yielding and can not be considered correct.

Better values could be obtained if the velocity of the plastic stress waves had been measured. Those values below the set level of the assumed dynamic yield were used for comparison of the stresses obtained in different tests. Tables 31 through 33 were prepared for this purpose. The stresses due to static loading are also included in these tables. Figures 87 and 88 show the longitudinal stresses of serrated multi-rib specimen under 16 kips static load at several loading locations. A direct and numerical comparison of the cited stress values for a given load level is not always possible, since impact force unlike static load can not be adjusted to a desired level.

The impact stress (Table 31) at extreme bottom fiber of the serrated single rib specimens SR-1-1 is 50.3 ksi and for SR-1-2 is above the assumed dynamic yield stress. The impacted closed single rib specimen CL-1-1 showed at the same location a stress value of 21.2 ksi. Static stresses at the same location both for closed and serrated single rib specimens were almost the same (6). The higher impact stresses at the extreme bottom fiber of the serrated rib specimen is assumed due to stress concentration or the notch effect at serration. This assumption is also supported by the test observations. Yield lines appeared in serrated ribs not only at the extreme bottom rib fibers but also on the serrated web side (Fig. 75). The comparison of static and impact stresses for the serrated three rib specimen is in Table 32 and for the serrated four rib specimens is in Table 33. Here again the notch effect due to serration is obvious.

Since the stresses measured at the deck plate were much lower than those at the ribs, they were not included in Tables 32 and 33. Deck plate stresses due to static loading were also lower than the

extreme rib stresses. The impact stresses of the multi-rib specimens reveal the beamlike action (Tables 23 to 30). The load was carried mainly by the impacted rib. If the impact was high enough to initiate yielding in the impacted rib, the rib bent stretching the deck plate laterally. Since the deck plate was supported by the unaffected neighboring ribs this created the transverse membrane stresses in the deck plate and also the distribution of the impact load among the ribs. The stress waves prefer to propagate in the direction of the material concentration. Therefore, since the test specimens had a higher material concentration along the ribs, then the beamlike action is understandable. This behavior of the orthotropic plate could not be recognized when they were statically loaded. It is important to point out that the load distribution between the ribs was less effective in the serrated rib specimens compared to the closed rib specimens.

The serrated specimen did not sustain loads to create a full plastic hinge as they were reported (6) under the static tests. When the rib showed the first sign of yielding at the lower extreme fibers buckling of the deck plate took place all along its width. The measured stresses indicated that none of the longitudinal deck stresses were close to dynamic yielding as buckling occurred. The buckling of the deck plate did not remain local, but spread all along the midspan section of the specimen resulting in total failure (Figs. 76 and 77). The pictures taken by a movie camera at a speed of 24 frames/sec. show how this buckling occurred in Test No. 133 on serrated four rib specimens. Figure 78 shows three consecutive film pictures taken at the instant of impact and buckling.

The following conclusions about the stress characteristics of the impacted orthotropic steel plates were drawn from the cited tables and plots:

(1) The longitudinal rib stresses due to impact at the extreme bottom fibers of the serrated single rib specimens were higher than those of closed rib specimens (Table 31).

(2) In serrated rib specimens yielding due to impact was visible not only at extreme bottom fibers of the rib but also around serration (Fig. 75).

(3) Early yielding and failure occurred in serrated rib specimens under impact because of the presence of notch or stress concentration effect at the serrations.

(4) Deck plate stresses in the longitudinal direction for both static and impact loading were lower than the longitudinal stresses at the lowest rib fibers.

(5) A close study of the impact stresses of the multi-rib specimen showed its beamlike behavior. Load was mainly carried by the impacted rib or ribs. Load distribution among the ribs occurred either in low level impact, or after the impacted rib fails.

(6) The serrated specimen did not sustain loads under impact tests to create a full plastic hinge. After the first sign of yielding at the lower extreme fiber, buckling of the deck plate took place all along its width. None of the deck stresses at this instant were close to yielding stress.

CHAPTER IV

CONCLUSIONS AND RECOMMENDATIONS

4.1. Conclusions

The impact behavior of the orthotropic steel plates and their primary single rib elements were studied. Certain correlations among the measured quantities were found revealing an insight into the complex nature of the impact response of the specimens tested. In the preceding sections the test results were discussed and concluding remarks were made.

The difference between the impact and static response of the orthotropic plates were described. Comparisons were made between the capacities of the multi-rib against single and closed versus serrated rib specimens.

The techniques employed in testing procedures and the measurements made are believed to be efficient for impact tests of orthotropic plates. All calculations were made with the help of computers.

The following are conclusions based on the present study:

(1) The orthotropic plate behaved differently under impact than under static load. The impact force needed to deflect the specimens by a given amount was higher than required static force. The more the initial impact velocity and the bigger the specimen the greater is the difference in responses.

(2) The maximum impact force recorded in multi-rib specimens is higher than the summation of the capacities of their primary single rib elements.

(3) Closed rib specimens are stiffer than the serrated rib specimens and require higher impact load for an equivalent deflection. In other words, for the same level of force serrated rib specimen deflect more.

(4) For serrated specimens, the rate of change of impulse is almost linear with the number of ribs. For closed rib specimen the rate of change is higher than that of the serrated ones.

(5) In all test series the specimens could be elastically deflected as much as L/400 (0.3 in.). When this was increased to 0.6 in. or L/200 the impacted multi-rib specimen yielded. The statically loaded single rib specimens also yielded within this limit but not the impacted single rib ones.

(6) The program used to predict the elastic central deflection of the closed rib specimens showed that the results were satisfactory as long as the shape of the forcing function was similar to the shape measured during the test. The error increased when the pulse shape differed from the real shape even if the impulse was kept unchanged.

(7) The central deflection of the plastically impacted closed single rib specimen can be calculated using the expression (19)

$$\delta_{collapse} = \frac{40}{27} \; P_{collapse} \frac{L^3}{48EI}$$

in which the collapse load would be replaced by the maximum impact force reached during the plastic impact test.

(8) Closed rib specimens have high reserve strength and high energy absorption capacities beyond initial yielding, whereas the serrated rib specimens failed sooner due to buckling of the deck plate.

(9) Closed rib specimens deformed until a plastic hinge was developed. At this stage the cross section of the rib also deformed due to local buckling of the top plate, the web and the lower chord of the rib. However, in serrated rib specimens, no plastic hinge could develop when its deck plate buckled. The stresses at the deck plate were well below yielding at this stage.

(10) Although in multi-rib specimens the recorded maximum impact force was higher than the summation of the maximum capacities of their primary single rib elements, the multi-rib specimens behaved more like beams than orthotropic plates. The load transfer through the plates occurred only when impacted rib (or ribs if the impact location was between two ribs) failed or deflected excessively.

(11) In all tests under impact, governing stresses occurred at the extreme fibers of the ribs. The longitudinal stresses of the deck plate were comparatively less than the rib stresses. In general, transverse deck stresses remained low except when the impacted rib excessively deformed pulling the deck plate with it.

(12) The notch effect or stress concentration due to serration could be observed clearly in impact tests. Longitudinal rib stresses in serrated specimens were much higher than those of closed rib specimens. Yielding was visible in serrated rib specimens not only at the extreme rib fiber but also around serrations.

(13) In only one of the tests the weld tip cracked when the serrated single rib specimen buckled and excessively deformed. This occurred when it was impacted by the mass released from the drop height of 120 in. There were no cracks or fractures observed throughout the remaining tests.

4.2. Recommendations

The following recommendations are made for further investigations of orthotropic plates under impact.

(1) Existing theoretical studies could be critically reviewed to find out the capability of predicting the behaviors of impacted beams and plates. The results of the present experimental study may be helpful in deciding on the shape, duration, and peak value of the forcing function to be used in the theoretical formulations. The calculated deflections, energy and stress values could be compared with the measured values reported herein.

(2) Dimensional analysis might be carried out together with experiments on different sizes of the same type of orthotropic plates to develop a generalized method to include the changes of geometric parameters.

(3) Further impact experiments should be conducted on improved closed multi-rib orthotropic plates with more load distributing capabilities between the ribs.

(4) Impact tests should be made in a way which more closely simulates field conditions. This includes the loading as well as the supporting of the specimen.

(5) The effect of the different supporting conditions of the same specimen should be experimentally investigated and also compared with the most suitable theory.

(6) The effect of repetitive impact within or beyond the elastic limit could also be studied, especially if further investigations on the biserrated orthotropic steel plates are desired.

TABLES

TABLE 1 TEST SPECIMENS

No.	Orthotropic Steel Plates		Detail in Figures
	Stiffened With	Abbreviation Used	
1	Closed single rib	CL-1-1	4
2	Closed single rib	CL-1-2	4
3	Biserrated single rib	SR-1-1	4
4	Biserrated single rib	SR-1-2	4
5	Closed three rib	CL-3-1	5
6	Biserrated three rib	SR-3-1	6
7	Closed four rib	CL-4-1	7
8	Biserrated four rib	SR-4-2	8
9	Biserrated four rib	SR-4-3	8

TABLE 2 SECTION PROPERTIES OF SINGLE RIB SPECIMENS

Specimen	Area A	Distance to c.g. Z	Moment of Inertia I	Section Modulus Top S_t	Bottom S_b	Plastic Modulus Z_p
	in^2	in	in^4	in^3	in^3	in^3
Closed rib	6.196	2.090	34.658	16.583	8.331	12.130
Serrated rib	5.444	2.217	33.736	15.217	8.365	11.444

TABLE 3 COUPON TESTS (3/16 inch thick)

	Upper Yield	Lower Yield	Mean Yield	Ultimate Stress	Ultimate Elongation	Yield Modulus
	ksi	ksi	ksi	ksi	%	ksi
	PARALLEL TO THE ROLL DIRECTION					
Mean of 5 coupons	41.51	38.90	40.19	59.25	28.66	31,320
	PERPENDICULAR TO THE ROLL DIRECTION					
Mean of 5 coupons	43.23	40.42	41.82	60.39	28.28	31,110
Average cross-sectional area of coupons .297 $in.^2$ Average value of Young Modulus 31.21 x (10^3) ksi						

TABLE 4 COUPON TESTS (1/4 inch thick)

	Upper Yield	Lower Yield	Mean Yield	Ultimate Stress	Ultimate Elongation	Young Modulus
	ksi	ksi	ksi	ksi	%	ksi
	PARALLEL TO THE ROLL DIRECTION					
Mean of 5 coupons	42.85	39.75	41.10	61.50	31.0	30,300
	PERPENDICULAR TO THE ROLL DIRECTION					
Mean of 5 coupons	43.51	40.14	41.82	62.54	28.9	31,390
Average cross-sectional area of coupons .3728 $in.^2$ Average value of Young Modulus 31.07 x (10^3) ksi						

TABLE 5

TEST RESULTS FROM THE CERTIFICATE OF THE STEEL PRODUCER

Plate thk.	Yield	Tensile	Elong.	Chemical Composition					Heat No.
in.	ksi.	ksi.	% of 8 in.	C	Mn	P	S	Si	
3/16	57.9	68.7	21.5	.19	.38	.01	.025	.05	80629
1/4	46.9	61.8	25.5	.17	.43	.01	.019	.07	13845

TABLE 6 SUMMARY OF THE FORCE/TIME RELATION DURING THE TEST ON CLOSED SINGLE RIB SPECIMENS

Test No.	Impact Location	Drop Height	Impact Velocity	Maximum Impact Force	At Instant After Impact	Impulse I	Impact Duration	Mean Impact Force
		In.	In./Sec.	K	Millisec.	K-Millisec.	Millisec.	K
6	1	10	87.9	15.4	37	446.7	64	7.0
7	1	15	107.6	21.8	40	588.3	67	8.8
8	1	15	107.6	21.5	43	592.8	70	8.5
9	1	18	117.9	20.5	35	570.9	57	10.0
11	1	20	124.3	23.0	38	624.7	65	9.6
12	1	30	152.2	28.2	38	907.1	64	14.2
13	1	40	175.7	27.6	37	856.5	61	14.0
25	1	50	196.5	30.4	34	1069.8	63	17.0
26	1	60	215.2	33.3	34	1153.5	64	18.0
27	1	72	235.2	31.9	41	1269.8	83	15.3
38	1	120	304.4	33.7	41	1507.0	85	17.7
39	1	120	304.4	48.1	42	1496.7	70	21.4
40	1	120	304.4	63.6	27	1686.5	86	19.6
28	1	240	430.5	71.0	35	2498.7	64	39.0

TABLE 7 SUMMARY OF THE FORCE/TIME RELATION DURING THE TEST ON SERRATED SINGLE RIB SPECIMEN

Test No.	Impact Location	Drop Height	Impact Velocity	Maximum Impact Force	At Instant After Impact	Impulse I	Impact Duration	Mean Impact Force
		In.	In./Sec.	K	Millisec.	K-Millisec.	Millisec.	K
SR-1-1 Specimen								
56	1	6	68.1	12.3	35	361.6	64	5.7
42	1	7	73.5	11.9	32	767.5	70	5.3
43	1	8	78.6	15.2	40	436.5	68	6.4
44	1	9	83.4	16.0	33	401.5	59	6.8
45	1	10	87.9	18.7	34	498.7	60	8.3
46	1	12	96.3	17.8	36	531.2	63	8.4
47	1	36	166.7	19.8	36	767.5	65	11.8
50	1	36	166.7	19.8	39	764.6	68	11.2
SR-1-2 Specimen								
57	1	10	87.5	17.9	34	517.3	61	8.5
58	1	14	104.0	19.4	34	607.3	63	9.6
59	1	16	112.2	21.4	40	649.3	68	9.6
60	1	18	117.9	17.2	39	561.8	68	8.3
61	1	20	124.3	19.8	35	639.9	64	10.0
62	1	26	141.7	18.8	40	708.2	80	8.9
66	1	36	166.7	21.8	37	934.3	92	10.2

TABLE 8 SUMMARY OF THE FORCE/TIME RELATION DURING THE TEST ON THREE RIB SPECIMEN

Test No.	Impact Location	Drop Height	Impact Velocity	Maximum Impact Force	At Instant After Impact	Impulse I	Impact Duration	Mean Impact Force
		In.	In./Sec.	K	Millisec.	K-Millisec.	Millisec.	K
CL-3-1 Specimen								
79	1	6	68.1	16.3	30	396.8	48	8.3
84	4	6	68.1	11.4	22	312.7	48	6.5
88	2	12	96.3	23.6	27	618.4	54	11.5
90	2	240	430.5	82.8	29	2023.1	54	37.5
89	2	480	608.8	330.8	25	8673.3	55	157.7
91	2	480	608.8	152.1	25	3067.0	65	47.2
SR-3-1 Specimen								
93	3	6	68.1	12.8	33	405.3	61	6.6
97	5	8	78.6	14.5	32	419.7	61	6.9
98	2	6	68.1	16.7	34	475.4	61	7.8
101	2	10	87.9	16.7	29	458.4	56	8.2
102	2	20	124.3	19.9	35	601.4	63	9.6
103	2	40	175.7	26.0	36	849.7	63	13.5
104	2	60	215.2	32.4	35	1019.3	62	16.4
105	2	240	430.5	80.2	34	2267.0	60	37.7
106	2	360	527.5	89.5	29	2250.0	68	33.1

TABLE 9 SUMMARY OF THE FORCE/TIME RELATION DURING THE TEST ON FOUR RIB SPECIMEN

Test No.	Impact Location	Drop Height	Impact Velocity	Maximum Impact Force	At Instant After Impact	Impulse I	Impact Duration	Mean Impact Force
		In.	In./Sec.	K	Millisec.	K-Millisec.	Millisec.	K
CL-4-1 Specimen								
137	5	8	78.6	13.3	31	437.5	63	6.9
142	2	8	78.6	12.8	33	466.9	63	7.4
147	6	8	78.6	13.9	32	450.0	60	7.5
153	6	60	215.2	32.1	42	1128.7	71	15.9
155	6	120	304.4	55.9	38	1667.6	87	19.2
157	6	552	652.9	138.6	24	2910.4	52	56.0
SR-4-2 Specimen								
109	5	10	87.9	17.9	39	515.8	63	8.2
113	2	6	68.1	17.1	33	430.2	49	8.8
112	2	10	87.9	21.4	31	506.0	52	9.7
118	6	6	68.1	17.1	32	427.4	50	8.6
SR-4-3 Specimen								
122	6	6	68.1	11.0	21	406.4	67	5.3
131	6	20	124.3	16.5	43	637.1	72	8.9
132	6	50	196.5	26.0	41	995.7	68	14.6
133	6	600	680.7	142.3	22	3268.1	64	51.1

TABLE 10 COMPARISON OF THE ULTIMATE LOADS OBTAINED IN STATIC AND IMPACT TEST

Test No.	Specimen	Impulse (kips-millisec)	P_{mean} (kips)	Failure Observed	$P_{max\ impact}$ (kips)	$P_{static\ ultimate}$ (kips)
47	Serrated Single rib	767.5	11.8	buckled	19.8	14.6
28	Closed Single rib	2498.7	39.0	Yielded previously in this test excessive deflection) 6in	71.0	19.1
105	Serrated	2267.0	37.7	previously yielded in this test yielded more	80.2	
106	Three rib	2225.0	33.1	Buckled	89.5	49.6
89	Closed	8673.3	157.0	Yielding Initiated	330.8	
91	Three rib	3067.0	47.0	Excessive deflection	152.8	
133	Serrated Four rib	3268.1	51.1	Buckled	142.3	73.0
157	Closed Four rib	2910.4	56.0	Yielded, deflection 2.5 in.	138.6	

TABLE 11
COMPARISON OF ULTIMATE STATIC AND IMPACT FORCES CARRIED BY TEST SPECIMENS

Referring to the capacities of the single rib specimens to be 100%.

Specimen	P Mean Impact	P Max Impact	P Static Ultimate
SR-1	100%	100%	100%
SR-3	320%	450%	340%
SR-4	433%	720%	500%
CL-1	100%	100%	100%
CL-3	403%	463%	
CL-4*	144%	195%	

Similarly, serrated and closed rib specimens will also be completed.

SR-1	100%	100%	100%
CL-1	330%	358%	130%
SR-3	100%	100%	100%
CL-3	416%	370%	
SR-4	100%	100%	100%
CL-4	110%	98%	

* See paragraph 3.2

TABLE 12 NATURAL FREQUENCIES OF A BEAM

ω_o	= Natural circular frequency		(rad/sec)
E	= 29.5×10^6	psi	
I_1	= 34.658	in^4	(Closed single rib)
I_2	= 33.736	in^4	(Serrated single rib)
L	= 120.0	in	
m_{b1}	= 0.5387	$Lbs\text{-}sec^2/in$	Total mass of closed rib specimen
m_{b2}	= 0.4730	$Lbs\text{-}sec^2/in$	Total mass of serrated rib specimen

$T = \frac{2\pi}{\omega_o}$ $\quad F = \frac{1}{T}$

	Closed single rib specimen		Serrated single rib specimen	
	ω_o sec^{-1}	f sec^{-1} (T) sec	ω_o sec^{-1}	f sec^{-1} (T) sec
(a) Beam mass (total)				
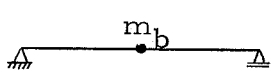 $\omega_o = 4\sqrt{\frac{3\,EI}{m_b L^3}}$		36.54		38.48
	229.61	0.027	241.76	0.026
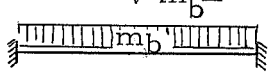 $\omega_o = \sqrt{\frac{384\,EI}{5m_b L^3}}$	290.44	46.22	305.80	48.67
	367.38	0.022		0.021
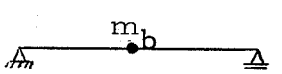 $\omega_o = \sqrt{\frac{48\,EI}{L^3\ 0.5m_b}}$		51.61		54.41
	324.74	0.019	341.89	0.018
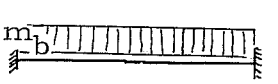 $\omega_o = 8\sqrt{\frac{EI}{L^3 m_b}}$		73.10		76.95
	459.22	0.013	483.52	0.013

TABLE 13 SOME HIGHLIGHTS DURING THE IMPACT TEST ON CL-3-1 SPECIMENS

Sequence Number	Test Number	Drop Height	Impact Velocity	Impact Location	Impact Force	Max. Displ. under Impact Loc.	Attained Energy	Remarks
		in.	in./sec.		K	in.	K-in.	
1	79	6	68.1	1	12.770	.358	3.969	Elastic
2	84	6	68.1	4	10.066	.214	1.663	Elastic
3	88	12	96.3	2	17.947	.317	4.866	Elastic
4	89	480	608.8	2	308.890	1.079	233.450	Yielding at central rib
					330.750	2.236	595.020	Yielding also at outer rib
					230.080	3.964	1005.900	
5	90	240	430.5	2	82.830	.986	52.869	Further yield
					61.518	1.041	57.272	Top plate slightly buckled
6	91	480	608.8	2	152.140	.585	55.908	
					75.640	2.457	233.840	

TABLE 14 SOME HIGHLIGHTS DURING THE IMPACT TEST ON SR-3-1 SPECIMENS

Sequence Number	Test Number	Drop Height	Impact Vel.	Impact Loc.	Impact Force	Max. Displ. under Impact Loc.	Attained Energy	Remarks
		in.	in./sec.		K	in.	K-in.	
1	93	6	68.1	3	10.785	.370	3.587	Elastic
2	97	8	78.5	5	12.798	.358	4.411	"
3	98	6	68.1	2	15.157	.306	3.800	"
4	100	6	68.1	2	12.712	.295	3.474	"
5	101	10	87.9	2	16.652	no record	no record	"
6	102	20	124.3	2	19.931	"	"	"
7	103	40	175.7	2	25.971	"	"	"
8	104	60	215.2	2	32.356	"	"	yield began
9	105	240	430.5	2	80.242 51.194	1.642 2.233	193.032 135.210	yielded
10	106	360	527.2	2	89.474 45.557	1.287 2.945	90.764 177.960	yielded & buckled

TABLE 15 SOME HIGHLIGHTS DURING THE IMPACT TEST ON CL-4-1 SPECIMENS

Sequence Number	Test Number	Drop Height	Impact Velocity	Impact Location	Impact Force	Max. Displ. under Impact Loc.	Attained Energy	Remarks
		in.	in./sec.		K	in.	K-in.	
1	137	8	78.6	5	10.401	.182	1.438	Elastic
2	142	8	78.6	2	10.747	.218	1.827	Elastic
3	145	8	78.6	2	9.220	.193	1.416	Elastic
4	147	8	78.6	6	10.603	.204	1.609	Elastic
5	153	60	215.2	6	32.154	.418	8.191	Elastic
6	154	60	215.2	6	32.298	.416	8.165	Slight yielding at rib 1 & 3
7	155	60	304.4	6	32.298	.655	22.151	Yielded further but not much
					48.663	.789	29.326	Almost no remaining strain
8	157	552	652.9	6	138.642	1.442	123.675	Yielded
					56.701	3.637	329.090	
9	158	360	527.2	6	102.512	1.439	103.084	Local buckling of top plate between the webs of rib 1
					85.571	1.507	109.789	
10	159	600	680.7	6	no record			
11	160	552	652.9	6	no record			Local buckling of top plate of rib 1&4

TABLE 16 SOME HIGHLIGHTS DURING THE IMPACT TEST ON SR-4-1 SPECIMENS

Sequence Number	Test Number	Drop Height	Impact Vel.	Impact Loc.	Impact Force	Max. Displ. Under Impact Loc.	Attained Energy	Remarks
		in.	in/sec		K	in.	K-in.	
1	107	10	87.9	5	12.137	-	-	Elastic
2	108	10	87.9	5	13.920	.276	3.161	"
3	110	10	87.9	5	14.006	-	-	"
4	115	6	68.1	2	11.188	.289	2.737	"
5	122	6	68.1	6	10.469	.184	1.792	"
6	129	6	68.1	6	6.655	.159	.979	"
7	130	6	68.1	6	9.982	.192	1.583	"
8	131	20	124.3	6	16.509	.295	3.082	"
9	132	50	196.5	6	24.893	.449	7.361	Yielding initiated
10	120	600	680.7	6	129.770	2.069	194.59	Yielded & buckled
11	133	600	680.7	6	142.329	1.668	205.151	Yielded & buckled
					107.467	2.490	273.231	
					43.506	5.756	477.546	

TABLE 17
COMPARISON OF INSTANTANEOUS IMPACT AND STATIC FORCES WHEN SPECIMENS REACH A SPECIFIED DEFLECTION VALUE

Specimen	Force kips	Force %		Test No.	P_{mean}	$\frac{P_{mean}}{P_{static}}$	Load. Locat.	Impact Velocity
When deflection at Load point δ = 0.3 in. = L/400								
SR-1	13.0	200	Impact	62	8.9	137	1	96.3
	6.5	100	Static			100		
CL-1	16.0	185	Impact	18	14.9	173	1	175.7
	8.6	100	Static			100		
SR-3	15.2	105	Impact	98	7.8	54	2	68.1
	14.5	100	Static			100		
CL-3	18.3		Impact	88			2	96.3
SR-4	16.5		Impact	131			6	124.3
	24.8	113	Impact	132*	10.5	48		196.5
	22.0	100	Static			100		
CL-4	30.2		Impact	154			6	215.3
When deflection at Load Point δ = 0.6 in. = L/200								
SR-1	13.8	121	Impact	62	8.9	78	1	96.3
	11.4	100	Static	(P_y =10.9K)		100		
CL-1	17.9	140	Impact	18	14.9	117	1	175.7
	12.8	100	Static	(P_y = 11.2K)		100		
SR-3	50.5	185	Impact	105*	37.8	145	2	480.3
	26.0	100	Static			100		
CL-3	230.0		Impact	89**			6	480.3
SR-4	70.0	182	Impact	120**	58.6	152	6	680.7
	38.5	100	Static			100		

* Specimen yielded after this test.

** Specimen buckled or remaining deflection more than 0.6 in.

TABLE 18
COMPARISON OF CALCULATED AND MEASURED PLASTIC MIDSPAN DEFLECTIONS OF THE CLOSED SINGLE RIB SPECIMEN

Test No.	Drop Height	Plastic Midspan Deflections		
		Calculated*	Measured	Ratio
	in.	in.	in.	in.
18	40	.273	1.566	5.85
26	60	.404	2.320	5.70
23	240	3.542	3.233	0.91
38	120	.695	1.928	2.83
39	120	.869	2.368	2.74

* Using Symonds formula (18).

TABLE 19
COMPARISON OF CALCULATED AND MEASURED PLASTIC MIDSPAN DEFLECTION OF THE CLOSED SINGLE RIB SPECIMEN

Test No.	Maximum Impact Force	Plastic Midspan Deflections		
		Calculated*	Measured	Ratio
	K	in.	in.	in.
18	28.47	1.485	1.566	1.05
26	33.31	1.738	2.320	1.33
23	79.38	4.141	3.233	0.78
38	33.74	1.760	1.928	1.10
39	48.15	2.512	2.368	0.94

* Using the formula to calculate midspan deflection of a simply supported beam when loaded by the static ultimate load at its midspan (19).

TABLE 20 SUMMARY OF ATTAINED ENERGY LEVELS IN SINGLE RIB SPECIMEN

Specimen	Drop Height	Test No.	Impact Force at Instant	Attained Maximum Energy (Kips-in.)						Maximum Deflection Reached
				Ultimate Value	Without Yielding	When Yielding Initiated at Ribs				When Failed	
						1	2	3	4		
	in.		Kips								in.
CL-1-1	40	18	27.9		38.8						1.181
	50	25	30.4			59.2					2.486
	240	23	79.4							233.1	3.233
			65.9	415.6							
CL-1-2	120	38	33.7			59.8					1.928
	120	39	48.1							92.3	5.163
			38.5	94.9							5.263
SR-1-1	36	47	18.0		30.3						1.710
			19.8			45.9					2.670
	120	48	24.2							55.9*	4.100
			17.1	108.0							6.500
SR-1-2	20	61	17.9		16.2						1.427
	26	62	18.6			30.4					2.098
	36	66	21.8							47.0*	3.650
			17.7	52.6							5.200

*Buckled.

TABLE 21 SUMMARY OF ATTAINED ENERGY LEVELS IN MULTIRIB SPECIMENS

Specimen	Drop Height	Test No.	Impact Force At Instant	Attained Maximum Energy (Ksi-in.)						Maximum Deflection Reached
				Ultimate Value	Without Yielding	When Yielding Initiated at Ribs				When Failed	
						1	2	3	4		
	in.		Kips								in.
CL-3-1	480	89	94.6		2.4						0.033
			109.6				5.4	5.4			0.062
			184.0			59.2					0.421
			330.8							595.0	2.236
			230.1	1051.9							3.964
SR-3-1	40	103	26.0		X						X
		104	32.4				X				X
		105	33.4		5.7						0.215
			88.2			93.0		93.0		93.0*	1.642
			51.2	135.2							2.233
CL-4-1	8	140	11.1		2.6						0.220
	120	155	22.0				6.0	6.0			0.504
	552	157	138.6			123.7			123.7	123.7	1.442
			56.7	329.1							3.637
SR-4-2	10	108	13.9		3.0						0.252
	10	109	17.5				X				X
	600	120	57.6		14.8						0.285
			61.5				20.8	20.8			0.386
			129.8			194.5			194.5	194.5	2.069
											4.300
SR-4-3	600	133	67.7		23.5						
SR-4-3	600	133	67.7		23.5						0.323
			78.7				35.4	35.4			0.444
			142.3			205.2			205.2	205.2*	1.668
			43.8	477.6							5.76

X displacement device was unattached
* buckled

TABLE 22
THE MOST CRITICAL VALUES* OF THE ATTAINED ENERGY IN DIFFERENT SPECIMENS

Specimens	CL-1	CL-3	CL-4	SR-1	SR-3	SR-4
Cases	(K-in.)					
Elastic	38.8	38.8**	38.8**	23.3	23.3**	23.3**
Yielding Initiated	59.2	59.2**	--	30. **	30. **	30. **
Totally Failed	92.3	595.0	--	47.0	93.0	194.5

* See Paragraph 3.4, also Tables 20 and 21
** Reasoning given in Paragraph 3.4; conclusion item 5.

TABLE 23 IMPACT STRESSES* - CLOSED THREE RIB SPECIMEN

Test No.	Mean Impact Force	Impact		Location	Stresses* Measured by the Gages at Locations (Ksi)							Attained Energy
		Force	Instant									
	K	K	millisec		1	2	3	4	4 tr.	6	7	K- in.
80	-	-	16	1	19.1	3.0	.8	-3.9	+4.7			+
85	6.7	12.6	21	4	26.4	22.9	11.2	-7.4	+8.3			+
		12.8	22	4	26.3	23.0	11.4	-7.4	+8.3			+
86	8.5	13.9	23	2	10.6	33.0	11.7	-6.1				+
		14.5	28		20.1	31.7	19.6	-9.1				
89	157.7	94.6	9	2	0.0	49.6		0.0	-6.6			2.4
		109.6	10		0.0	77.2**		0.0	-9.1			5.4
		184.0	15		49.4			-12.2	-15.5			59.2
		208.5	16		73.9**			-20.2	-14.7			80.1
		307.7	19					-37.2	-6.4			180.9
		308.9	20					-34.8	-0.2			233.5
		315.2	23					-2.7	-23.9			435.4
		330.8	25					0.0	-37.8			595.0
		329.9	26					0.0	-45.7			673.3
		323.0	27						-55.9			745.7

\+ could not be calculated
* unless otherwise specified, longitudinal stresses are given in this table; tr. indicates transversal
** stress values above 60 ksi should only be regarded as an indication of plastic range rather than the stress level reached at that instant
*** position of the loading pad 24 in. long side across the ribs

TABLE 24 IMPACT STRESSES* - SERRATED THREE RIB SPECIMEN

Test No.	Mean Impact Force	Impact		Location	Stresses* Measured by the Gages at Locations (Ksi)							Attained Energy
		Force	Instant									
	K	K	millisec		1	2	3					K- in.
94	7.5	12.7	24	3			33.6	-2.4	+4.0	-5.9	-6.5	+
		14.8	28					-4.0	+5.6	-6.9	-6.3	+
		14.2	29					-4.3	+5.2	-6.7	-6.5	+
95	6.4	11.5	24	5	7.2	22.5		-7.3				+
97	6.9	13.4	23	5				-5.5	+3.9		1.6	3.68
		12.8	25					-5.7	+3.6		1.6	4.19
100	5.9	12.7	37	2		30.4	18.2					3.47
101	8.2	13.3	20	2	15.7	39.6			+6.4			+
102	9.6	16.1	28	2	16.9	49.0			+12.3		+9.2	+
103	13.5	21.5	30	2	15.0	58.5			+17.6		+12.4	+
		17.3	49		17.8	55.7			+12.0		+11.6	+
104	16.4	27.0	30	2	24.2	76.96**			+24.2		+19.6	+
105	37.7	72.8	30	2		175.5**	58.2		+45.2			61.54
		80.2	34			previously yielded	73.3** 107.2**		+40.8 +20.7			93.03 134.98

\+ could not be calculated
* unless otherwise specified, longitudinal stresses are given in this table; tr. indicates transversal
** stress values above 60 ksi should only be regarded as an indication of plastic range rather than the stress level reached at that instant
*** position of the loading pad 24 in. long side across the ribs

TABLE 25 IMPACT STRESSES* - CLOSED FOUR RIB SPECIMEN

Test No.	Mean Impact Force	Impact		Location	Stresses* Measured by the Gages at Locations (Ksi)							Attained Energy
		Force	Instant									
	K	K	millisec		1	2	3	4	5	6	7	K- in.
139***	6.0	9.7	20	5	20.6	19.8	6.9	0.9				1.39
		10.0	21		20.4	19.6	7.3	2.0				1.45
		10.1	22		20.0	19.1	7.4	2.9				1.45
		9.9	24		18.7	17.5	7.2	3.9				-
140	7.1	13.3	12	2	1.1	23.9	0.9	0.0				0.81
		11.1	16		6.9	57.2	6.2	0.8				2.61
		10.3	17		9.3	61.8**	8.3	1.5				2.95
		9.8	19		13.9	64.5**	12.0	3.7				-
		11.4	21		16.0	60.7**	13.9	6.4				-
		13.4	24		11.7	53.7	11.2	9.0				-
									5	5 tr.		
141	6.9	10.5	12	2	1.6	54.6			-1.3	1.5		0.09
		10.2	13		2.7	80.3**			-1.8	1.8		1.24
		9.5	17		9.8	yielded			-4.7	2.5		2.43
		11.0	21		11.6	↓			-5.8	2.0		2.54
											6	
144***	6.4	5.9	8	2	0.1	39.7			-0.4		-0.3	0.00
		7.8	9		0.1	86.7**			-0.6		-0.5	0.01
		10.3	20		11.6	yielded			-7.0		-5.1	1.65
		10.3	21		12.0	↓			-7.1		-5.3	1.65
		10.0	22		11.7				-6.9		-5.4	-

\+ could not be calculated
* unless otherwise specified, longitudinal stresses are given in this table; tr. indicates transversal
** stress values above 60 ksi should only be regarded as an indication of plastic range rather than the stress level reached at that instant
*** position of the loading pad 24 in. long side across the ribs

TABLE 26 IMPACT STRESSES* - CLOSED FOUR SPECIMEN - continued

Test No.	Mean Impact Force	Impact		Location	Stresses* Measured by the Gages at Locations (Ksi)							Attained Energy
		Force	Instant									
	K	K	millisec		1	2	3	4	5	5 tr.	7	K- in.
155	19.2	45.3	30	6	10.6		55.3		-7.6	15.0		10.36
		47.4	31		10.9		57.9**		-7.9	16.0		11.29
		49.4	32		11.7		61.2**		-8.3	16.8		12.51
		51.2	33		13.1		65.0**		-8.8	17.5		13.91
		52.8	34		14.9		70.1		-9.4	18.1		15.22
		55.9	37		21.6		yielded		-11.4	20.3		20.18
		50.8	42		29.0		↓		-14.2	23.3		28.45
		48.7	43		29.2				-14.4	23.1		29.33
156***	29.5	33.8	17		9.2		53.3		-5.0	13.0		10.24
		35.0	18		11.8		59.2		-6.0	14.0		11.98
		45.9	25		20.3		yielded		-10.7	19.4		21.54
		48.0	26		20.0		↓		-10.9	19.7		22.37
		61.4	34		19.1				-11.3	19.6		23.21
		50.9	38		20.9				-12.0	21.6		25.38
		47.7	39		21.9				-12.1	21.4		25.63
			41		23.8				-12.2	19.2		-
			42		24.5		↓		-12.0	17.3		-

\+ could not be calculated
* unless otherwise specified, longitudinal stresses are given in this table; tr. indicates transversal
** stress values above 60 ksi should only be regarded as an indication of plastic range rather than the stress level reached at that instant
*** position of the loading pad 24 in. long side across the ribs

TABLE 27 IMPACT STRESSES* - CLOSED FOUR RIB SPECIMEN - continued

Test No.	Mean Impact Force	Impact		Location	Stresses* Measured by the Gages at Locations (Ksi)							Attained Energy
		Force	Instant		1	2	3	4	5	5 tr.	7	
	K	K	millisec									K- in.
157	56.0	51.9	16	6	8.3		48.7		-6.1	21.6		16.93
		58.3	17		13.3		64.2**		-7.9	24.5		22.49
		138.6	24		57.2**		yielded		-20.4	43.0		123.68
		129.0	25		61.1**				-21.2	48.4		150.66
		114.6	26		64.6**				-22.0	53.5		177.68
		86.1	29		yielded				-26.0	60.2**		244.33
		83.8	30						-28.2	59.3		212.70
		73.7	34						-37.9	45.7		312.24
		57.8	38						-41.8	38.1		328.51
		57.5	40						-40.4	38.5		329.09
		59.6	42						-37.2	37.8		-

\+ could not be calculated
* unless otherwise specified, longitudinal stresses are given in this table; tr. indicates transversal
** stress values above 60 ksi should only be regarded as an indication of plastic range rather than the stress level reached at that instant
*** position of the loading pad 24 in. long side across the ribs

TABLE 28 IMPACT STRESSES*- SERRATED FOUR RIB SPECIMEN

Test No.	Mean Impact Force	Impact		Location	Stresses* Measured by the Gages at Locations (Ksi)							Attained Energy
		Force	Instant									
	K	K	millisec		1	2	4	5	5 tr.	6 tr.	7 tr.	K- in.
107	8.4	12.2	22	5	22.4	25.8	.9					+
		12.9	24		24.6	28.4	1.8					+
		12.2	27		24.9	32.1	3.7					+
		13.6	30		21.5	37.5	4.5					+
		16.1	37		17.4	46.3	-0.01					+
		10.1	47		17.7	59.7	1.4					+
108	7.7	13.0	24	5	21.2	29.0		-5.9	-1.7			2.05
		14.7	27		23.9	41.3		-7.1	-1.4			2.81
		13.9	30		22.3	55.6		-6.7	-0.8			3.16
109	8.2	15.5	30	5		yielded			-2.3	-3.6	1.7	+
		17.9	35					Gage	-2.8	-3.3	1.7	+
		17.5	37					Location	-2.9	-3.6	1.6	+
								3				
111	8.6	13.9	17	2	7.6	68.8**	1.2	7.1				3.45
		15.3	20		15.06	yielded	4.8	12.9				5.11
		15.4	21		17.00		6.5	14.4				5.49
		15.2	22		18.00		8.3	15.4				5.78
		18.3	30		2.3		1.8	9.8				-
		18.7	31		1.0		-0.8	8.7				-
		18.5	32		.6		-3.2	7.6				-

\+ could not be calculated
* unless otherwise specified, longitudinal stresses are given in this table; tr. indicates transversal
** stress values above 60 ksi should only be regarded as an indication of plastic range rather than the stress level reached at that instant
*** position of the loading pad 24 in. long side across the ribs

TABLE 29 IMPACT STRESSES* - SERRATED FOUR RIB SPECIMEN - continued

Test No.	Mean Impact Force	Impact		Location	Stresses* Measured by the Gages at Locations (Ksi)							Attained Energy
		Force	Instant									
	K	K	millisec		1	2	3	4	5	6	7 tr.	K- in.
117	7.0	11.2	21	6	8.3	20.6	21.7	9.7				1.26
		11.3	22		8.6	20.5	22.4	9.7				-
		11.5	24		7.7	20.2	23.2	8.3				-
118	8.6	8.3	12	6	-0.2	5.1				0.9	-2.2	0.00
		11.1	14		0.01	9.5				0.5	-2.4	0.31
		12.1	18		3.1	20.5				-1.6	-1.1	1.23
		15.7	25		11.1	30.3				-5.0	-0.2	2.76
		16.3	27		10.4	29.9				-5.0	-0.6	2.81
		17.1	32		4.6	24.9				-3.8	-1.0	-
								6	6 tr.	7	7 tr.	
119	8.2	15.6	21	6		26.7		-2.3	0.4	-4.6	2.8	+
		17.7	23			28.3		-3.1	0.5	-5.2	2.5	+
		18.5	25			27.9		-3.4	0.3	-5.5	1.7	+
		17.1	28			25.7		-2.9	-0.01	-4.9	1.1	+
								6	6 tr			
132	10.1	13.9	22	6		26.7	29.7	+0.01	1.7			2.83
		25.1	47			52.2	37.6	-3.6	4.8			7.24
		24.8	48			52.3	36.7	-3.6	4.6			7.36

\+ could not be calculated
* unless otherwise specified, longitudinal stresses are given in this table; tr. indicates transversal
** stress values above 60 ksi should only be regarded as an indication of plastic range rather than the stress level reached at that instant
*** position of the loading pad 24 in. long side across the ribs

TABLE 30 IMPACT STRESSES* - SERRATED FOUR RIB SPECIMEN - continued

Test No.	Mean Impact Force	Impact		Location	Stresses* Measured by the Gages at Locations (Ksi)							Attained Energy
		Force	Instant									
	K	K	millisec		1	2	3	4	5 tr.	6	7	K- in.
120	58.6	57.6	14	6	2.0	42.4			5.7	3.0		14.78
		61.5	15		2.7	62.6**			7.7	2.9		20.80
		127.2	23		47.2	yielded			47.4	18.0		166.19
		129.8	24		51.0				66.7**	22.2		194.59
		-	26		60.4**				yielded	29.4		
		-	27		75.6**					32.8		
		-	32		yielded					44.7		
		-	34							41.0		
										6	6 tr.	
126***	5.2	8.7	23	6	7.2	23.0				-5.3	8.5	1.42
		8.7	25		8.0	22.0				-5.5	8.4	-
										6		
133	51.1	56.8	14	6		42.6	48.9			-2.5		8.84
		67.7	15			65.2**	58.1			-3.3		14.64
		78.7	16			yielded	67.1**			-3.4		23.49
		142.3	22							34.3		167.47
		67.7	28							40.3		341.10

\+ could not be calculated
* unless otherwise specified, longitudinal stresses are given in this table; tr. indicates transversal
** stress values above 60 ksi should only be regarded as an indication of plastic range rather than the stress level reached at that instant
*** position of the loading pad 24 in. long side across the ribs

TABLE 31 COMPARISON OF STRESSES AT SINGLE RIB SPECIMEN

Specimen	Loading		Time after Impact	Stress Measured at Midspan Section		Attained Energy at that Instant
	Static	Impact		Bottom Gage	Top Gage	
	K	K	millisecond	Ksi	Ksi	K-in
CL-1-1	10.6 (6,p.141)	P_{mean}=7.0	-	35.3	-21.4 at center line	
Test no. 6		10.5	23	19.2	-4.7 one inch from the	6.86
		10.9	27	21.2	-4.5 edge of the top plate	8.40
SR-1-1	9.3 (6,p.183)	P_{mean}=7.4	-	32.5	-15.0 at center line	
Test no. 53		11.9	21	49.3	-17.2	9.46
		10.5	23	50.3	-17.1 at serrated side	9.96
SR-1-2	9.3	P_{mean}=8.0		32.5	-15.0 at center line	
Test no. 68		11.2	30	64.4	-23.8	10.96
		12.8	32	63.0	-24.0 at serrated side	11.09

TABLE 32 COMPARISON OF STRESSES IN SERRATED THREE RIB SPECIMENS

Test No.	Loading	Pad	Load Location	Load	Instant	Rib Stresses (Ksi)				Displacement Under Load	Attained Energy
				K	Millisec.	1	2	3	4	in.	K-in.
P1-E1	Static a)	24"x10"	4	16.0	-	23.7	28.7	5.8			
P1-E1	Static b)	24"x10"	5	16.0	-	5.1	22.5	29.8		.27	
95	Impact	10"x24"	5	11.5	24	7.2	22.5	-		-	+
P1-E1	Static c)	24"x10"	2	16.0	-	13.0	29.0	13.3		.28	
P1-E1	Static d)	24"x10"	2	16.0	-	7.8	33.0	8.6		.32	
100	Impact	10"x24"	2	12.7	37		30.4	18.2		.18	3.47
101	Impact	10"x24"	2	13.3	20	15.7	39.6			not recorded	+
102	Impact	10"x24"	2	16.1	28	16.9	49.0				+
103	Impact	10"x24"	2	21.5	30	16.0	58.5				+
				17.3	49	17.8	55.7				+
104	Impact	10"x24"	2	27.0	30	24.2	yielded				+
105	Impact	10"x24"	2	72.8	30		yielded	58.2		1.24	61.54
				80.2	34		yielded	yielded		1.64	93.03

+ could not be calculated

TABLE 33 COMPARISON OF STRESSES IN SERRATED FOUR RIB SPECIMENS

Test No.	Loading	Pad	Load Location	Load	Instant	Rib Stresses (Ksi)				Displacement Under the Load	Attained Energy
				K	millisec	1	2	3	4	in.	K-in.
P2-E1	Static a)	24"x10"	2	16.3	-	10.7	31.9		3.4	-	-
107	Impact	10"x24"	5	12.9	24	24.6	28.4	-	1.8		
				12.2	27	2 .9	32.1	-	3.7		
				13.6	30	21.5	37.5	-	4.5		
				10.1	47	17.7	59.7	-	1.4		
111	Impact	10"x24"	2	13.9	17	7.6	yielded	7.1	1.2	.26	3.45
				15.2	22	18.0	in test	15.4	8.3	.41	5.78
							no. 109				
P2-E1	Static b)	24"x10"	6	16.0		4.5	21.5	24.9	5.5	.25	
126	Impact	24"x10"	6	8.7	23	7.2	23.0			.17	1.37
				8.7	25	8.0	22.0			.18	1.42
P2-E1	Static c)	10"x24"	6	16.0		4.6	19.2	24.0	5.5	.27	
117	Impact	10"x24"	6	11.3	22	8.6	20.5	22.4	9.7	.14	1.2
118	Impact	10"x24"	6	15.7	25	11.1	30.3	-	-	.23	2.8
120	Impact	10"x24"	6	57.6	14	2.0	42.4	-	-	.29	20.8
				61.5	15	2.7	yielded	-	-	.39	28.0
				127.2	23	47.2		-	-	1.81	166.2
				129.8	24	yielded		-	-	2.07	194.6

TABLE 34 RATIO OF SPECIMEN MASS TO THE IMPACTING MASS

Specimen	Weight lbs/ft	Specimen Weight* lbs	Additional Weight**	Total Weight (3) + (4)	Half of Specimen & Additional Weight	Ratio 1 6/9	Ratio 2 5/9	Weight of the Impacting Mass
1	2	3	4	5	6	7	8	9
CL-I-1 CL-I-2	23.60	236	286	522	404	.3375	.4361	1197
SR-I-1 SR-I-2	21.05	210	286	496	391	.3266	.4144	1197
CL-III-1	114.20	1142	286	1428	857	.7160	1.1930	1197
SR-III-2	106.55	1066	286	1352	819	.6842	1.1290	1197
CL-IV-1	153.12	1531	286	1817	1052	.8788	1.5180	1197
SR-IV-2 SR-IV-3	142.92	1429	286	1715	1001	.8363	1.4330	1197

* 10 foot length span without supports.

** (steel load distributing pad, confining pipe, plunger, cushioning)

FIGURES

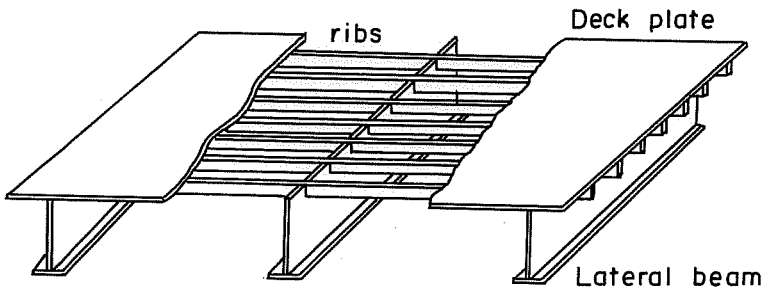

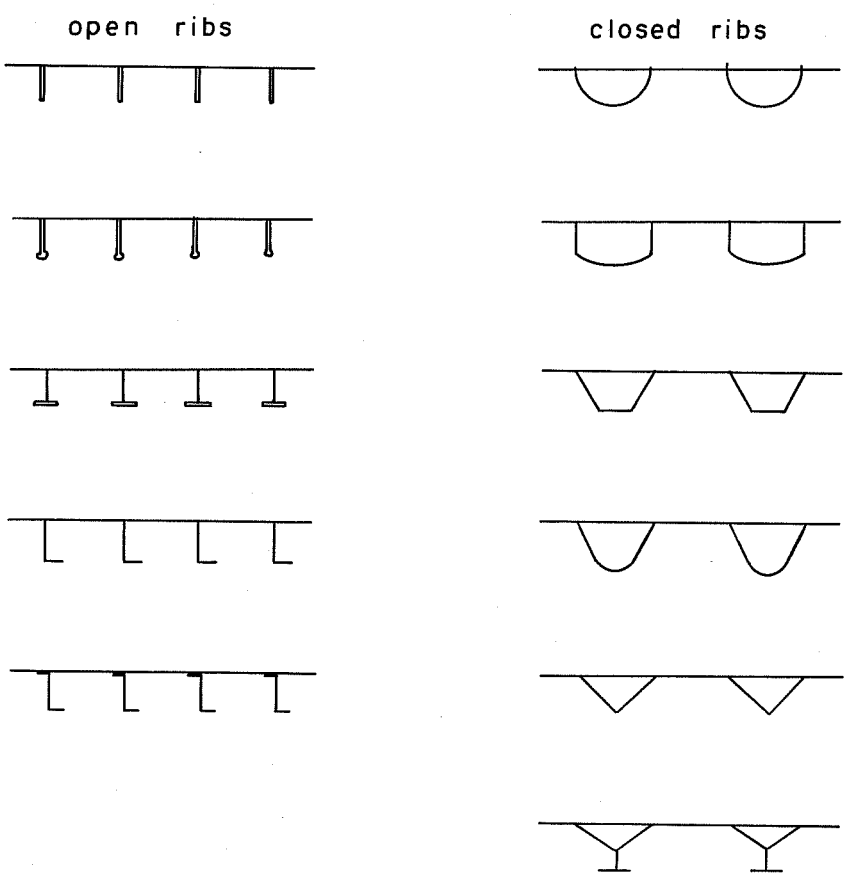

Fig. 1 Orthotropic Steel Plate and Developed Rib Forms

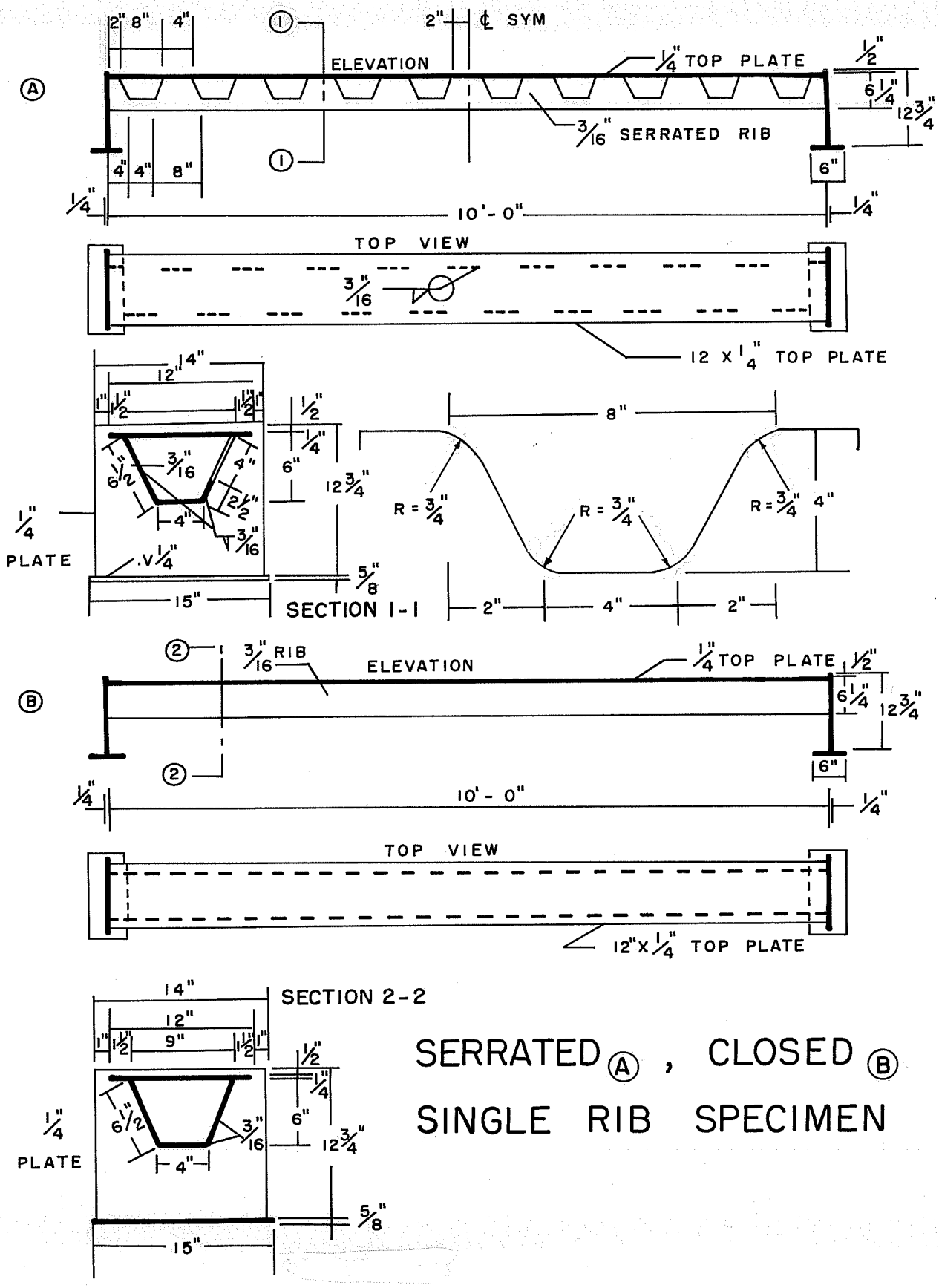

Fig. 4 Detail of the Single Rib Specimens

CLOSED THREE-RIB SPECIMEN

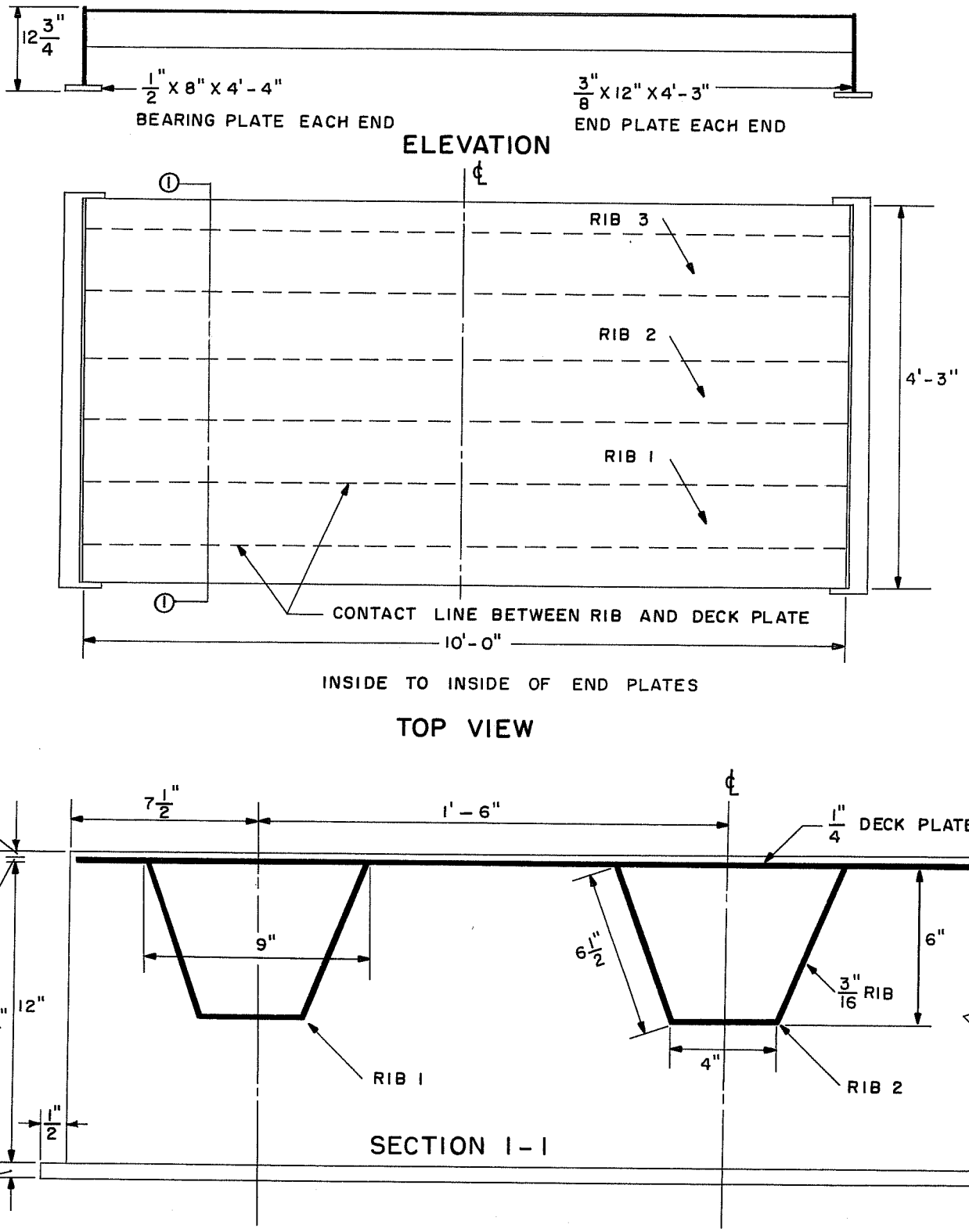

Fig. 5 Detail of the Closed Three Rib Specimen

SERRATED THREE-RIB SPECIMEN

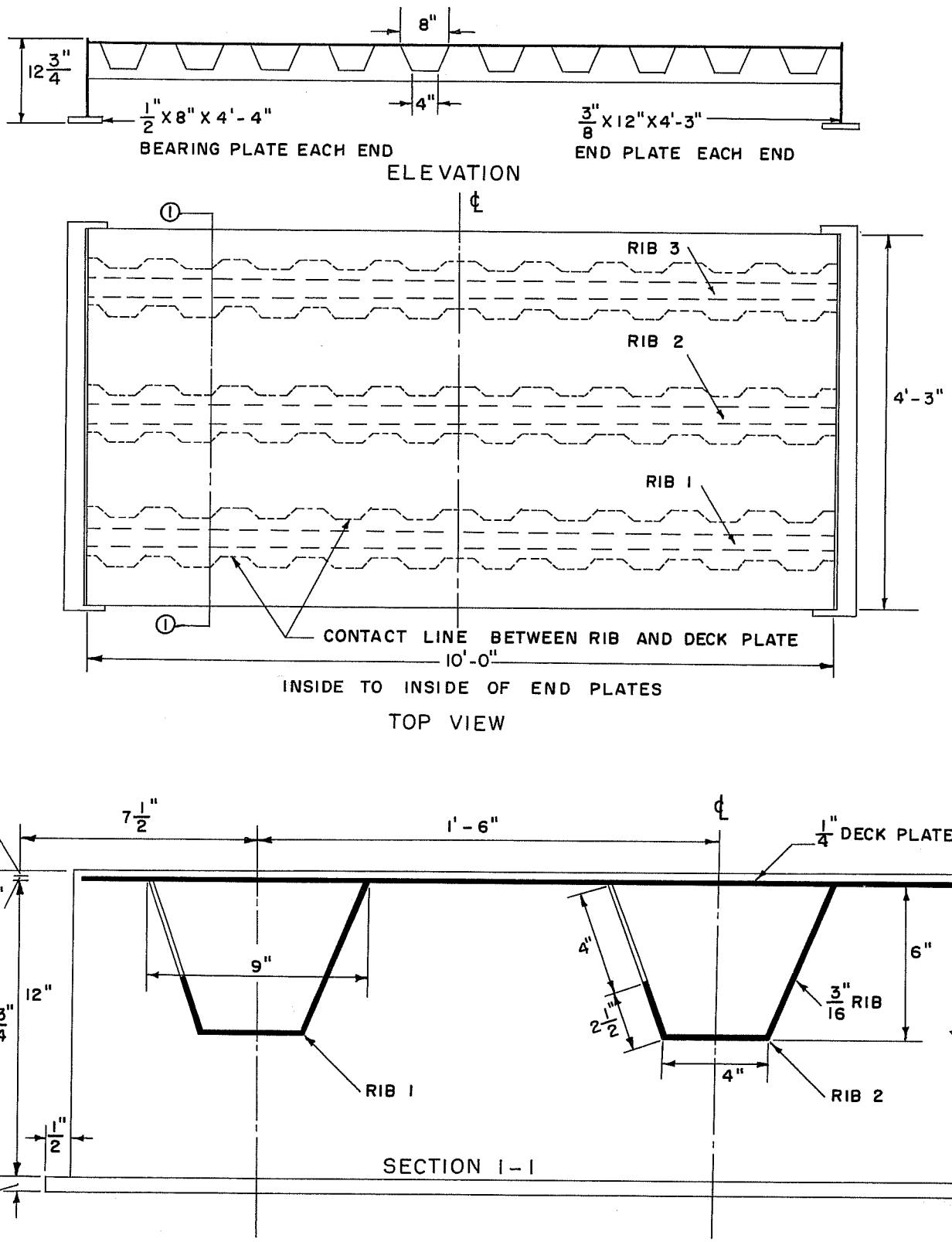

Fig. 6 Detail of the Serrated Three Rib Specimen

CLOSED FOUR-RIB SPECIMEN

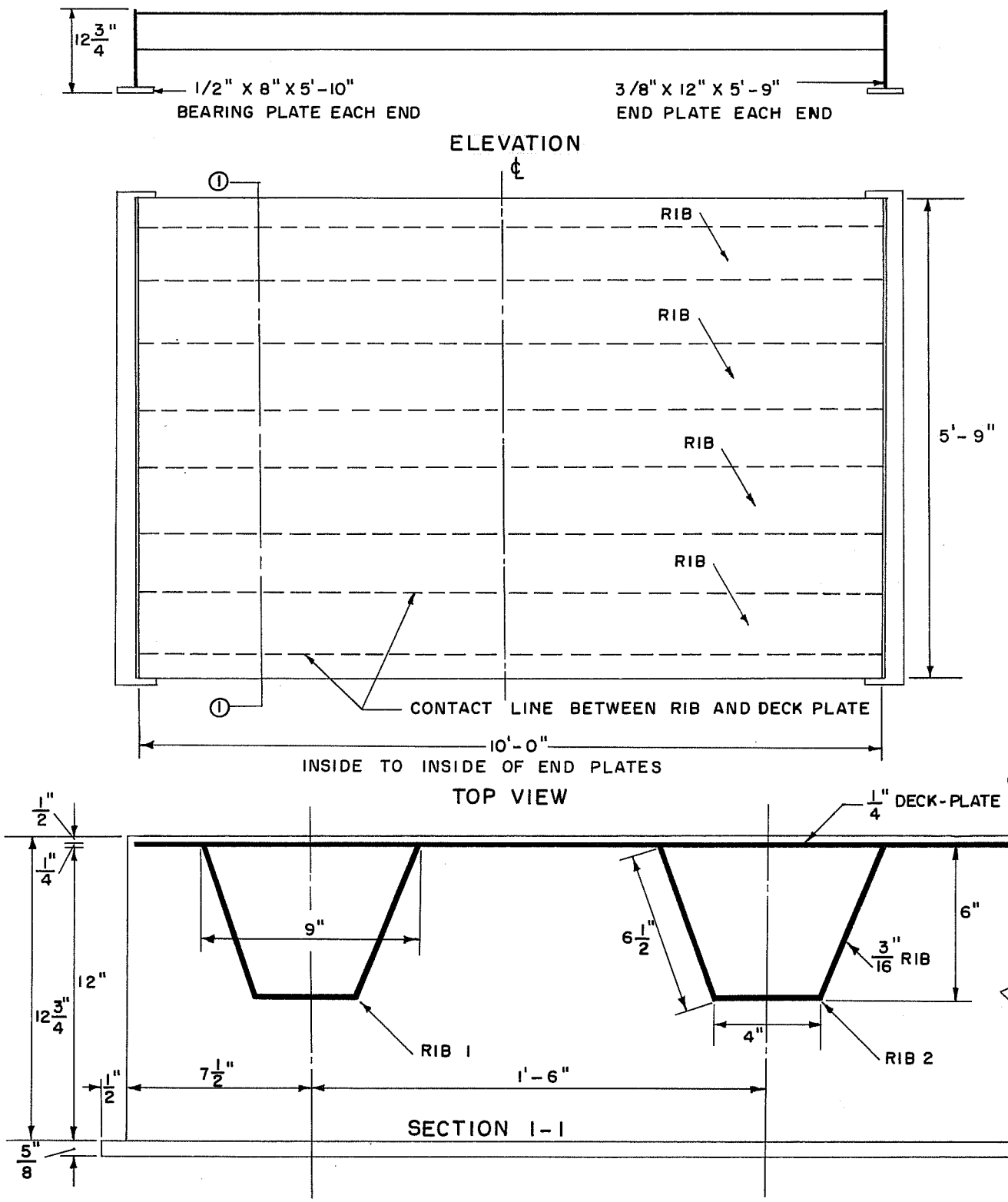

Fig. 7 Detail of the Closed Four Rib Specimen

SERRATED FOUR-RIB SPECIMEN

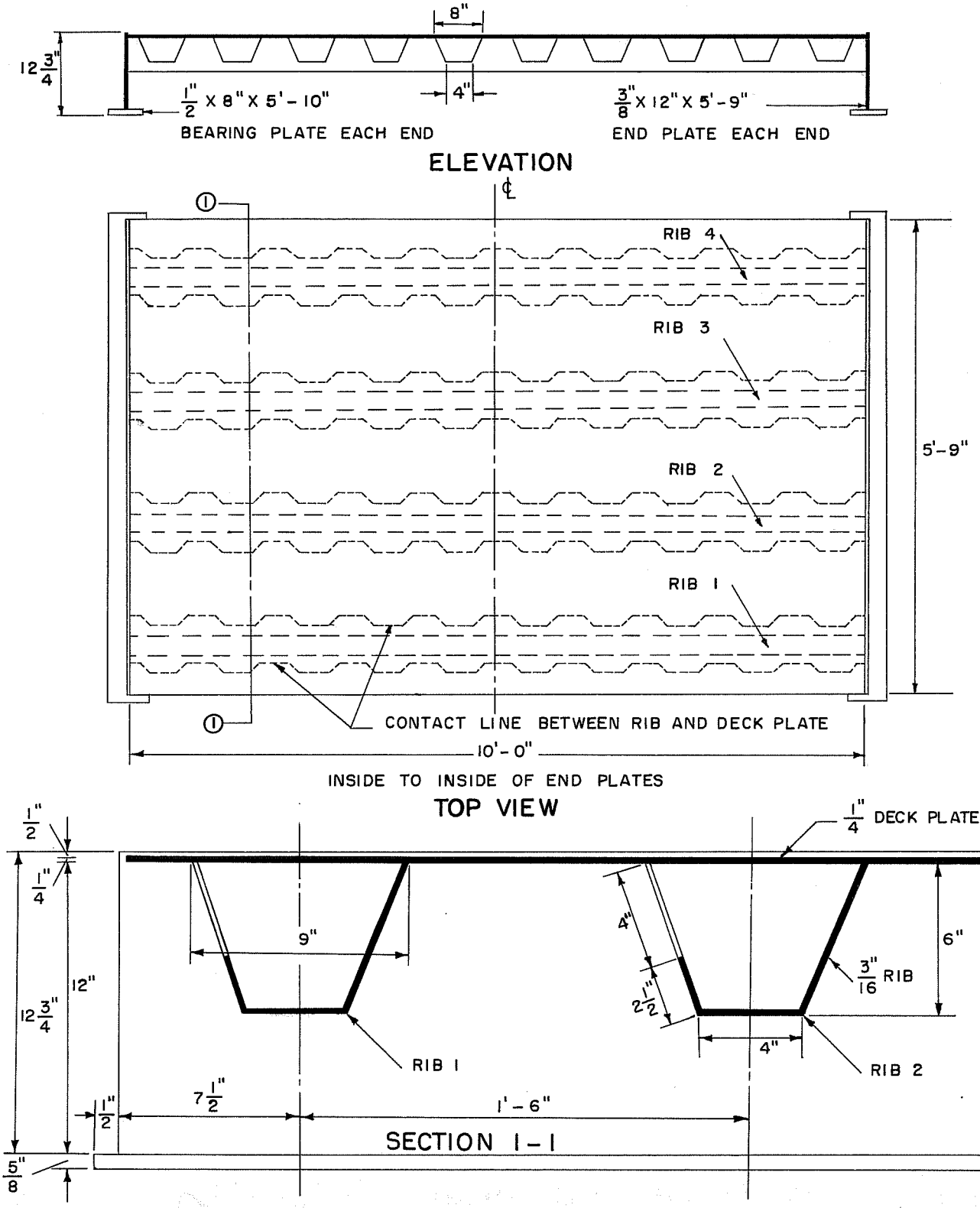

Fig. 8 Detail of the Serrated Four Rib Specimen

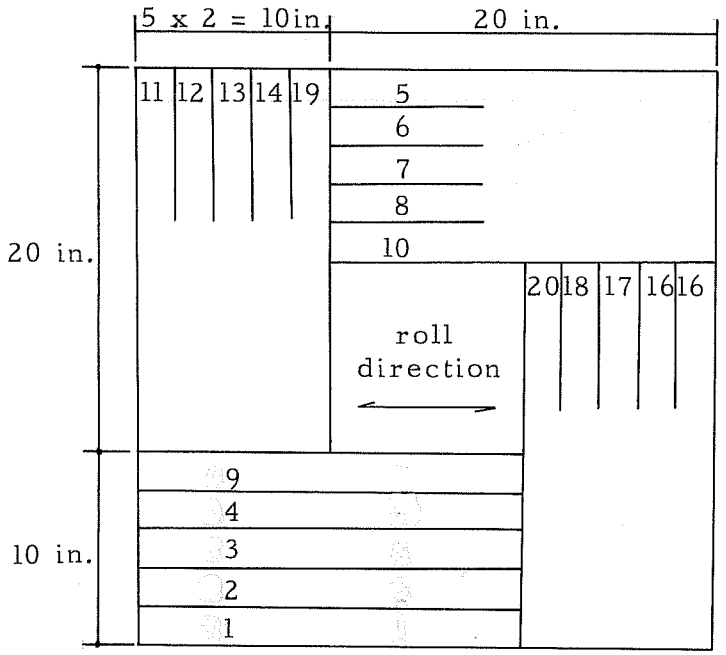

No. 1 to 10 coupons parallel to the roll direction
(9, 10 one side flame cut)

No. 11 to 20 coupons perpendicular to the rolling
(19, 20 one side flame cut)

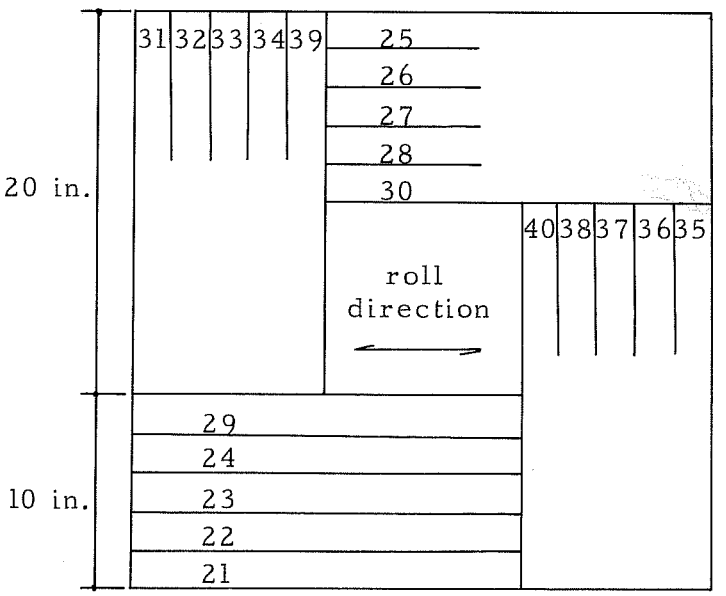

No. 21 to 30 coupons parallel to the roll direction

No. 31 to 30 coupons perpendicular to the rolling

Fig. 11 Pattern and Numbering of the Coupon Cut

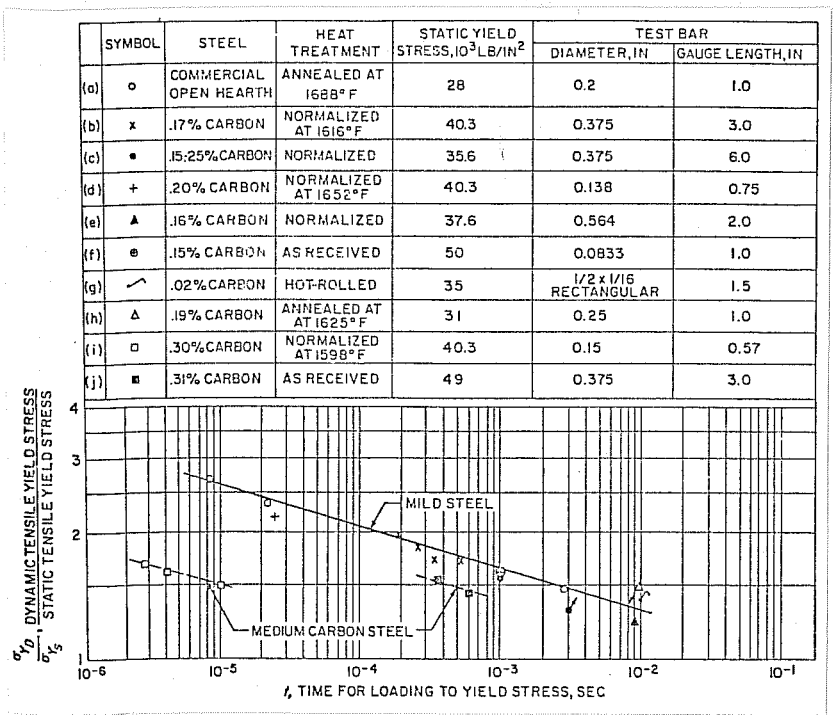

Fig. 12 Ratio of Dynamic and Static Tensile Yield Stress as a Function of Loading Time for Mild and Medium Carbon Steel

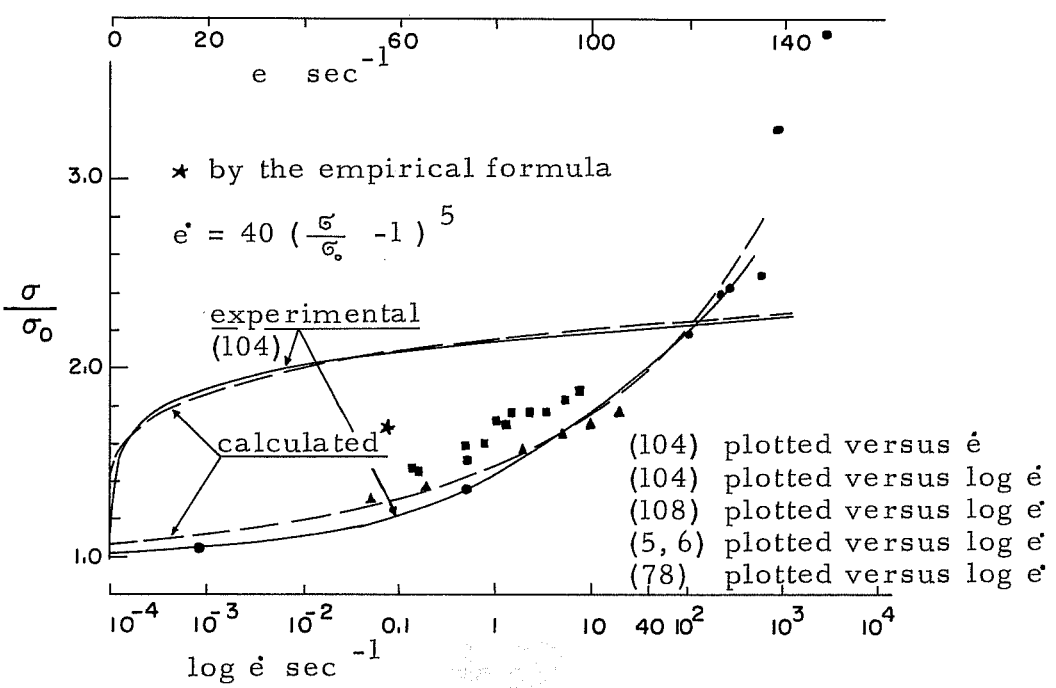

Fig. 13 Dependence of the Lower Yield Stress of Mild Steel on the Strain Rate

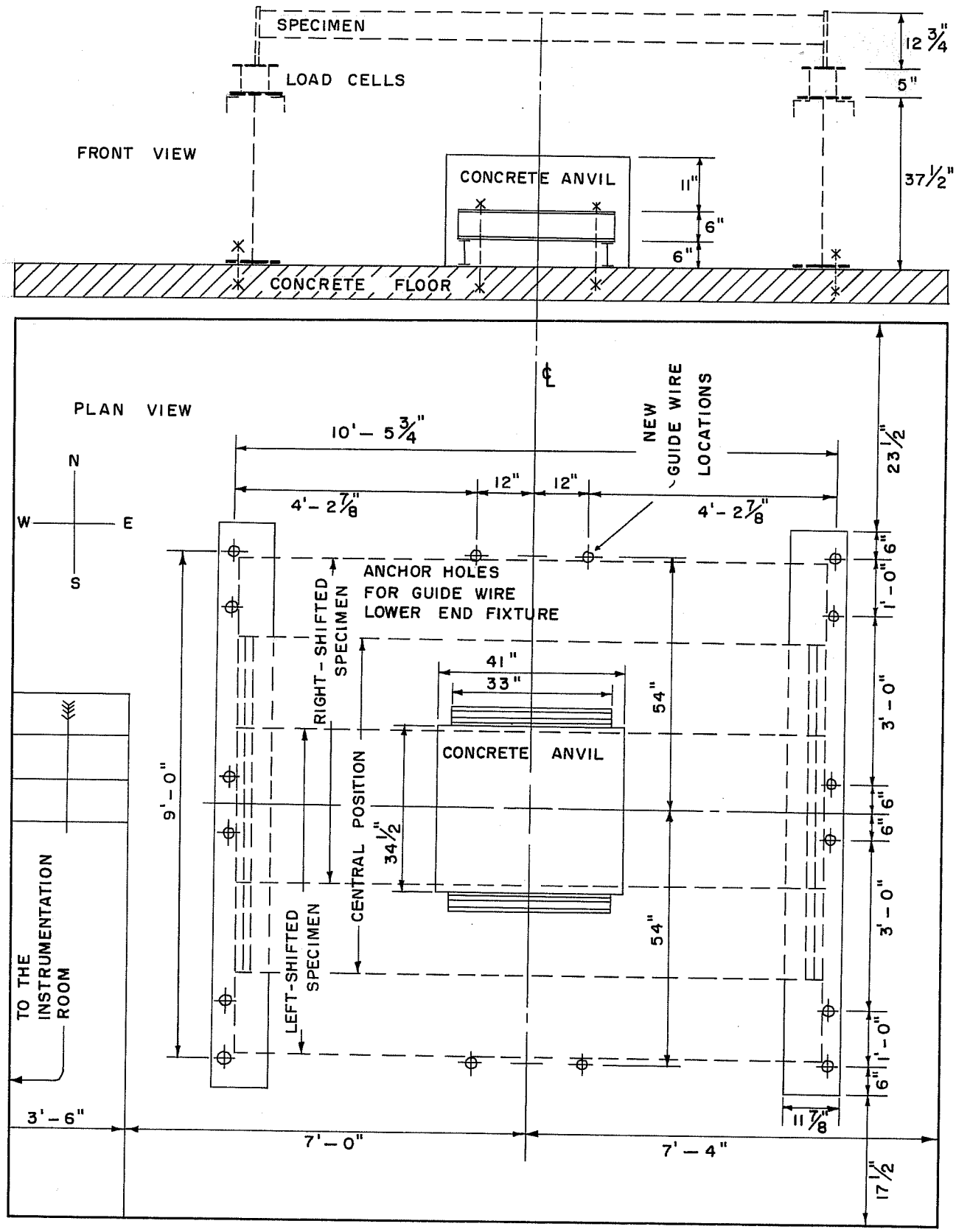

Fig. 18 The Test Site

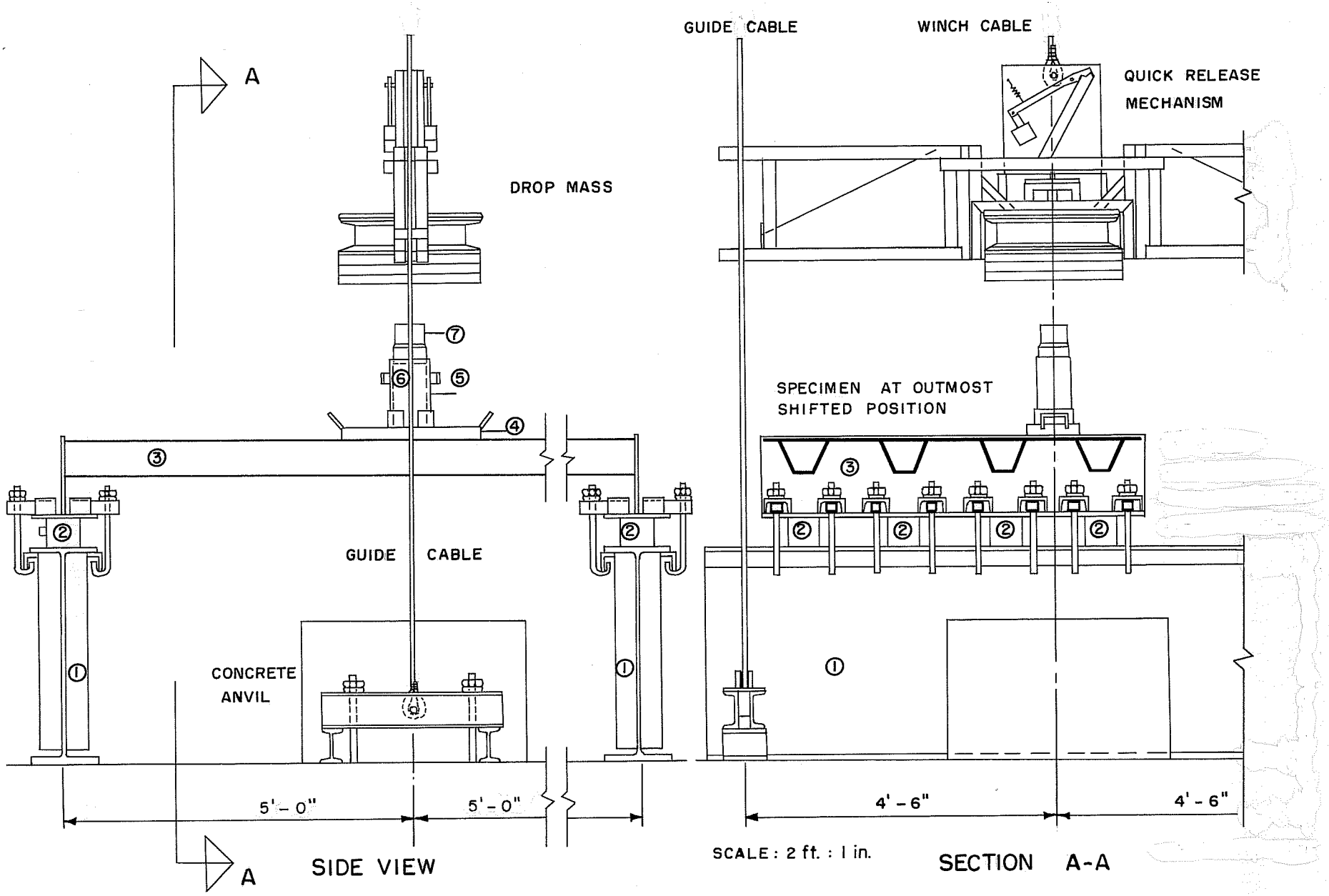

Fig. 19 Test Set-up

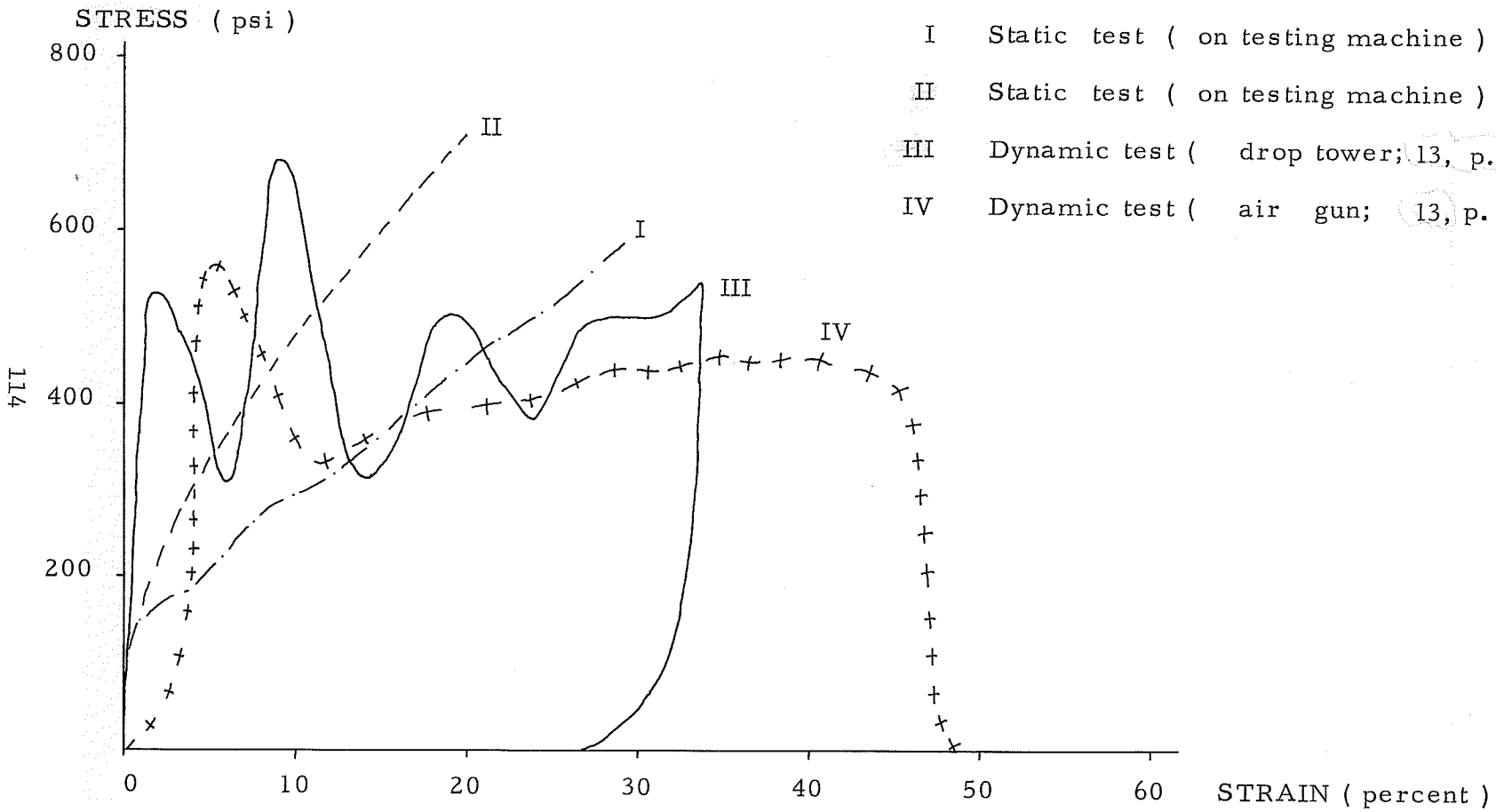

Fig. 20 Static and Dynamic Stress - Strain Curves of the Vermiculite Cushioning Material

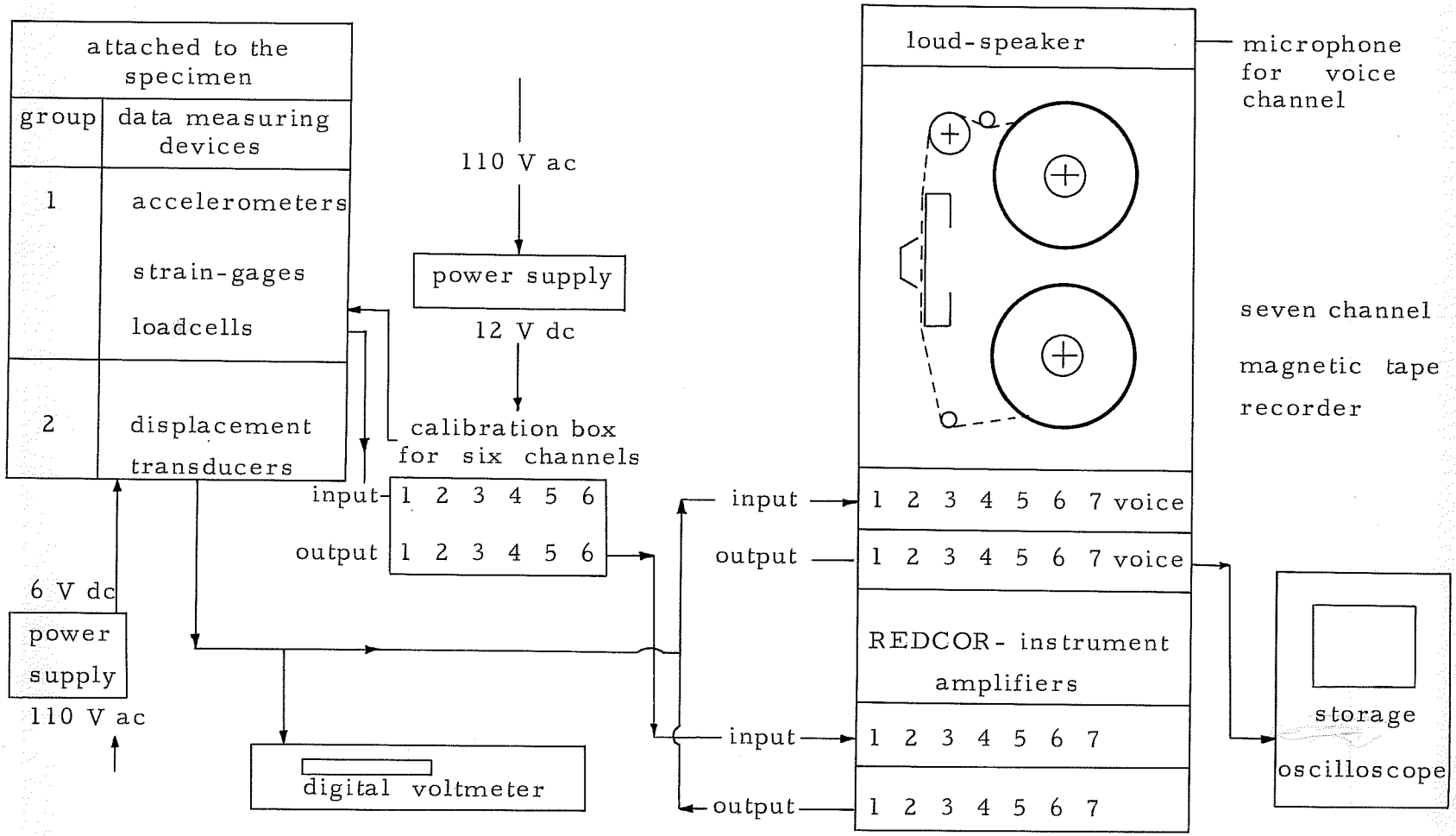

Fig. 21 Schematic representation of the data measuring recording instruments

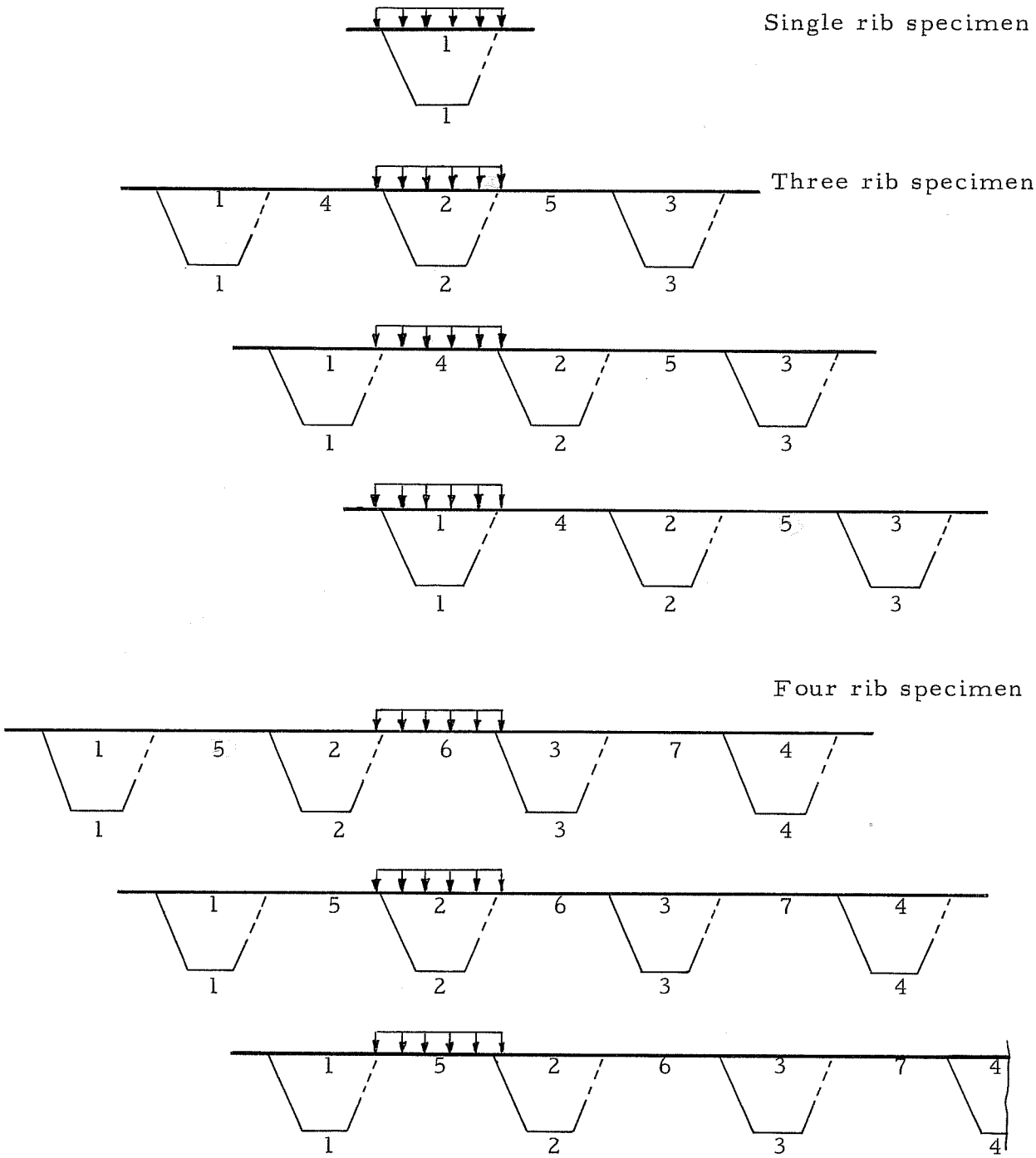

Fig. 26 Impact positions and the numbering of instrument locations

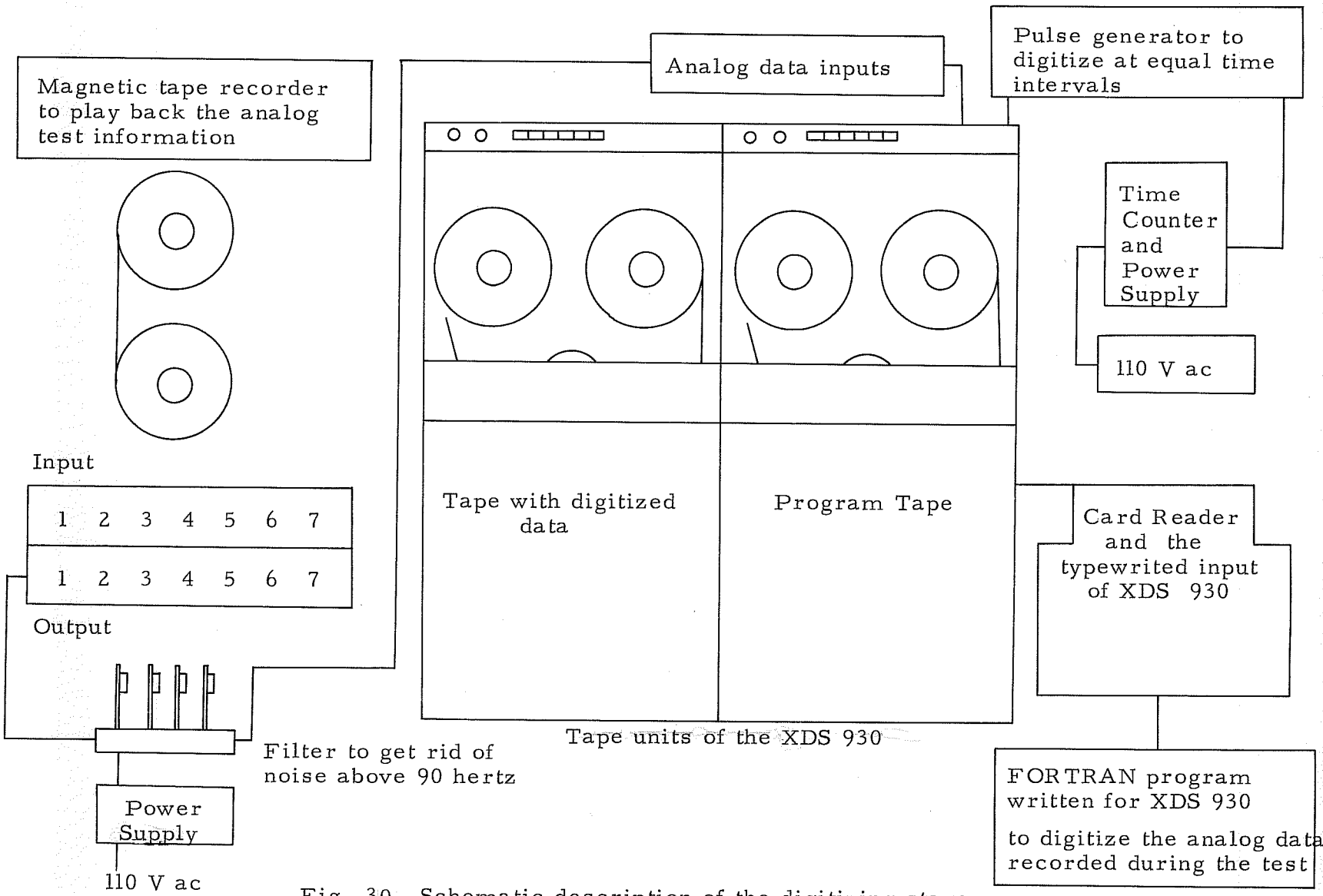

Fig. 30 Schematic description of the digitizing stage

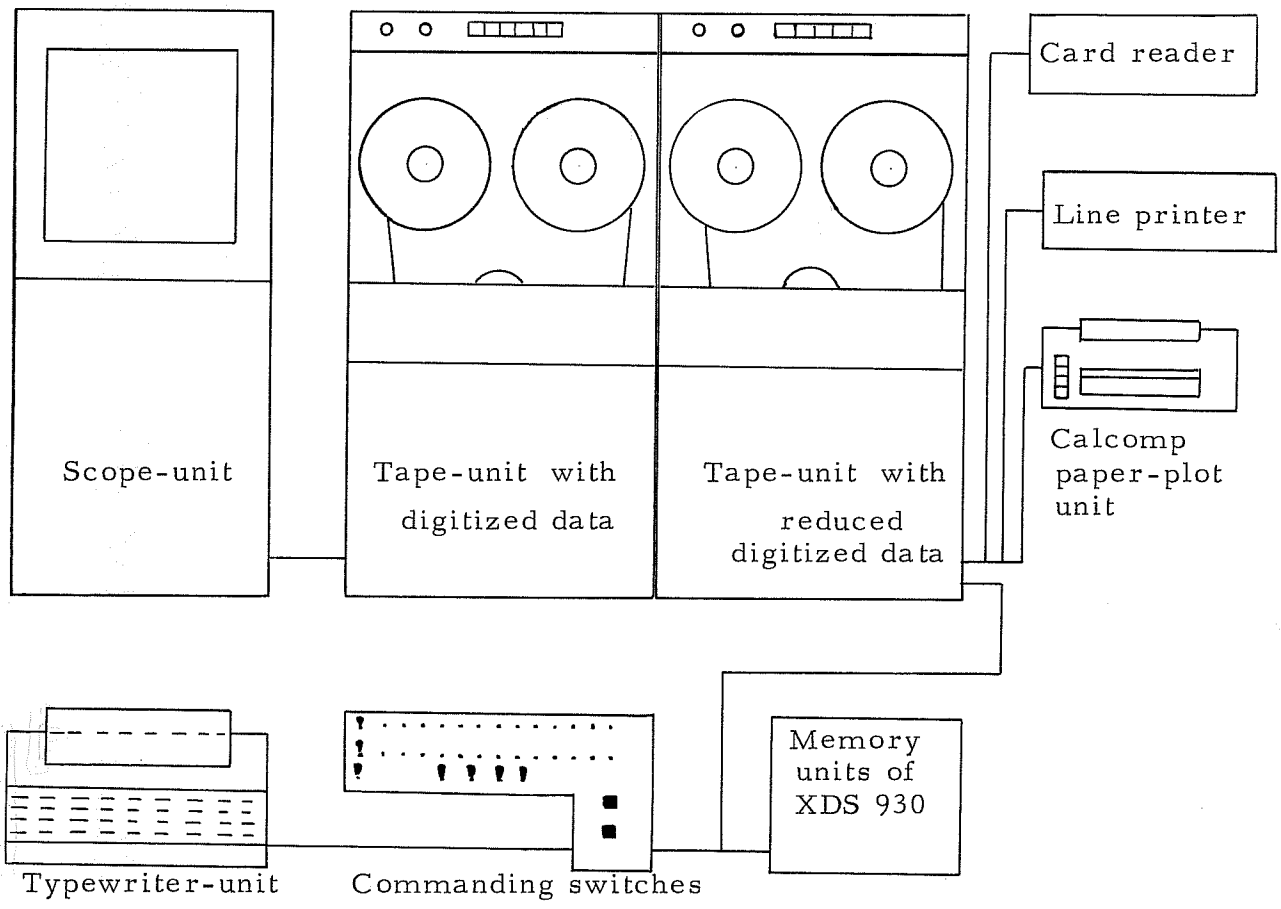

FORTRAN PROGRAM

1. to read information from digitized tape
2. to display the data for each channel of record on the scope
3. to shift the location of the data begin-point to the right of left side of the scope
4. to stretch or compress the figure shown on the scope keeping the beginning point the same
5. to plot the figure shown on the scope using the calcomp-unit
6. to write the same data on a tape
7. to print the same data on line printer

Fig. 33 Schematic Description of the First Step Data Reduction on the XDS 930

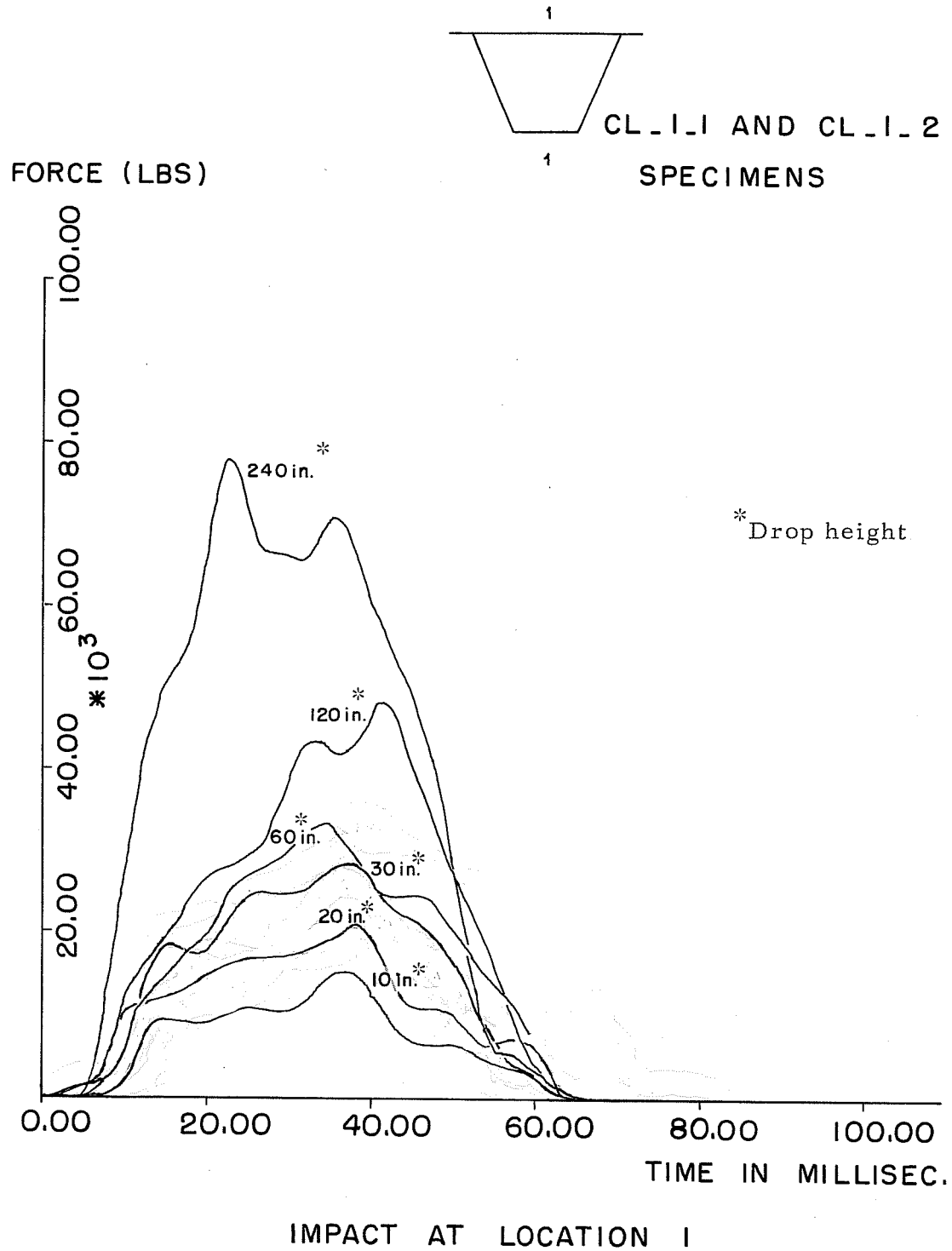

Fig. 34 Impact Force / Time relations obtained on closed single rib specimens

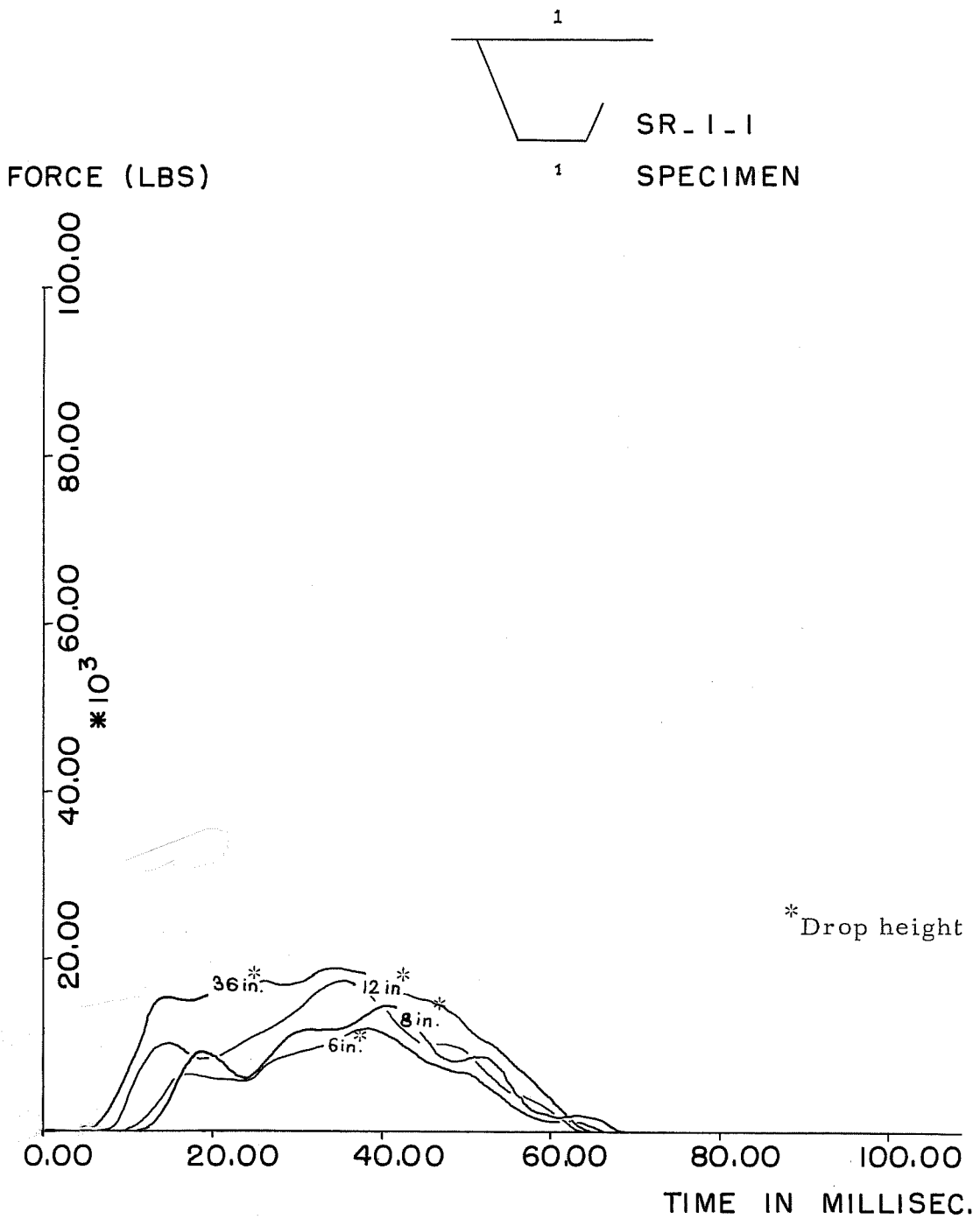

Fig. 35 Impact Force / Time relations obtained on biserrated single rib specimen

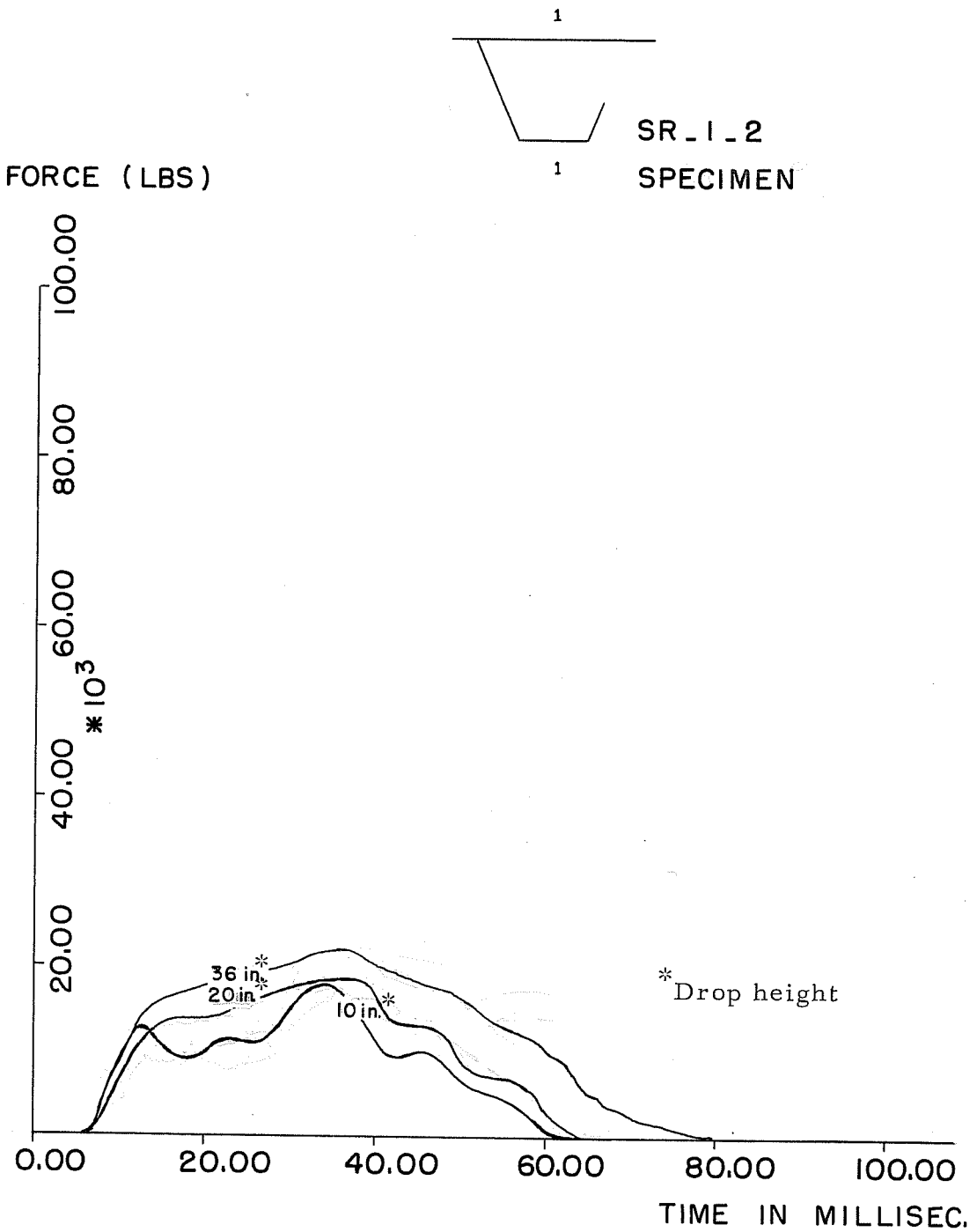

Fig. 36 Impact Force / Time realtions obtained on biserrated single rib specimen

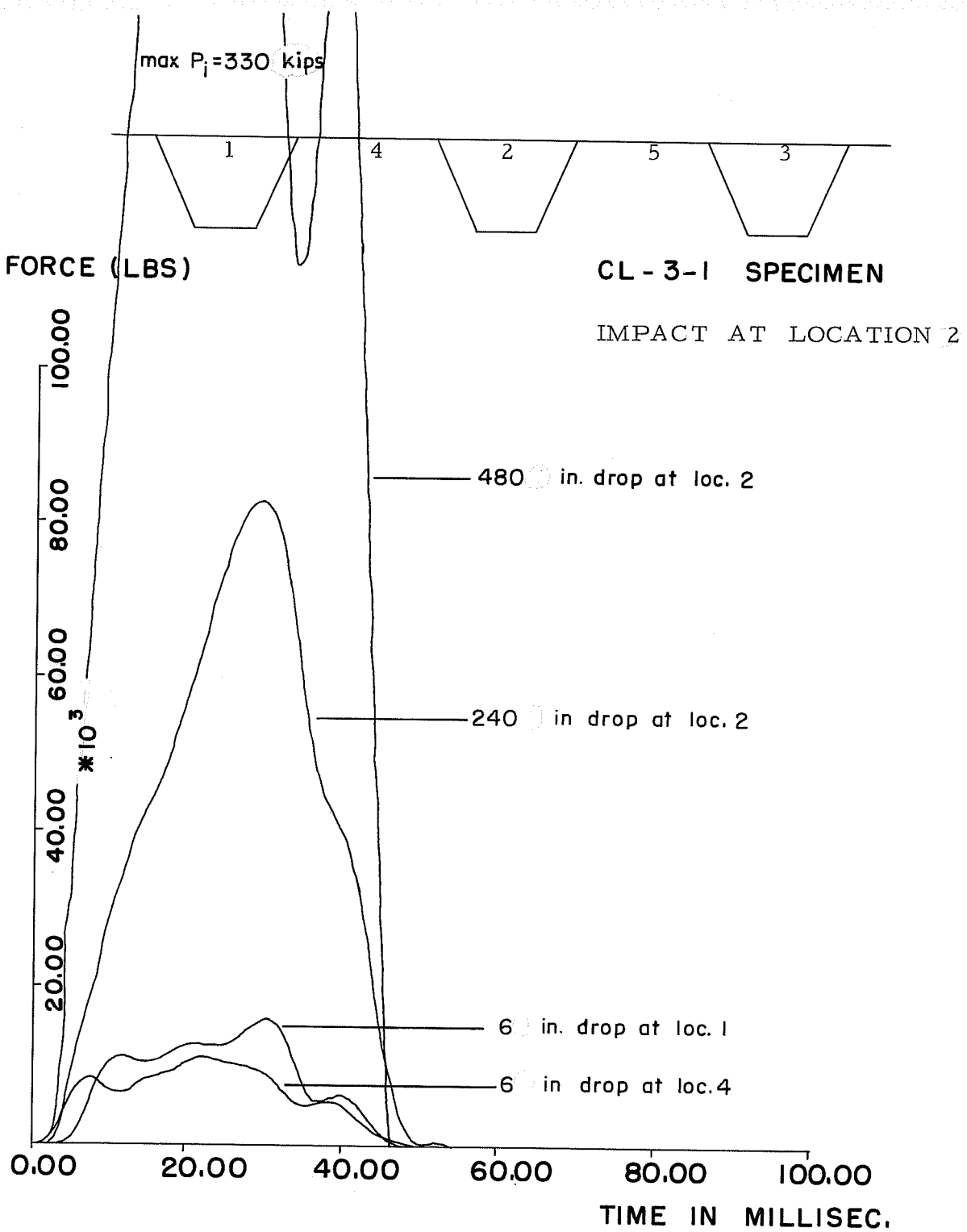

Fig. 37 Impact Force / Time relations obtained on closed three rib specimen

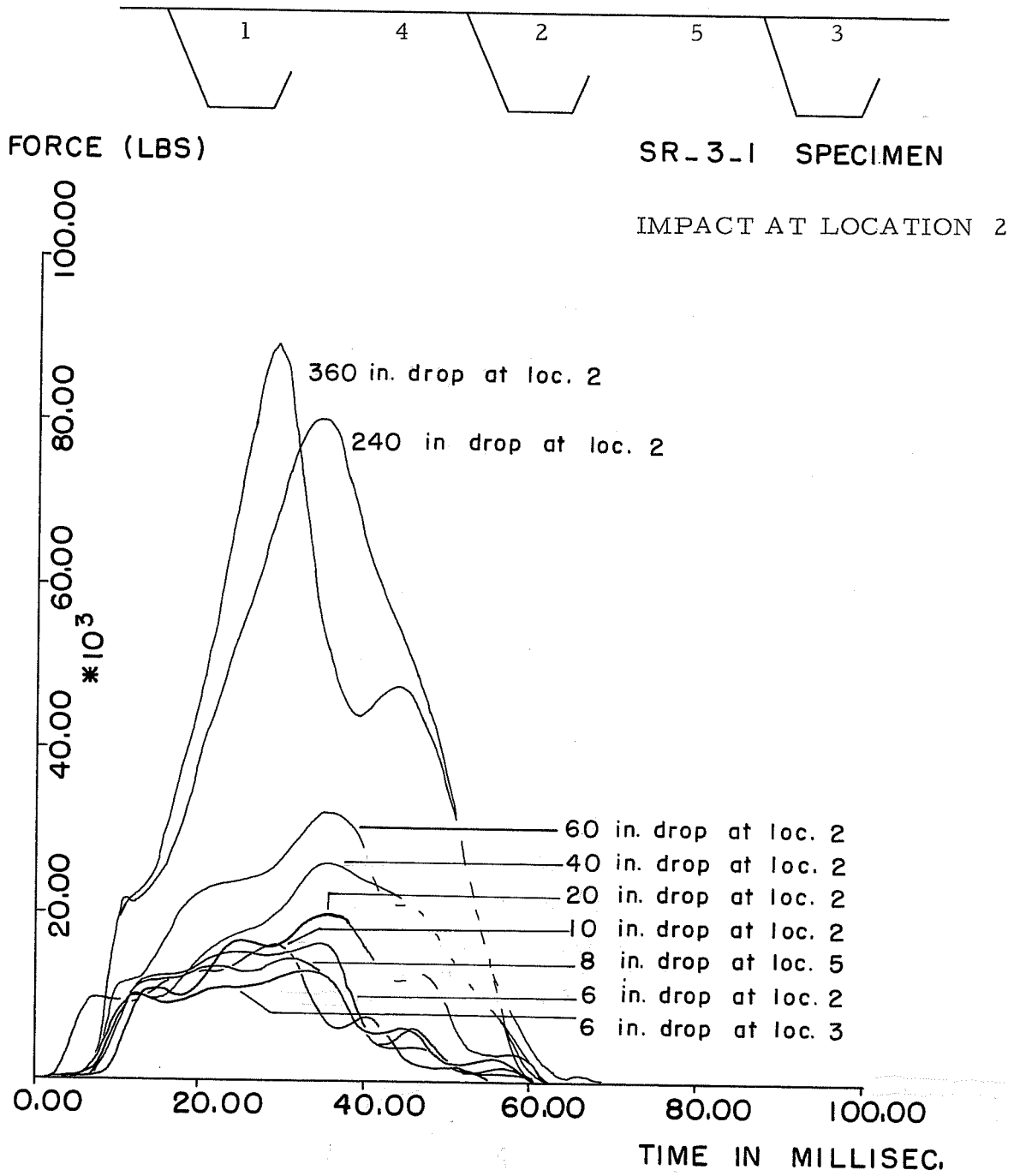

Fig. 38 Impact Force / Time relations obtained on biserrated three rib specimen

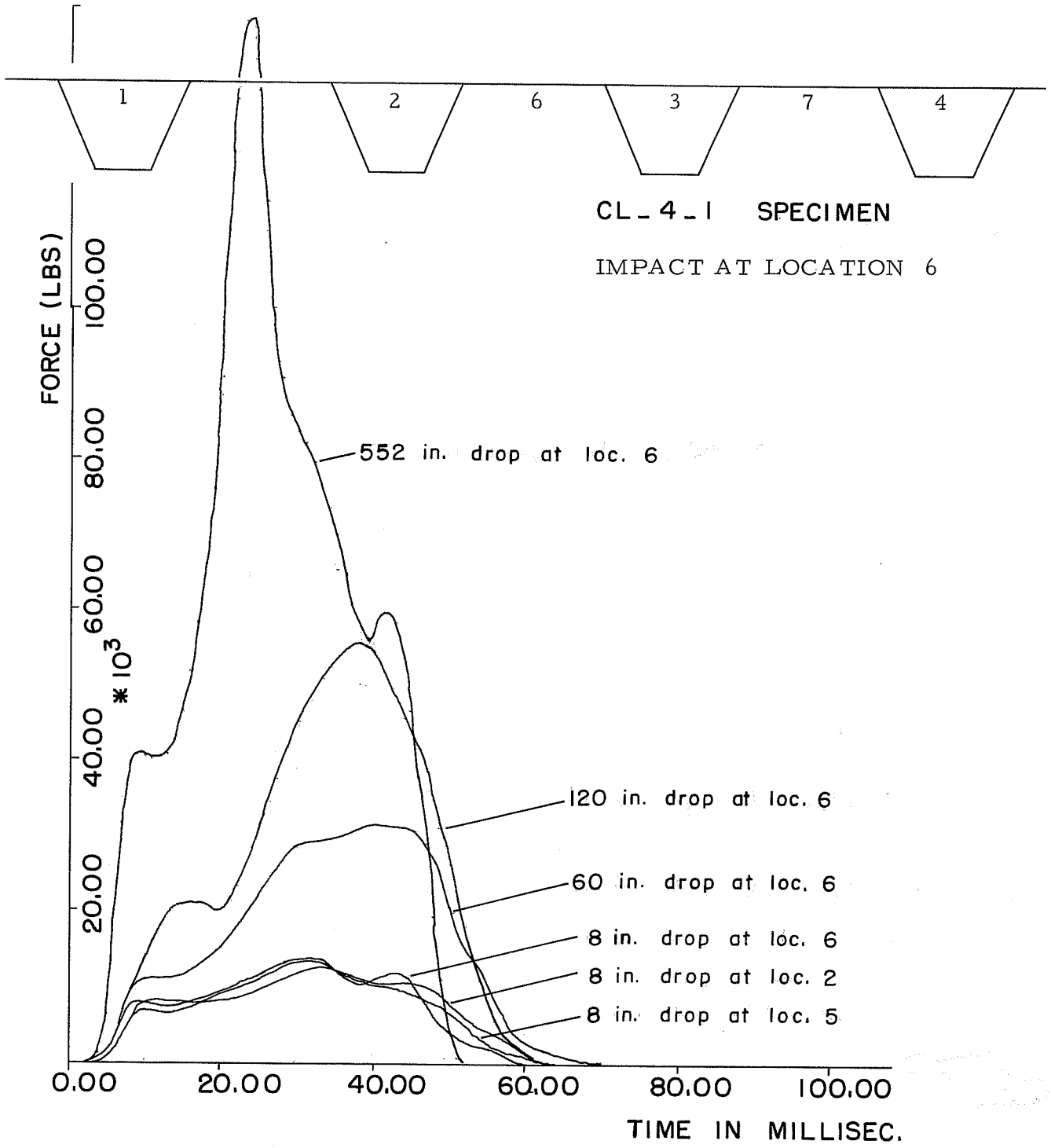

Fig. 39 Impact Force / Time relations obtained on closed four rib specimen

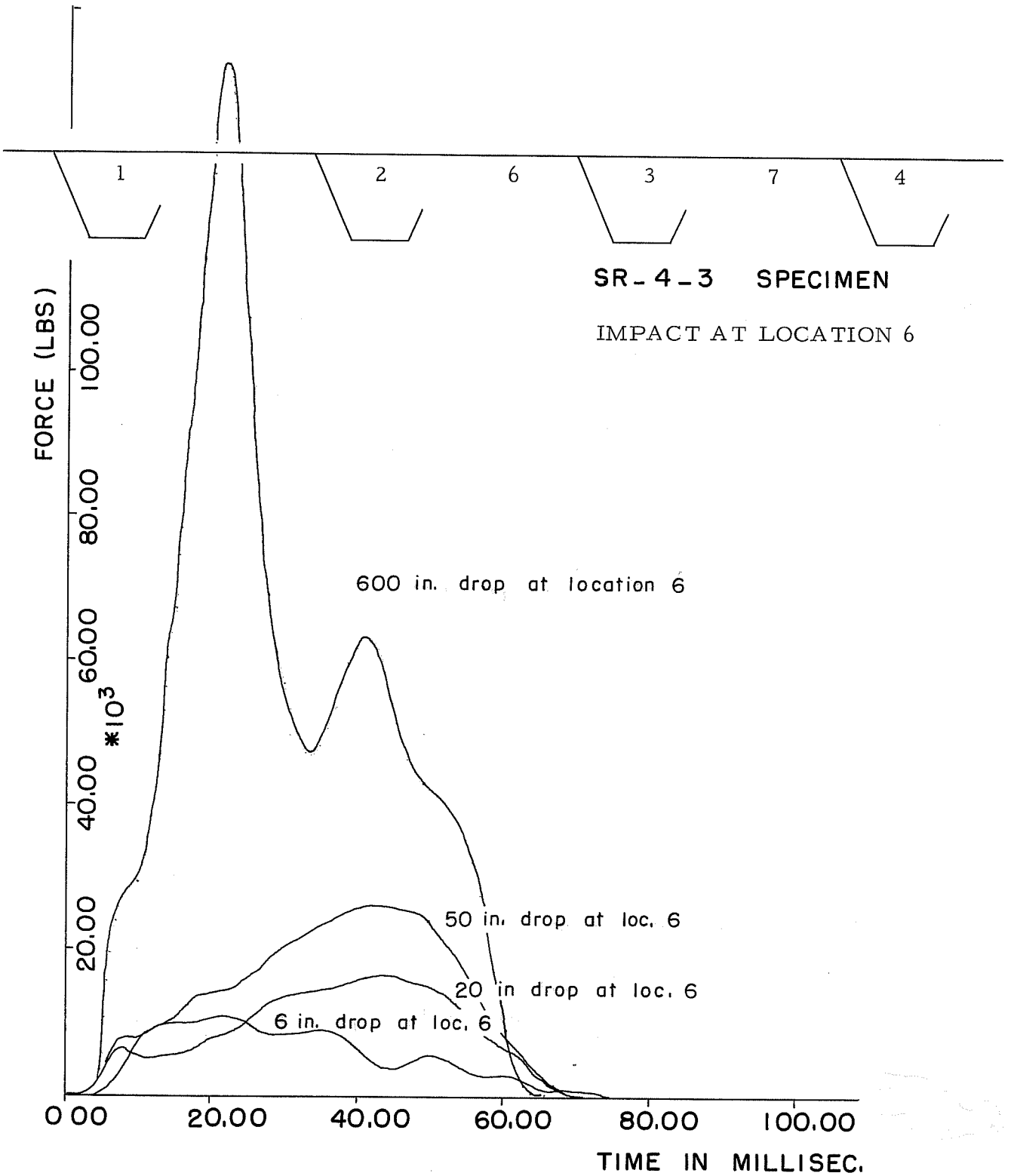

Fig. 40 Impact Force / Time relations obtained on biserrated four rib specimen

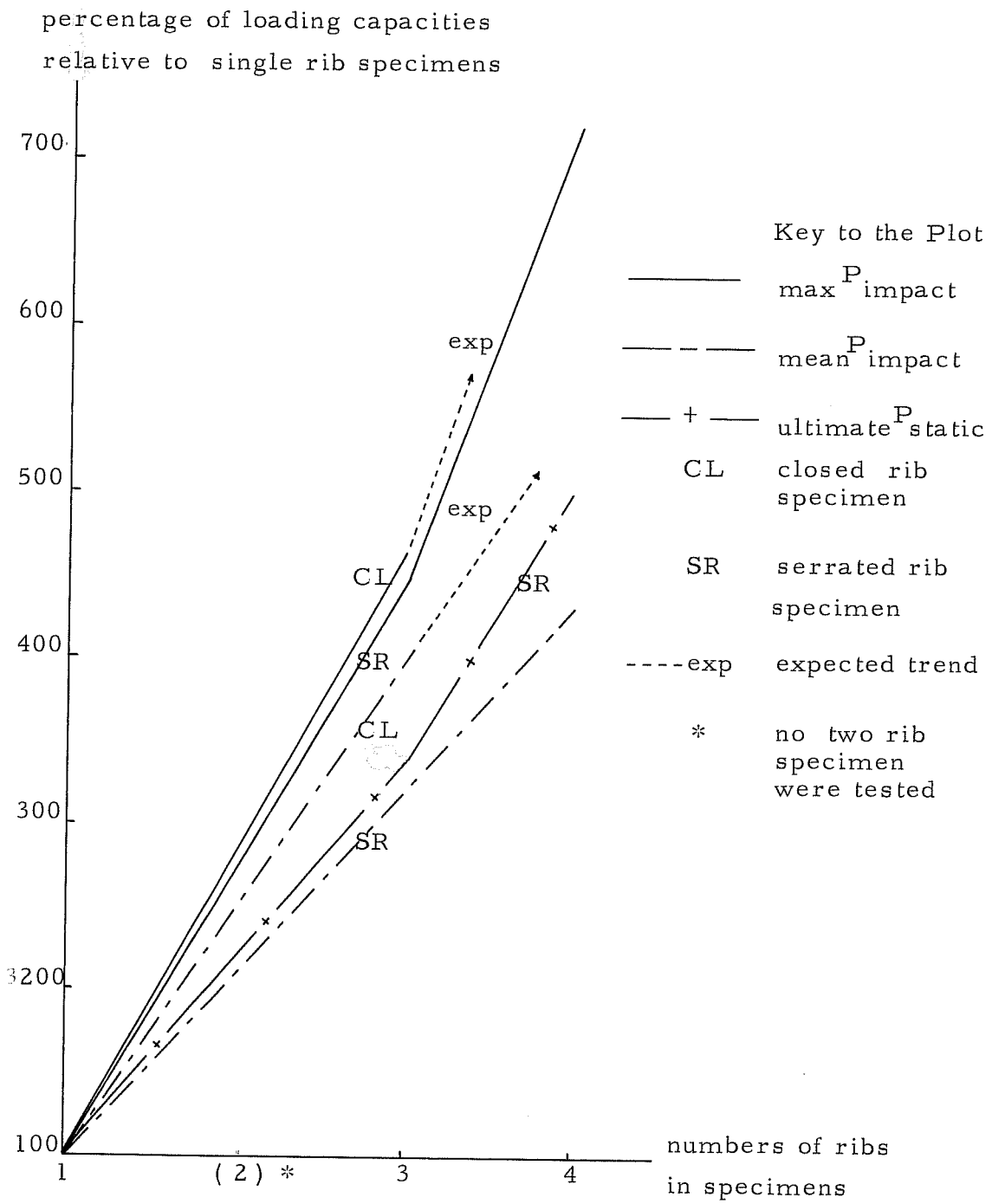

Fig. 41 Comparison of the Ultimate Loading Capacities of the Specimens with Regard to the Capacity of their Single Rib Elements

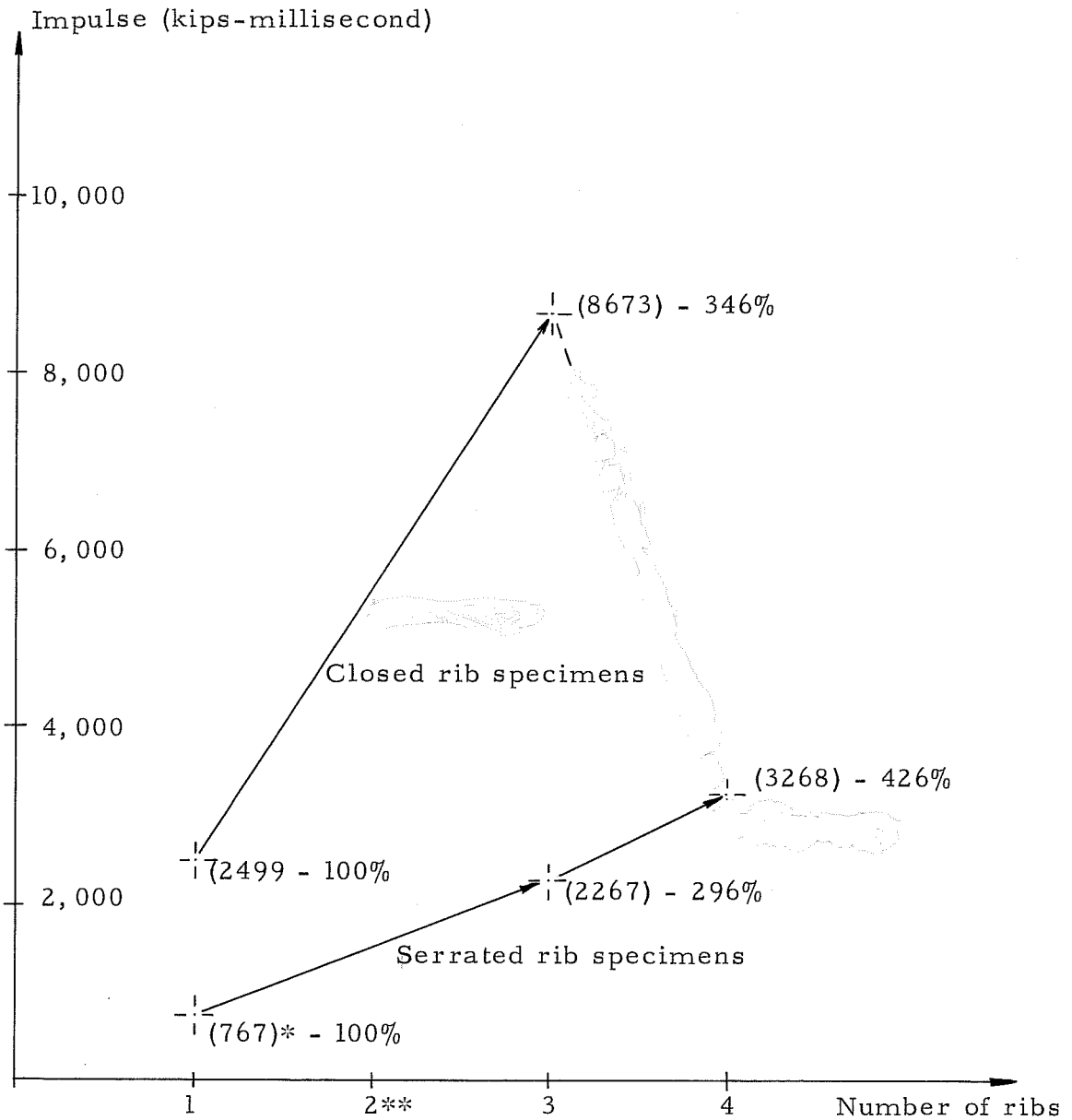

Fig. 42 Impulse Obtained from Ultimate Impact Tests for Various Specimens

* Ordinate values in kips-millisecond
** No two rib specimens were tested

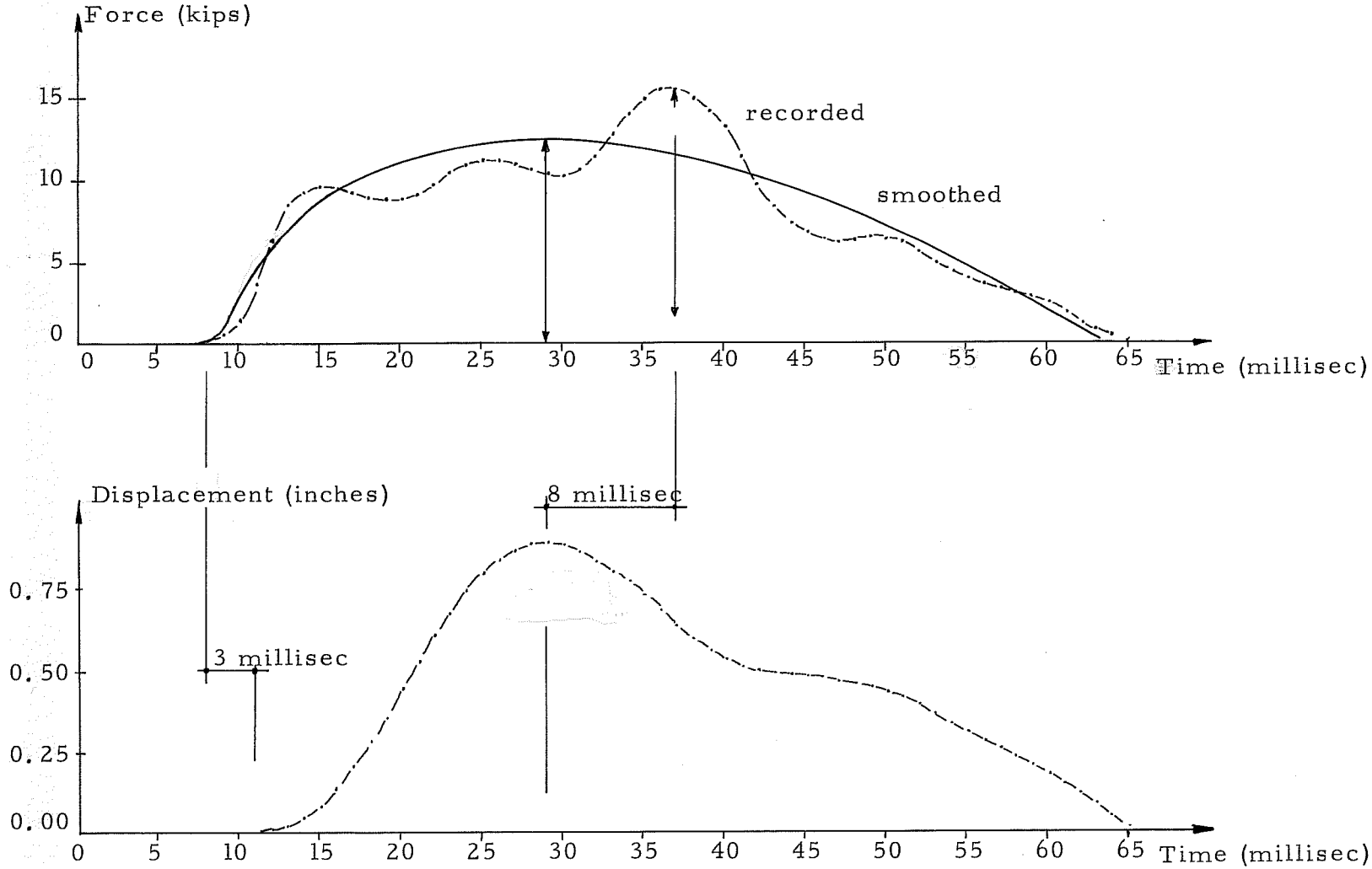

Fig. 43 Force/Time and Displacement/Time Relation
Test No. 6, 10 in. Drop on CL-1-1 Specimen

SPECIMEN CL-1-1 DROP HEIGHT 10.0 INCH IMPACT VELOCITY 87.9 INCH/SEC MASS 1197 LBS

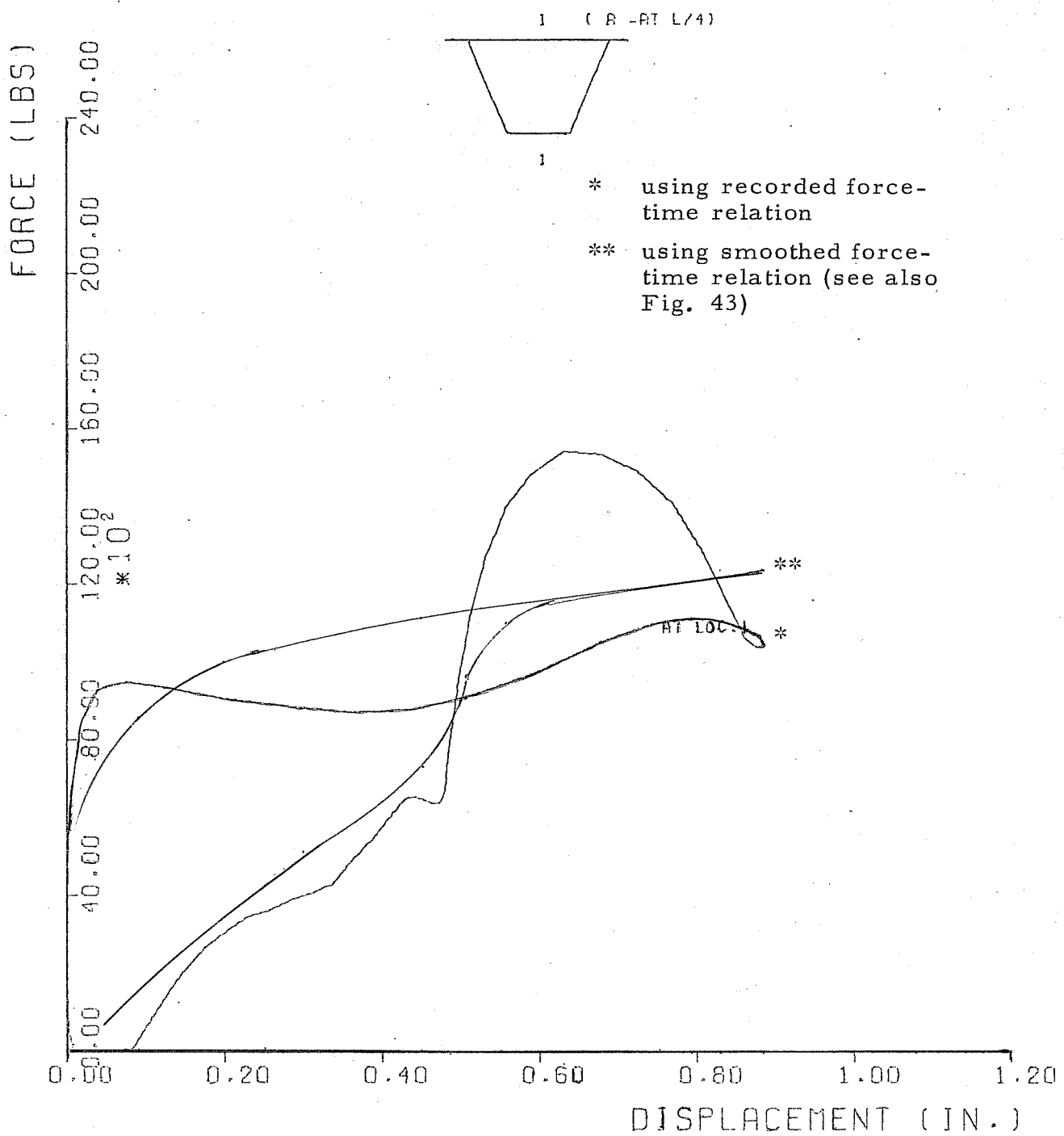

TEST NO. 6

FORCE - DISPLACEMENT RELATION

IMPACT AT LOCATION 1

Fig. 44

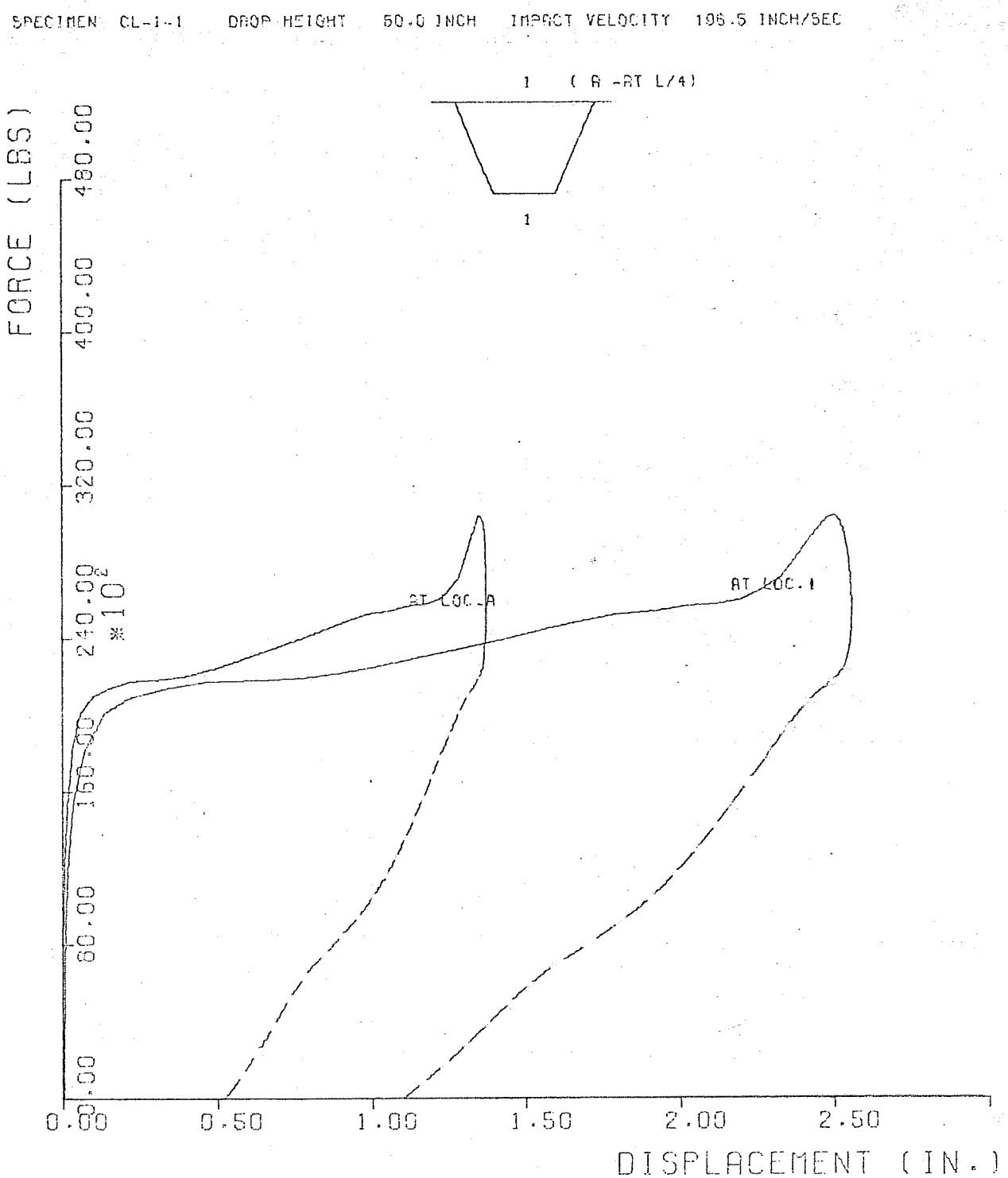

TEST NO. 20

FORCE - DISPLACEMENT RELATION

IMPACT AT LOCATION 1

Fig. 45

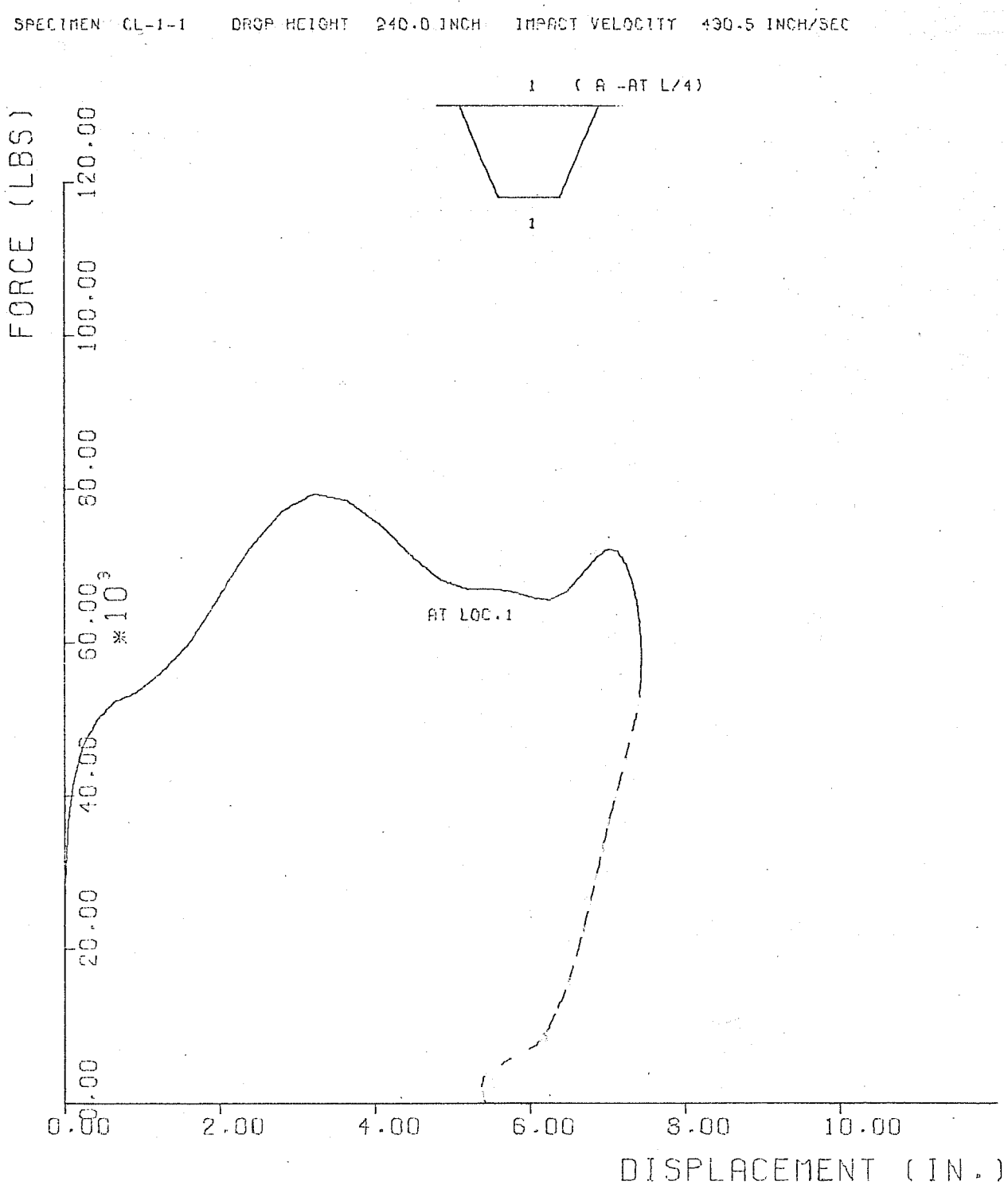

TEST NO. 23

FORCE - DISPLACEMENT RELATION

IMPACT AT LOCATION 1

Fig. 46

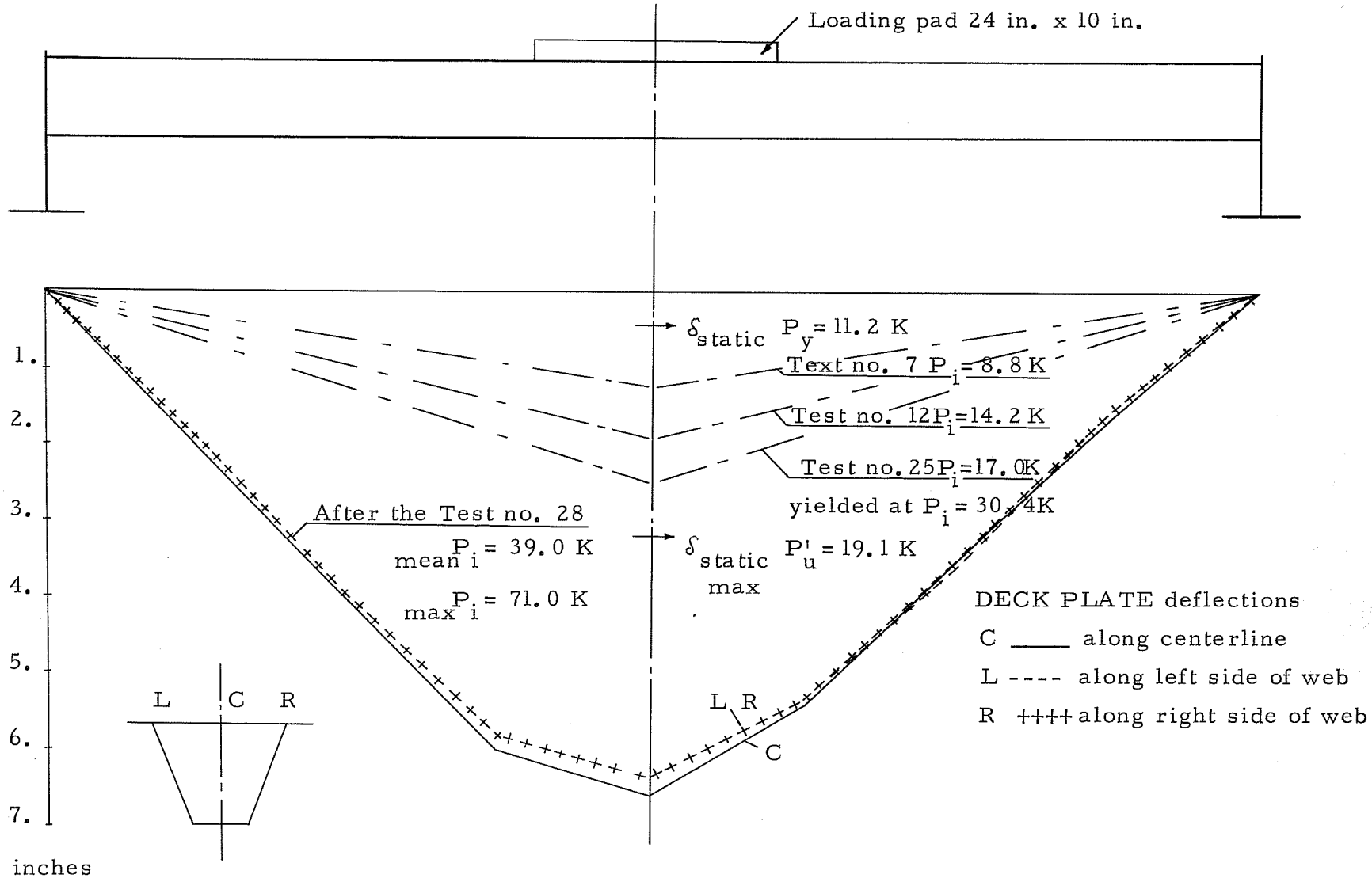

Fig. 47 Deflection of the Specimens CL-1-1

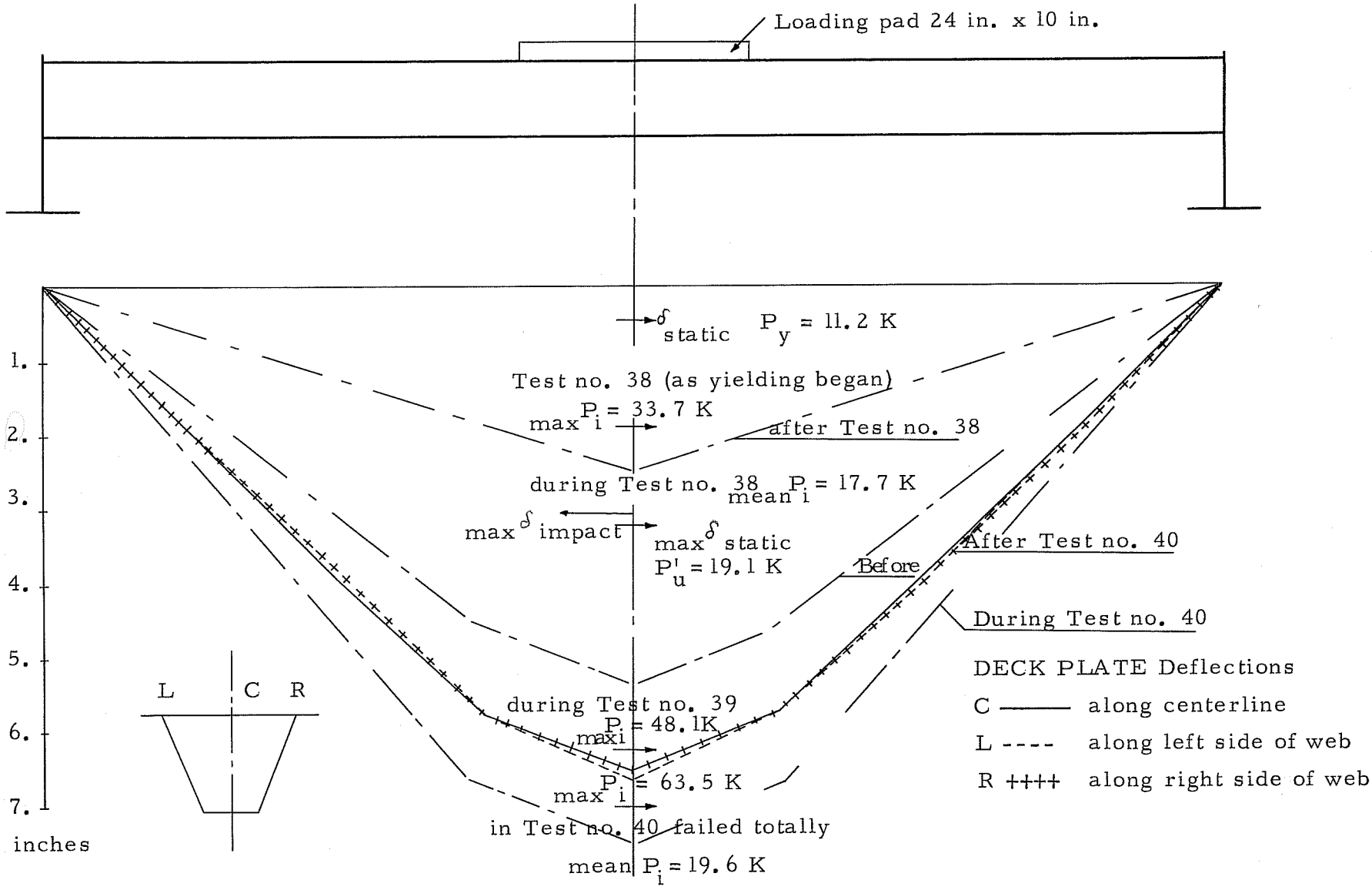

Fig. 48 Deflection of the Specimen CL - 1 - 2

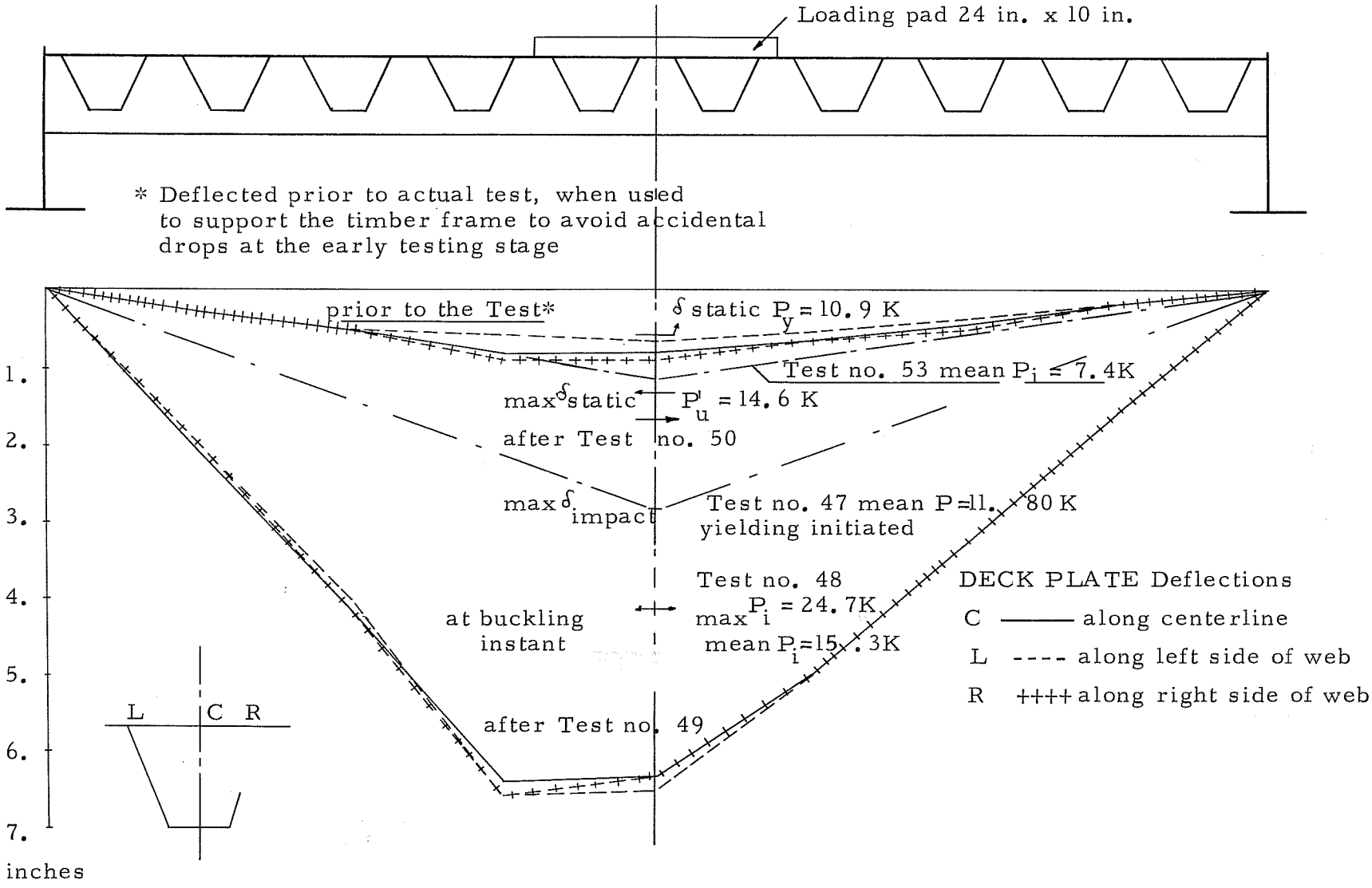

Fig. 49 Deflection of the Specimen SR-1-1

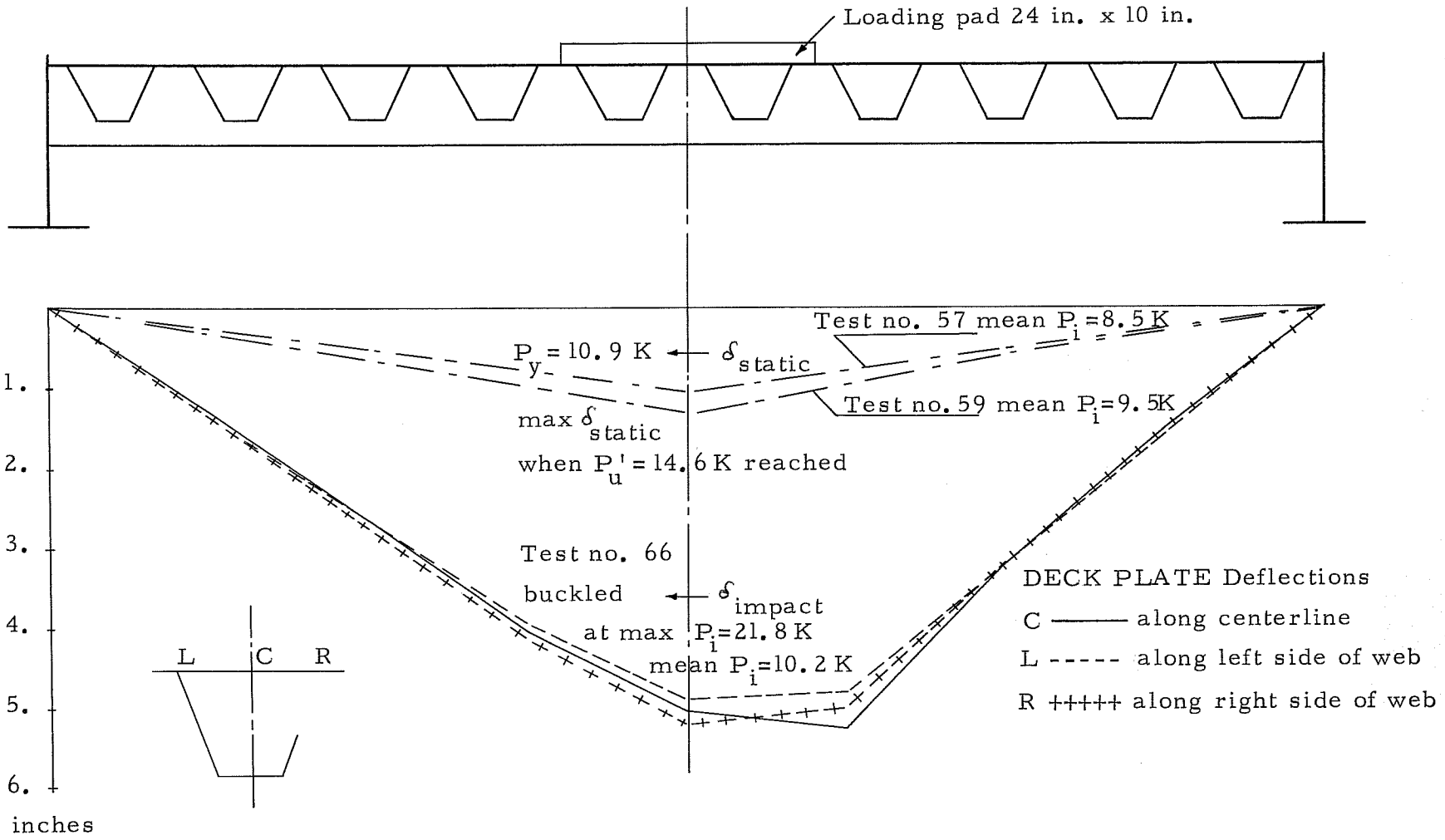

Fig. 50 Deflection of the Specimen SR-1-2

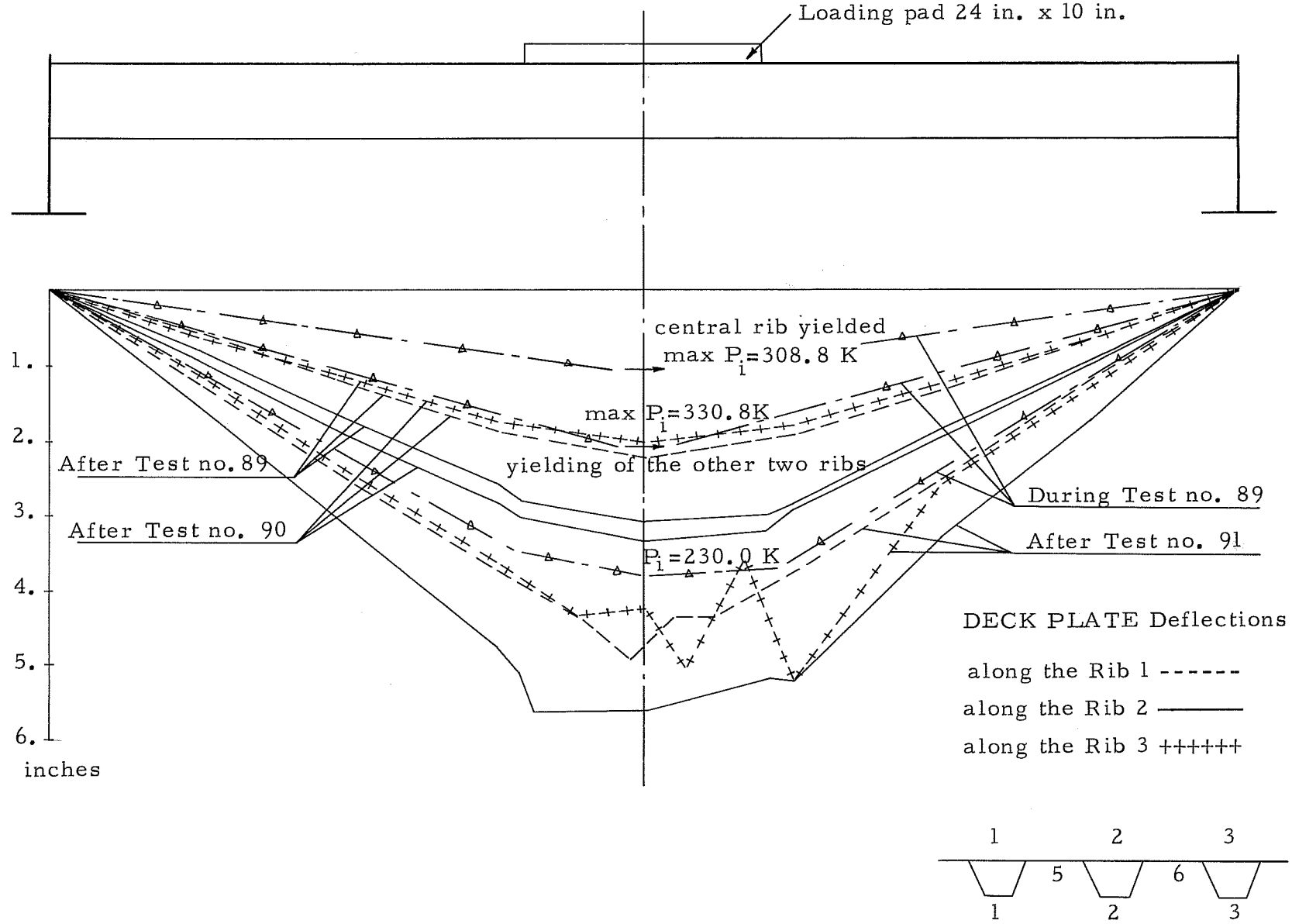

Fig. 51 Deflection of the Specimen CL-3-1